CALCULATION OF FLOW PAST MULTIPLE BODIES BY VORTEX CLOUD METHOD

By

Mohammad Raza Rizvi

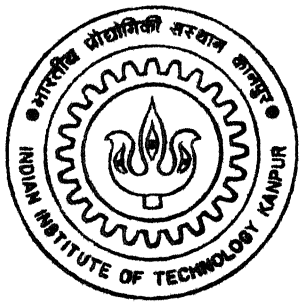

DEPARTMENT OF AEROSPACE ENGINEERING

INDIAN INSTITUTE OF TECHNOLOGY KANPUR

MAY, 2001

CALCULATION OF FLOW PAST MULTIPLE BODIES BY VORTEX CLOUD METHOD

Thesis submitted in partial fulfillment of the requirements for the degree of

Master of Technology

By

Mohammad Raza Rizvi

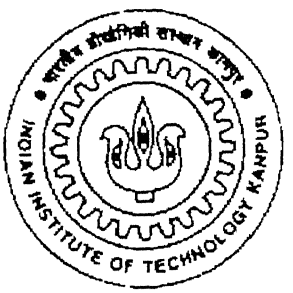

DEPARTMENT OF AEROSPACE ENGINEERING

INDIAN INSTITUTE OF TECHNOLOGY

KANPUR - 208016

May, 2001

Release Caution Money

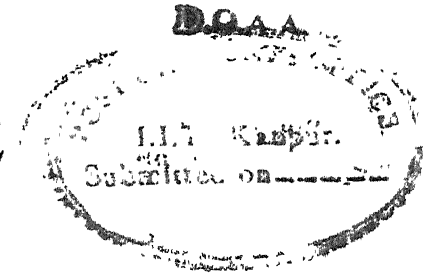

CERTIFICATE

It is certified that the work contained in the thesis ***Calculation of Flow Past Multiple Bodies by Vortex Cloud Method*** by Mohammad Raza Rizvi has been carried out in my supervision and has not been submitted elsewhere for a degree.

Vijay Gupta
Professor
Department of Aerospace Engineering
Indian Institute of Technology Kanpur

1 May 2001

Acknowledgments

I take this opportunity to express my indebtedness and deep sense of gratitude to my thesis supervisor Dr. V. Gupta for introducing me into the exciting field of Vortex methods. His inspiring guidance, systematic approach, stimulating discussions and extensive care helped to shape my thesis as well as my personal attitude towards academics. It is my immense good fortune to be under his tutelage and I am profoundly grateful to him. I would also like to thank Dr Sanjay Mittal for his guidance and help.

I am grateful to my friends Desai Tapshil, Ashok, Vivek for accompanying me through out my stay and always try to understand me in an otherwise difficult time

I extend my profound thanks to my friends Satya, Vinod, Goel, Jain, Kumar Sarvesh, Yadav and all of my friends at hall-5 , who have made my stay here a most memorable one and who have directly or indirectly helped in the completion of the thesis.

This work could not have been completed without the blessings of my parents. Even to think of thanking them is to trivialize all that they have done for me. My profoundest debts to them therefore, remain silent and unacknowledged.

Mohammad Raza Rizvi
IIT Kanpur

Dedicated

to

My Parents

Abstract

Aerodynamic drag on moving vehicles consists the major cost element of transportations. There have been recent developments, where suppression of wake by the use of edge treatment have promised dramatic savings in fuel costs.

In present work a 'full vortex cloud' scheme has been used as a tool for numerical investigation of unsteady, incompressible flows past some two dimensional bodies. Four geometries have been considered, first geometry is circular cylinder for validation of the code, second one is a square cylinder to be used as a model for trucks, third is a similar square cylinder with edge modifications, and forth is a rotating circular cylinder. The drag obtained for square cylinder are compared with the available results, and it is found that the results are in good agreement with the available results It is also found that the the drag of square cylinder can be reduced to a good extent by using a drag suppressor. We have also tried to develop the flow past rotating circular cylinder.

Contents

List of Figures

List of Tables

Nomenculature

W_∞	Free stream resultant velocity
U_∞	Free stream velocity in the x-direction
V_∞	Free stream velocity in the y-direction
M	Number of elements
Re	Reynolds number
ν	Dynamic viscosity
$ds, \Delta s$	Element length
s	Distance around profile
r_{mn}	Distance vector between m and n vortices
β_n	Slope at element n
Γ	Circulation
$\gamma(s)$	Vorticity strength
$K(s_m, s_n)$	Coupling coefficient
q	Velocity vector
Z	Number of shed vortices
$dt, \Delta t$	Time step
t	Time
P_i, Q_i	Random numbers
ϵ	Offset
ϕ	Angle
ρ	Fluid density
p_{stg}	Stagnation pressure

C_l	Lift coefficient
C_d	Drag coefficient
f	Frequency of vortex shedding
St	Strouhal number

Chapter 1

Introduction

1.1 Literature survey

The origin of vortex methods can be traced back to 1930s in the works of Rosenhead(1931) who approximated the motion of a two dimensional vortex sheet by following the movement in time of a system of point vortices, using their locations as quadrature points. Performing his calculations by hand, he was not able to conduct simulations for extended times.

Westwater(1935) was first to apply the approach of Rosenhead to the vortex sheet roll-up behind a wing. With the advent of high speed computers, a number of researchers e.g.Takami(1964), Moore(1974), Clements and Maull(1973) extended this approach to the vortex sheet roll-up behind a wing. Some researchers Kuwahara and Takami(1973) and Chorin and Bernard(1973) introduced vortices with small but finite area instead of using point vortices.

In 1973 Moore presented a numerical study for the roll-up of finite vortex sheet. In his work he introduced tip vortex to represent the tightly rolled portion of vortex sheet, the chaotic motion which was a feature of some of the earlier studies, was eliminated and details of the outer portion of the spiral were calculated.

In 1973 Chorin presented a scheme to simulate viscous effects. In his scheme vortices move under mutually induced velocity of field modified by a diffusion component due to viscosity. In his method of random walk particles undergo a Brownian-like motion to simulate the effects of viscosity.

In 1979 Baker used a numerical method to calculate the time evolution of vortex

sheet by adapting "Cloud in Cell" technique. Krasny in 1987 studied numerically the two vortex sheet evolution problems arising in the aerodynamics(*e.g.* aircraft wake).

Other researchers worked for the development of vortex methods include Sarpkaya(1989), Smith and Stansby(1988), Saffman(1981), Milizzano and Saffman(1977) and Leonard(1980) etc.

1.2 Present Work

The present work is in essence an extension of the work started in 1993 by Parag Kumar continued by Verma(1994) and Manish Kumar Jain(1996). Parag Kumar studied the motion of the vortices shed from sharp corners by a method of conformal transformation. Jain and Verma worked on operator splitting method to solve the Navier-Stokes equation and developed a full-vortex cloud method. They solved the flow past circular and square cylinder and provided basic technique for flow past multiple objects.

The present work is focused on developing the technique further to study complex shapes.

Chapter 2

THE FLOW PAST SQUARE CYLINDER

2.1 Introduction

Vortex methods were originally conceived as tools to model the evolution of unsteady, incompressible, high Reynolds number flows of engineering interest. Vortex methods simulate flows of this type by discretizing only the vorticity carrying regions and tracking the computational elements in a Lagrangian frame.

The "full-vortex cloud theory" attempts to develop the real flow past two-dimensional bodies of arbitrary shape. Vorticity is created over the whole body surface, *i.e.* body is covered with discretized vortex panels. The strength of which is determined using Martensen method which is based on satisfying the zero tangential velocity condition by postulating a vortex sheet at the body surface. Thereafter this vortex sheet is diffused in the flow field and is convected downstream as a cloud of discrete vortices during a sequence of small time steps, ultimately shedding naturally from sharp edges or boundary layer natural separation points. The ultimate aim is nothing less than a full simulation of real fluid flow with minimum human intervention.

2.2 The full-vortex cloud approach

In this method, the traditional discrete vortex methods are modified so as to account for viscous diffusion as well. This permits calculations for finite Reynolds numbers as opposed to traditional methods which are valid only for infinite Reynolds number. The surface of two-dimensional body is covered by discretized vortex panels. These panels then diffuse into the flow region with every time step as well as convect according to the local flow velocity.

The complex diffusion convection problem is handled by an operator-splitting strategy first proposed by Chorin(1973, 1978) and later developed extensively by Smith and Stansby(1987), Lewis and Porthouse(1983) and Verma(1994).

Thus the Navier-Stokes equation

$$\frac{\partial q}{\partial t} + q.\nabla q = \frac{-\nabla p}{\rho} + \nu \nabla^2 q \tag{2.1}$$

is first converted into the two dimensional vorticity transport equation

$$\frac{\partial \omega}{\partial t} + q.\nabla \omega = \nu \nabla^2 \omega \tag{2.2}$$

and then split into two equations

$$\bullet\ convection \quad \frac{\partial \omega}{\partial t} + q.\nabla \omega = 0 \tag{2.3}$$

and

$$\bullet\ diffusion \quad \frac{\partial \omega}{\partial t} = \nu \nabla^2 \omega \tag{2.4}$$

The above two equations are solved one after the other. The process starts with the calculation of potential flow about the body with the vortex sheet replacing the body surface. This sheet is then discretized into a number of elements. These elementary vortices first diffuse according to equation 2.4 and, then, are convected according to equation 2.3. The convection velocity is determined by the influence of all the vorticity elements, the free-stream of the new vortex sheet required to satisfy tangency condition. After these two equations have been solved, the Navier-Stokes equation reduces to

$$\frac{\partial q}{\partial t} = -\frac{\nabla p}{\rho} \tag{2.5}$$

which when solved will give pressure distribution.

The numerical scheme is developed in this chapter. The flow diagram in Fig. 2.1 shows the strategy for the full-vortex cloud analysis.

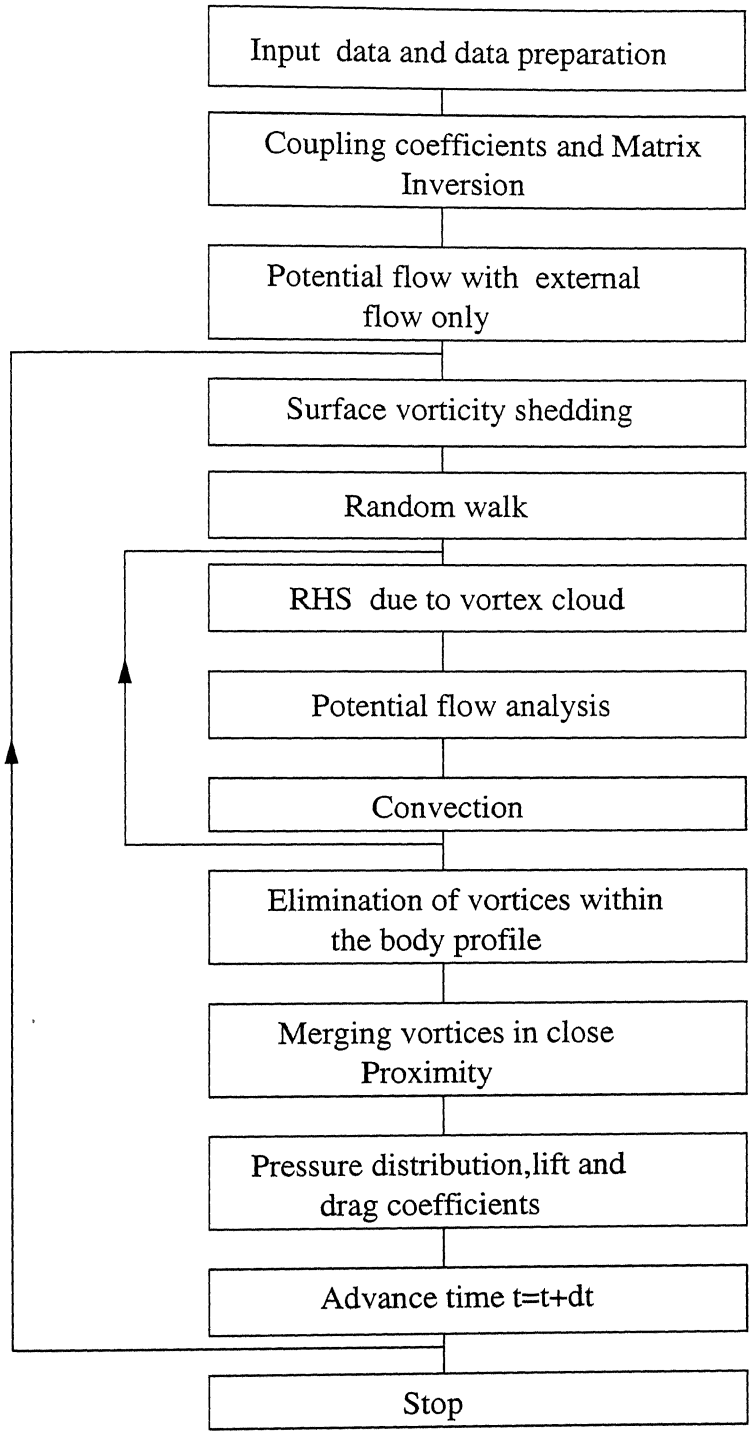

Figure 2.1: Flow diagram for full-vortex cloud model

2.3 Martensen method

Consider a discretized two-dimensional body which is immersed in a uniform flow W_∞ at an angle of attack α_∞ measured with respect to the x-axis as shown in Fig 2 2. Let the length of n^{th} panel be ds_n and has vorticity sheet of strength $\gamma(s)$ per unit length Then from Biot-Savart law, the induced velocity at s_m, dq_{mn} due to a small vorticity $\gamma(s_n)ds_n$ located at s_n on the body is

$$dq_{mn} = \frac{\gamma(s_n)ds_n}{2\pi r_{mn}} \tag{2.6}$$

where r_{mn} is the distance between the elements m and n.

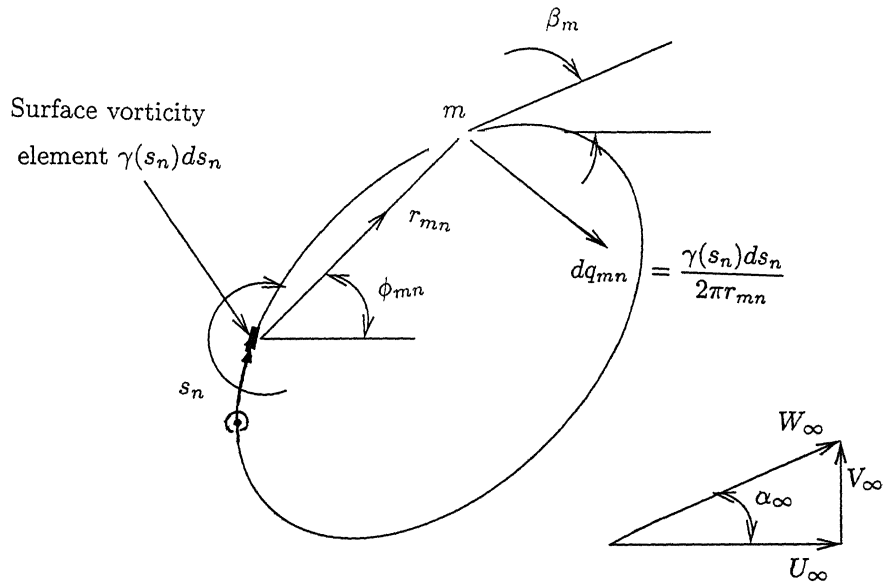

Figure 2 2: Martensen method

Resolving dq_{mn} parallel to s_m, we obtain the following tangential velocity component

$$dv_{s_{mn}} = \frac{1}{2\pi}\left\{\frac{(y_m - y_n)cos\beta_m - (x_m - x_n)sin\beta_m}{(x_m - x_n)^2 + (y_m - y_n)^2}\right\}\gamma(s_n)ds_n \tag{2.7}$$

Stating the Dirichlet boundary condition at s_m

$$-\frac{1}{2}\gamma(s_m) + \oint k(s_m, s_n)\gamma(s_n)ds_n + (U_\infty cos\beta_m + V_\infty sin\beta_m) = 0 \tag{2.8}$$

Coupling coefficient $k(s_m, s_n)$ is given by

$$k(s_m, s_n) = \frac{1}{2\pi}\left\{\frac{(y_m - y_n)cos\beta_m - (x_m - x_n)sin\beta_m}{(x_m - x_n)^2 + (y_m - y_n)^2}\right\} \tag{2.9}$$

Coupling coefficient $K(s_m, s_n)$ can be written as

$$K(s_m, s_n) = k(s_m, s_n)\Delta s_n \tag{2 10}$$

In special case when $n = m$, the coupling coefficient can be modified as follows,

$$K(s_m, s_m) = -\frac{1}{2} + K'_{mm} \tag{2.11}$$

where K'_{mm} can be evaluated using $L-$Hospital's rule

$$K'_{mm} = \frac{\Delta s_m}{2\pi} \lim_{s_m \to s_n} \left\{ \frac{(y_m - y_n)cos\beta_m - (x_m - x_n)sin\beta_m}{(x_m - x_n)^2 + (y_m - y_n)^2} \right\} \tag{2 12}$$

or

$$K'_{mm} = \frac{\Delta s_m}{4\pi r_m} \approx -\frac{\Delta \beta_m}{4\pi} \tag{2 13}$$

Lewis gave a simple relation for self induced coupling coefficient,

$$K(s_m, s_m) = -\frac{1}{2} - \frac{1}{8\pi}(\beta_{m+1} - \beta_{m-1}) \tag{2 14}$$

Equation 2.8 can be written in the following numerical form

$$\sum_{n=1}^{M} K(s_m, s_n)\gamma(s_n) = -(U_\infty cos\beta_m + V_\infty sin\beta_m) \tag{2.15}$$

Martensen method in presence of cloud of vortices

In presence of the cloud of vortices, the boundary integral equation will yield,

$$-\frac{1}{2}\gamma(s_m) + \oint k(s_m, s_n)\gamma(s_n)ds_n + (U_\infty cos\beta_m + V_\infty sin\beta_m)$$

$$+\sum_{j=1}^{Z} \Delta\Gamma_j (U_{mj} cos\beta_m + V_{mj} sin\beta_m) = 0 \tag{2.16}$$

or in numerical form

$$\sum_{n=1}^{M} K(s_m, s_n)\gamma(s_n) = -(U_\infty cos\beta_m + V_\infty sin\beta_m) - \sum_{j=1}^{Z} \Delta\Gamma_j (U_{mj} cos\beta_m + V_{mj} sin\beta_m) \tag{2.17}$$

Where the unit velocities U_{mj}, V_{mj} are given by

$$U_{mj} = \frac{1}{2\pi}\left[\frac{y_m - y_j}{r_{mj}^2}\right] \tag{2.18}$$

$$V_{mj} = -\frac{1}{2\pi}\left[\frac{x_m - x_j}{r_{mj}^2}\right] \tag{2.19}$$

Where $r_{mj}^2 = (x_m - x_j)^2 + (y_m - y_j)^2$

Helmholtz theorem states that the vorticity at any moment in the flow should be conserved. Thus

$$\sum_{n=1}^{M} \gamma(s_n)\Delta s_n + \sum_{j=1}^{Z} \Delta\Gamma_j - \Gamma_{circ} = 0 \tag{2.20}$$

Where Γ_{circ} is the sum of strength of all the vortices removed from the flow field. The above equation (2 11) must be added to equation (2.11) to ensure vorticity conservation. Thus

$$\sum_{n=1}^{M}(K(s_m, s_n) + \Delta s_n)\gamma(s_n) = -(U_\infty cos\beta_m + V_\infty sin\beta_m)$$

$$-\sum_{j=1}^{Z} \Delta\Gamma_j(U_{mj} cos\beta_m + V_{mj} sin\beta_m + 1) + \Gamma_{circ} \tag{2.21}$$

2.4 Input data and data preparation for body geometry

The body surface is discretized into small elements, the numbering of the elements is done in clockwise direction starting from the leading edge. The last point on the body coincides with the first point. The profile slope and profile pivotal points are calculated at the middle of each element.

$$\Delta s_n = \sqrt{(x_{n+1} - x_n)^2 + (y_{n+1} - y_n)^2} \tag{2.22}$$

profile slopes and pivotal points which are located at the centre of each element, are then given by

$$cos\beta_n = \frac{(x_{n+1} - x_n)}{\Delta s_n} \tag{2.23}$$

$$sin\beta_n = \frac{(y_{n+1} - y_n)}{\Delta s_n} \tag{2.24}$$

$$x_n = \frac{1}{2}(x_{n+1} + x_n) \tag{2.25}$$

$$y_n = \frac{1}{2}(y_{n+1} + y_n) \tag{2.26}$$

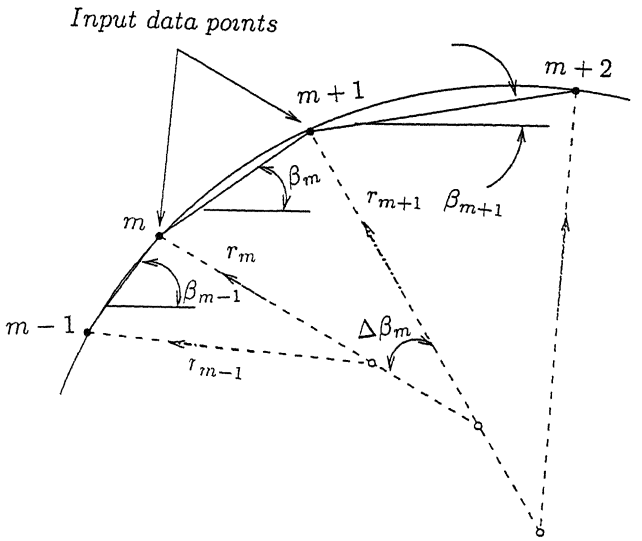

Figure 2.3: Surface element geometry

2.5 Calculation of coupling coefficients

The calculation of coupling coefficient is straight forward except for some complications in special circumstances, such as for thin bodies. For thin body shapes, the coupling coefficients are unable to represent correctly the mutual interference of opposite elements correctly. For thick body shapes on the other hand this problem does not arise and the coupling coefficient matrix is diagonally dominant.

While in case of thin bodies, the error level of back diagonal coefficient of the matrix, namely $K(s_m, s_{M+1-m})$, may dominate leading to erroneous results. To eliminate the error the following techniques are used.

1. Use of sub-elements

A standard Martensen numerical model implies the replacement of the line vorticity elements by a concentrated vortex of strength $\gamma(s_n)ds_n$ at each pivotal point *i.e.* at the middle of each element.

The representation of the true element vorticity influence can be improved when $K(s_m, s_n)$ is calculated as the average value of coupling coefficients for elements.

Consider a case in which an element s_n is broken-up into N sub-elements each of length ds_n/N. The coupling coefficient of the m^{th} element is then given by

$$\overline{K}(s_m, s_n) = \frac{1}{\Delta s_m} \int_0^{\Delta s_m} k(s_m, s_n) ds_n \tag{2.27}$$

In numerical form,

$$\overline{K}(s_m, s_n) = \frac{1}{2\pi N} \sum_{i=1}^{N} \left\{ \frac{(y_m - y_i)cos\beta_m - (x_m - x_i)sin\beta_m}{(x_m - x_i)^2 + (y_m - y_i)^2} \right\} \tag{2.28}$$

Where the location of i_{th} sub-element is given by

$$x_i = x_n + \left(i - \frac{1}{2}(1+N) \right) \frac{\Delta s_n cos\beta_n}{N} \tag{2.29}$$

$$y_i = y_n + \left(i - \frac{1}{2}(1+N) \right) \frac{\Delta s_n sin\beta_n}{N} \tag{2.30}$$

It is found that two or three sub-elements give better results than using more sub-elements.

2. Back-diagonal correction

Back diagonal correction is used to enforce zero internal circulation From Kelvin's theorem the net circulation $\Delta\Gamma_m$ around the profile interior induced by surface vorticity element $\gamma(s_m)\Delta s_m$ should be zero. If this condition is forced upon the coupling coefficients,

$$K(s_{opp}, s_m) = -\frac{1}{\Delta s_{opp}} \sum_{n=1, n\neq opp}^{M} K(s_n, s_m)\Delta s_n \quad (opp = M + 1 - m) \tag{2.31}$$

The back diagonal matrix coefficients $K(s_{M+1-m}, s_m)$ are replaced by the value given by this equation, thereby, ensuring net circulation around the profile interior implied by the numerical model is made to zero.

2.6 Shedding of vortices from the body

Following potential flow analysis at each time step, the surface vorticity $\gamma(s_n)\Delta s_n$ created at every boundary element is shed from the surface into the fluid as a new discrete vortex The vorticity is released at some offset from the body. The offset is taken as $\sqrt{4\nu\Delta t/3}$. However at very high Reynolds number, the offset is very small. The usual approach is to choose a value for the offset related to element size(say 25% of the average surface element length).

2.7 Diffusion of vortices

As given by Chorin in 1973, the diffusion of vortices in a flow is modeled by a random walk method. The diffusion model is such that the vortices move randomly in θ-direction with flat probability, and walking in the r-direction with normal distribution

Let P denotes the probability that a given vorticity element will lie somewhere within the circle of radius r,

$$P = 1 - e^{-r^2/4\nu t} \tag{2.32}$$

for the random walk process, we generate a random number P_i between 0 to 1 with uniform distribution. The i_{th} vortex element will be found at radius r_i such that

$$P_i = 1 - e^{\frac{-r_i^2}{4\nu t}} \tag{2.33}$$

the radial shift of vortex can be calculated from the above equation as $r_i = \sqrt{4\nu t \ln(1/P_i)}$. We generate two random numbers P_i and Q_i. Thus during time step Δt, the element i will undergo the following movement,

$$\bullet \ angular\ shift\ \Delta\theta_i = 2\pi Q_i \tag{2.34}$$

$$\bullet \ radial\ shift\ \Delta r_i = \sqrt{4\nu\Delta t \ln(1/P_i)} \tag{2.35}$$

Thus after the increment of time step Δt the new location of the i^{th} element will be

$$x_i' = x_i + \Delta r_i cos\Delta\theta_i \tag{2.36}$$

$$y_i' = y_i + \Delta r_i sin\Delta\theta_i \tag{2.37}$$

2.8 Convection of vortices

After shedding and diffusion having been taken place, vortices undergo convection under the influence of all other vortices in the flow plus vorticity bound to the body surface plus the external flow field.

If the m^{th} vortex is at (x, y) and there are total Z vortices in the flow field, then the convection velocity of the vortex is the sum of individual velocities imparted

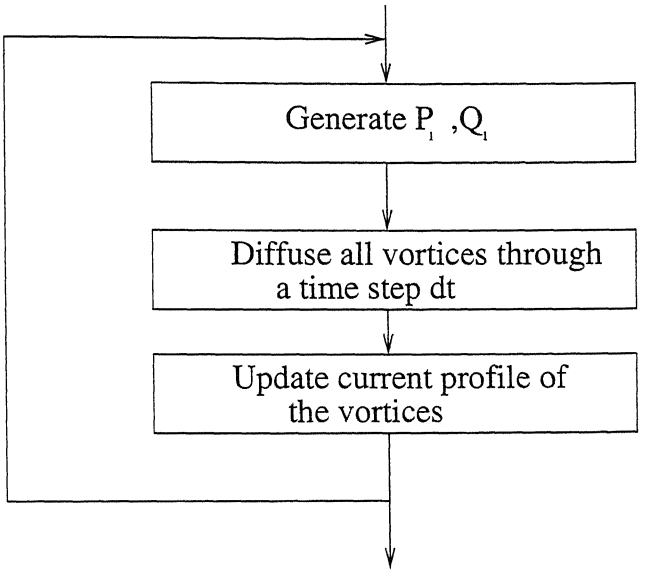

Figure 2.4: Random number generator

by each vortex on this particular vortex, plus sum of velocities imparted by the bound vorticity of the body plus free stream velocity. In numerical form,

$$u = U_\infty + U_{vortex\ cloud} + U_{bound} \tag{2.38}$$

$$v = V_\infty + V_{vortex\ cloud} + V_{bound} \tag{2.39}$$

where $U_\infty = W_\infty cos\alpha$ and $V_\infty = W_\infty sin\alpha$

If we consider n^{th} vortex in the cloud located at the position (x_j, y_j), the velocity at m due to vortex n will then be given by Biot-Savart law. Summing up the influence of Z vortices as

$$U_{vortex\ cloud} = \sum_{j=1, j\neq m}^{Z} \frac{\Gamma_j}{2\pi}\left(\frac{y - y_j}{r^2}\right) \tag{2.40}$$

$$V_{vortex\ cloud} = -\sum_{j=1, j\neq m}^{Z} \frac{\Gamma_j}{2\pi}\left(\frac{x - x_j}{r^2}\right) \tag{2.41}$$

If there are M discrete panels on the body surface with distributed vorticity of the strength $\gamma(s_n)ds_n$ at the n^{th} element,

$$U_{bound} = \sum_{j=1}^{M} \frac{\gamma(s_j)ds_j}{2\pi}\left(\frac{y - y_j}{r^2}\right) \tag{2.42}$$

$$V_{bound} = -\sum_{j=1}^{M} \frac{\gamma(s_j)ds_j}{2\pi}\left(\frac{x-x_j}{r^2}\right) \tag{2.43}$$

where $r = \sqrt{(x-x_j)^2+(y-y_j)^2}$

Now after convection velocity of each vortex has been calculated, their new position after convection is ascertained by displacing them by amounts $\Delta x = u\Delta t$ and $\Delta y = v\Delta t$ and adding these displacements to their original location coordinates will give their new location coordinates.*i.e*

$$x' = x + u\,\Delta t \tag{2.44}$$

$$y' = y + v\,\Delta t \tag{2.45}$$

After convection of all the vortices, if we now re-calculate the convection velocities (u', v') at their new locations (x', y'), we can estimate the better location by using the central difference scheme. That is

$$x'' = x + \frac{1}{2}(u+u')\Delta t \tag{2.46}$$

$$y'' = y + \frac{1}{2}(v+v')\Delta t \tag{2.47}$$

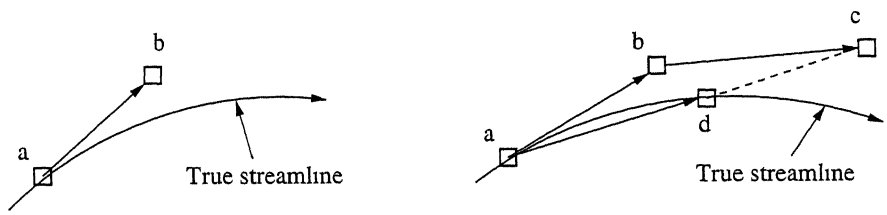

(a) Forward difference method

(b) Central difference method

Figure 2.5: Estimates of streamline path

2.9 Merging of vortices

As the vortices move away from the body, their effect diminishes with increasing the distance from body. we know that CPU time required for the N particles in the flow is of the order $O(N^2)$. So reducing the number of vortices by merging them is the effective way to reduce their number. The total strength of the newly formed vortex after merging will be the algebraic sum of the strength of individual vortices.

2.10 Reflection of vortices

Vortices if drifted very close to the body, can produce serious potential flow errors So vortices are pushed back in the direction normal to the body to some fixed distance(say offset ϵ) in order to prevent the possible errors in Martensen analysis or in convection

2.11 Calculation of lift and drag coefficient and Strouhal number

Since we are using operator splitting technique for the solution of Navier-Stokes equation, after diffusion $\nu\nabla^2 q$ and convection $q.\nabla q$, the remaining part of the equation is,

$$-\frac{\nabla p}{\rho} = \frac{\partial q}{\partial t} \tag{2.48}$$

At any point s_n on the body surface, the velocity $q = \gamma(s_n)$ parallel to the surface. Then the pressure gradient along the surface at s_n is given by,

$$\frac{\partial p_s}{\partial s} = -\rho\frac{\partial \gamma(s_n)}{\partial t} \tag{2.49}$$

which can be written in the following form,

$$\Delta p_n = -\rho\frac{\gamma(s_n)\Delta s_n}{\Delta t} = -\rho\frac{\Delta \Gamma_n}{\Delta t} \tag{2.50}$$

for pressure change over the surface element n during the discrete time step Δt. The integration of above equation will give pressure change at any element on the body surface.

$$p_m = p_1 + \sum_{n=1}^{m} \Delta p_n \tag{2.51}$$

The average pressure on any element will then be,

$$\overline{p}_n = \left(\frac{p_n + p_{n+1}}{2}\right) \tag{2.52}$$

After calculating average pressures on all the elements, the lift and drag coefficient can be calculated by the following equations,

$$C_l = \frac{L}{\frac{1}{2}\rho W_\infty^2 l} = -\frac{2}{\rho W_\infty^2 l}\sum_{n=1}^{M} \overline{p}_n cos\beta_n \Delta s_n \tag{2.53}$$

$$C_d = \frac{D}{\frac{1}{2}\rho W_\infty^2 l} = \frac{2}{\rho W_\infty^2 l} \sum_{n=1}^{M} \overline{p}_n sin\beta_n \Delta s_n \tag{2.54}$$

where l is the characteristic length.

To determine the Strouhal number St of vortex shedding, spectral analysis is first used to determine the dominant frequency of the pressure data. Then the dominant frequency is used to determine the St using the following equation

$$St = \frac{f\,d}{W_\infty} \tag{2.55}$$

where d is the diameter of the cylinder, and W_∞ is the free-stream velocity.

2.12 Results and Discussions

We have first run the code for the case of circular cylinder for the purpose of validation of the code. The results obtained for circular cylinder are then compared with the available results The Fig. 2.6A shows the available numerical results(*Ref*.11, *pp*.422) and Fig. 2.6B shows the results obtained in the present study. The Fig. 2.6A predict the average lift and drag of circular cylinder as zero and 1.5 respectively at Re=20000. And from the present study, the lift and drag obtained are zero and 1.53 respectively at Re=20000. Thus the results obtained are in fair agreement with the available numerical results. After validation, the flow past a square cylinder at various Reynolds number is calculated.

Flow past square cylinder

To solve flow past square cylinder, the side of square cylinder is taken as 1.0, mainstream flow W_∞ is 1.0 and $\alpha_\infty = 0$. Here we have discretized the body into 56 elements. The time step is taken sufficiently small at 0 05 to maintain reversibility during convection and the code is run for a minimum of 650 steps($T_{min} = 32.5$) which is sufficiently large to cover several oscillations of the vortex sheet. The lift and drag coefficients along with Strouhal number are calculated at various Reynolds number($20,000$, $30,000$, $40,000$, $50,000$, $60,000$, 1×10^5, 1.2×10^6). For eliminating numerical noise, we are averaging the lift and drag coefficients for 10 steps. The flow diagram for different Reynolds numbers shown in Fig. 2.8 to Fig. 2.12. The variation of lift and drag coefficients with respect to time are shown from Fig. 2.13 to Fig. 2.15. The Table 2.1 shows the average values of life and drag coefficients with Strouhal number.

The average drag obtained from the present study for square cylinder is around 2.18 at $Re = 1\times10^5$. The experimental results(Ref. 25) show the drag of square cylinder around 2.10. Thus the results obtained numerically are in good agreement with the available results. Fig. 2.7 shows the variation of drag with increasing Reynolds number. The drag although slightly higher than the experimental results, is in good agreement with the experimental results.

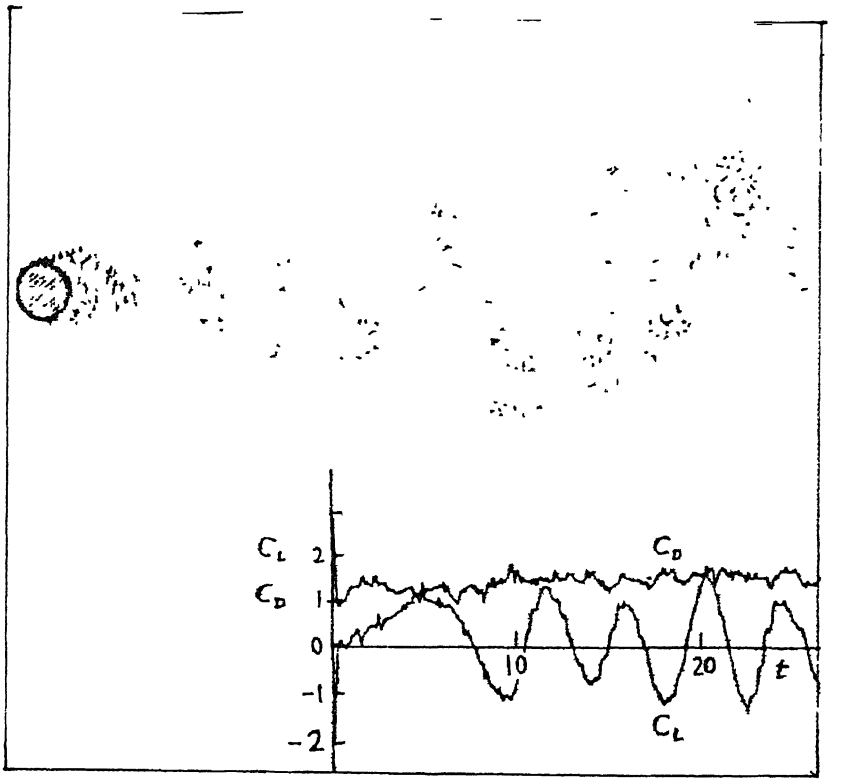

Figure 2.6A: Vortex cloud solution to flow past circular cyliner at Re=20,000(*Ref*.11, *pp*.422)

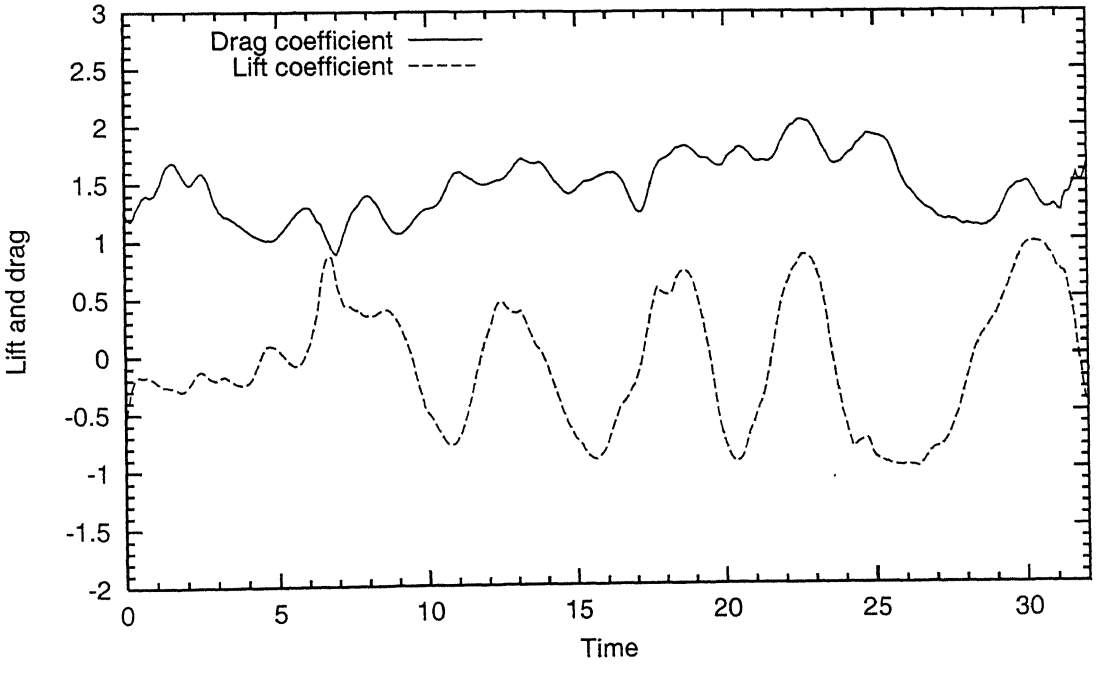

Figure 2.6B:Vortex cloud solution obtained for flow past circular cylinder at Re = 20000 for validation of the code

Re	*Average lift coefficients,* C_l	*Average drag coefficients,* C_d	*Strouhal No. St*
20000	0.011405	2.299080	0.1953
30000	-0.054072	2.154425	0.2013
40000	0.137076	2.113487	0.2106
50000	-0 015132	2 328437	0.2216
60000	-0.011620	2.177026	0.1973
1×10^5	0.127729	2.177774	0 1946
$1\ 2 \times 10^6$	-0.098907	2.190457	0.1920

Table 2 1· Lift and Drag for the case of square cylinder

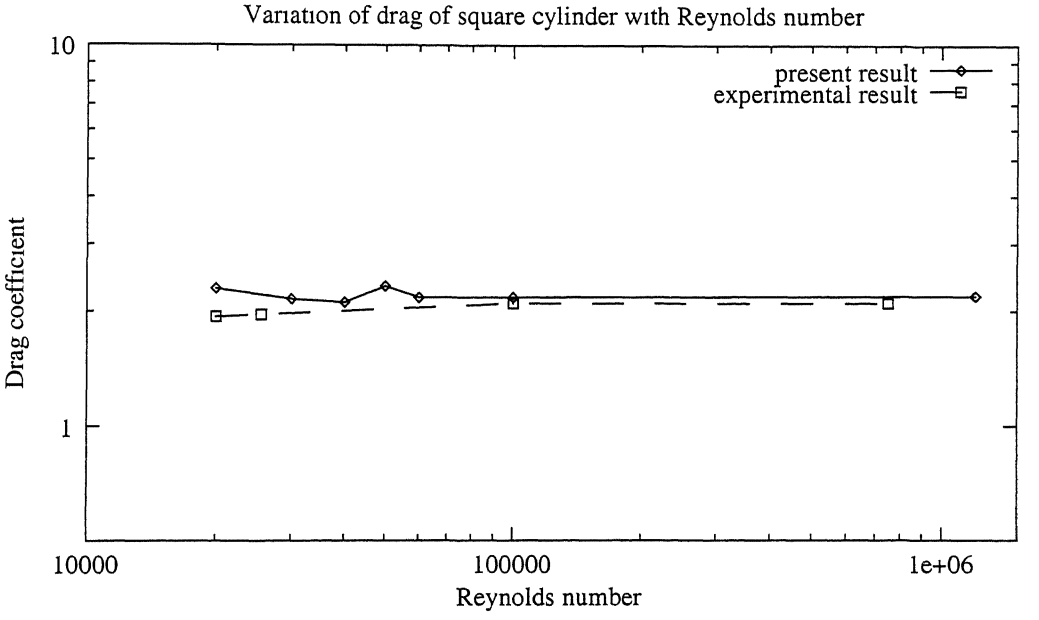

Figure 2.7: Comparison of drag of square cylinder with available experimental results(*Ref.* 25)

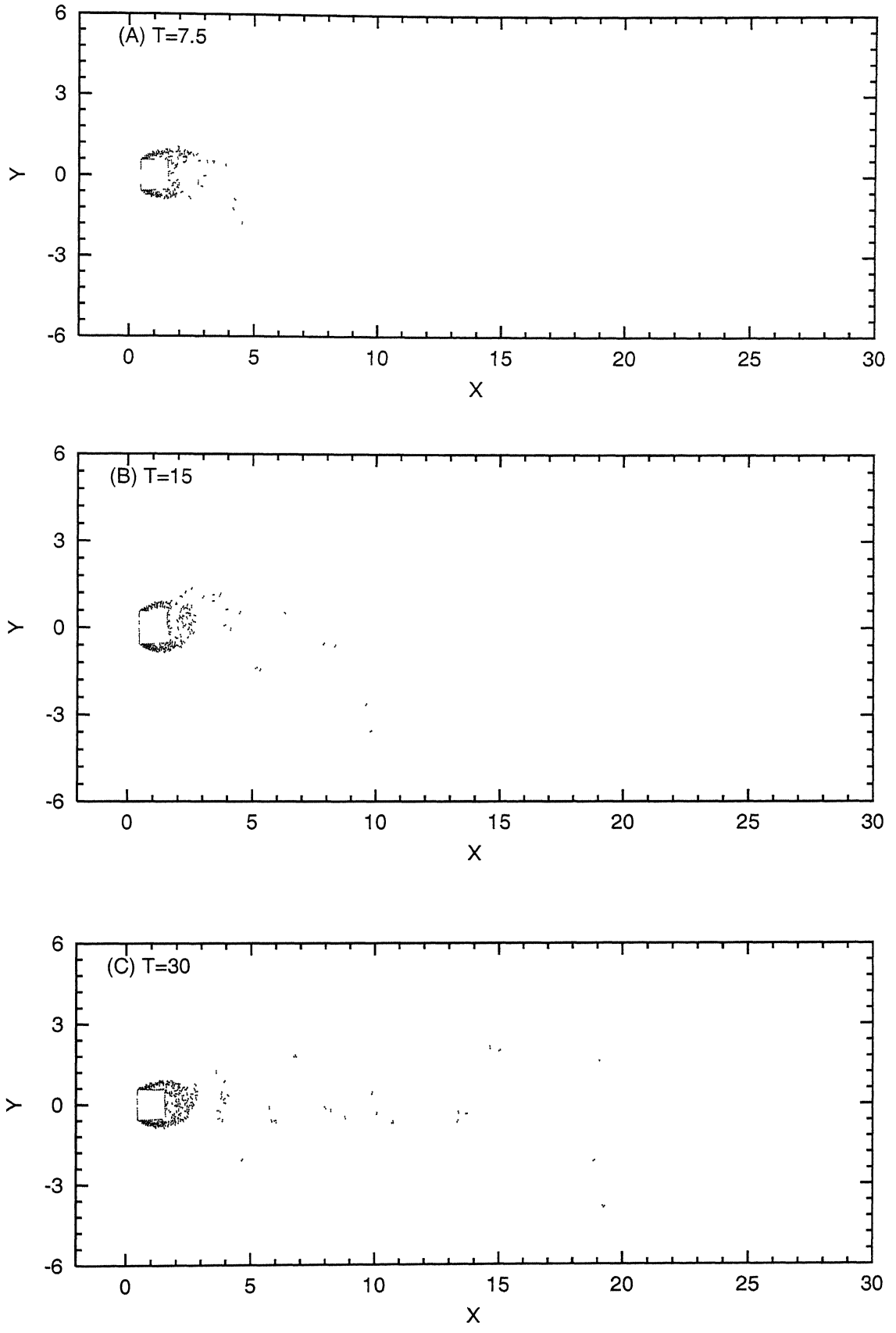

Figure 2.8: Flow diagram for square cylinder at $Re = 20000$

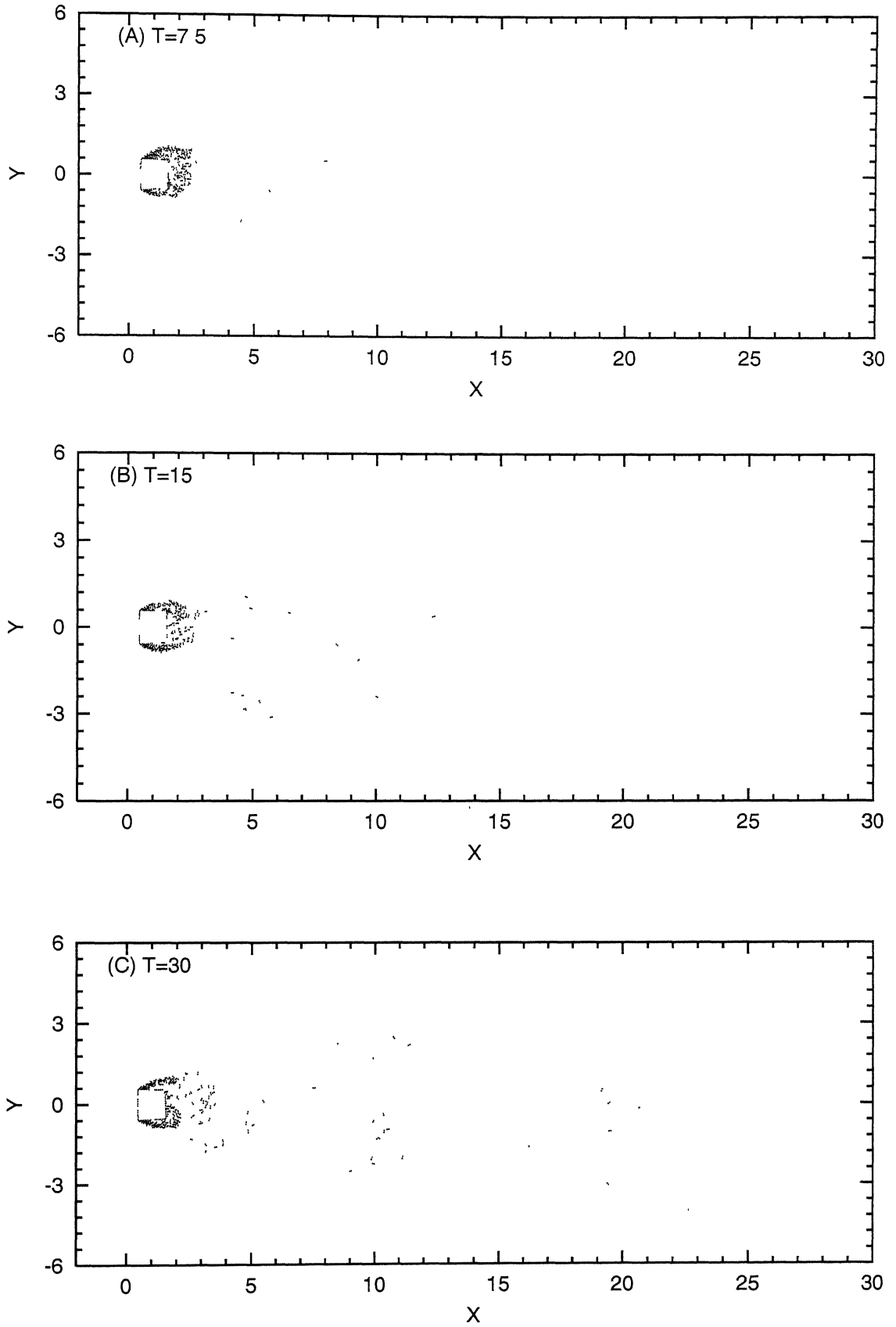

Figure 2.9. Flow diagram for square cylinder at $Re = 40000$

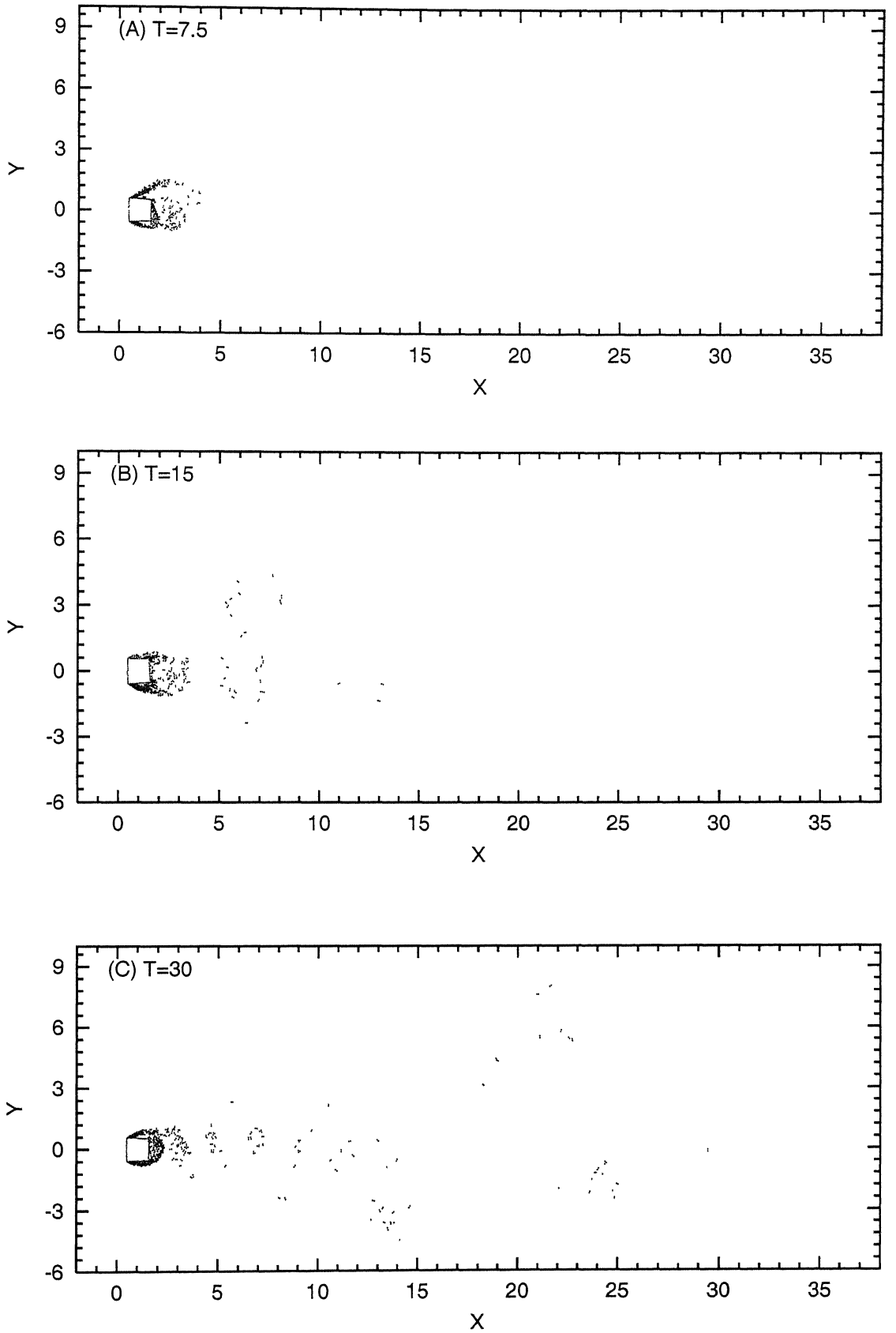

Figure 2.10: Flow diagram for square cylinder at $Re = 60000$

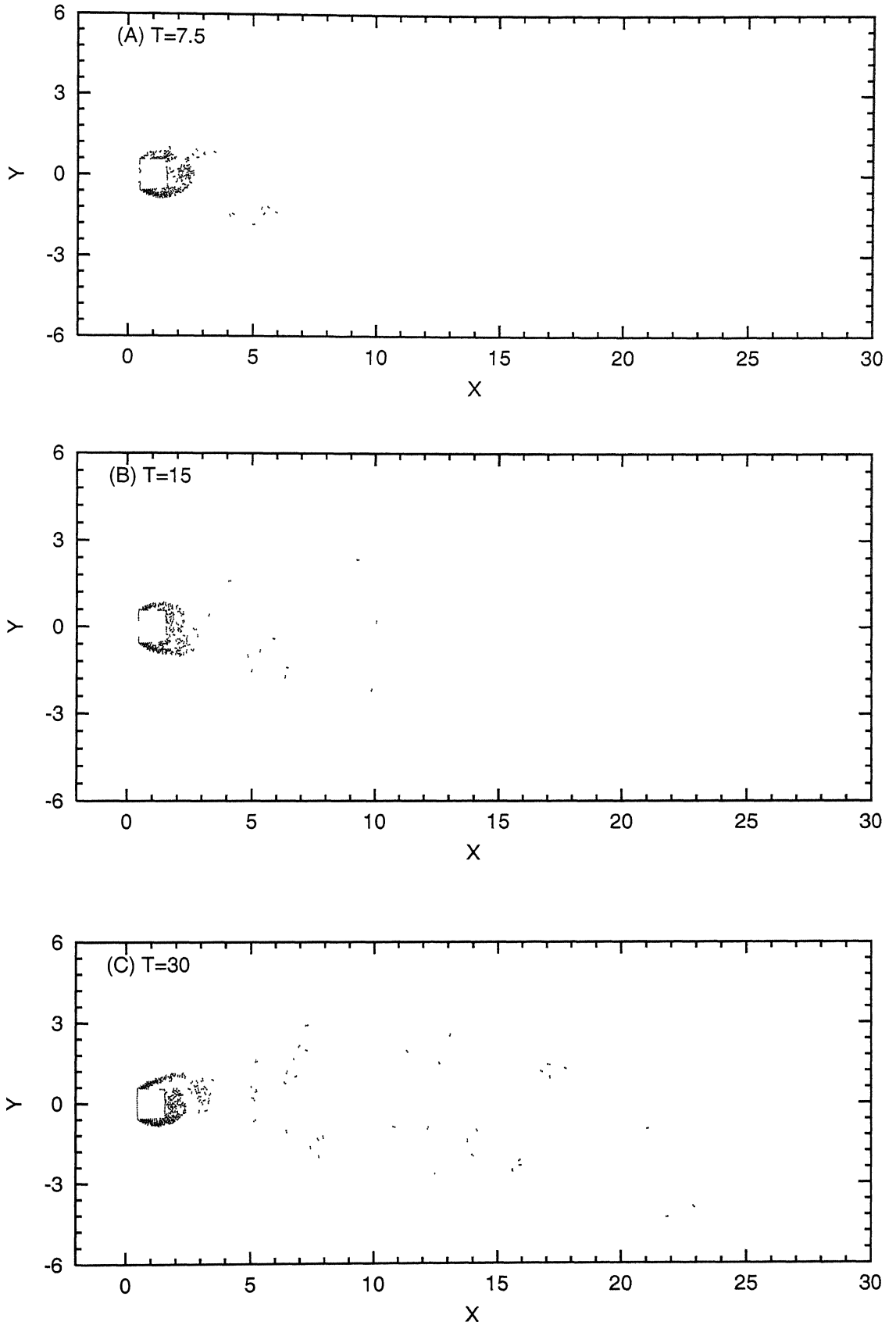

Figure 2.11: Flow diagram for square cylinder at $Re = 1 \times 10^5$

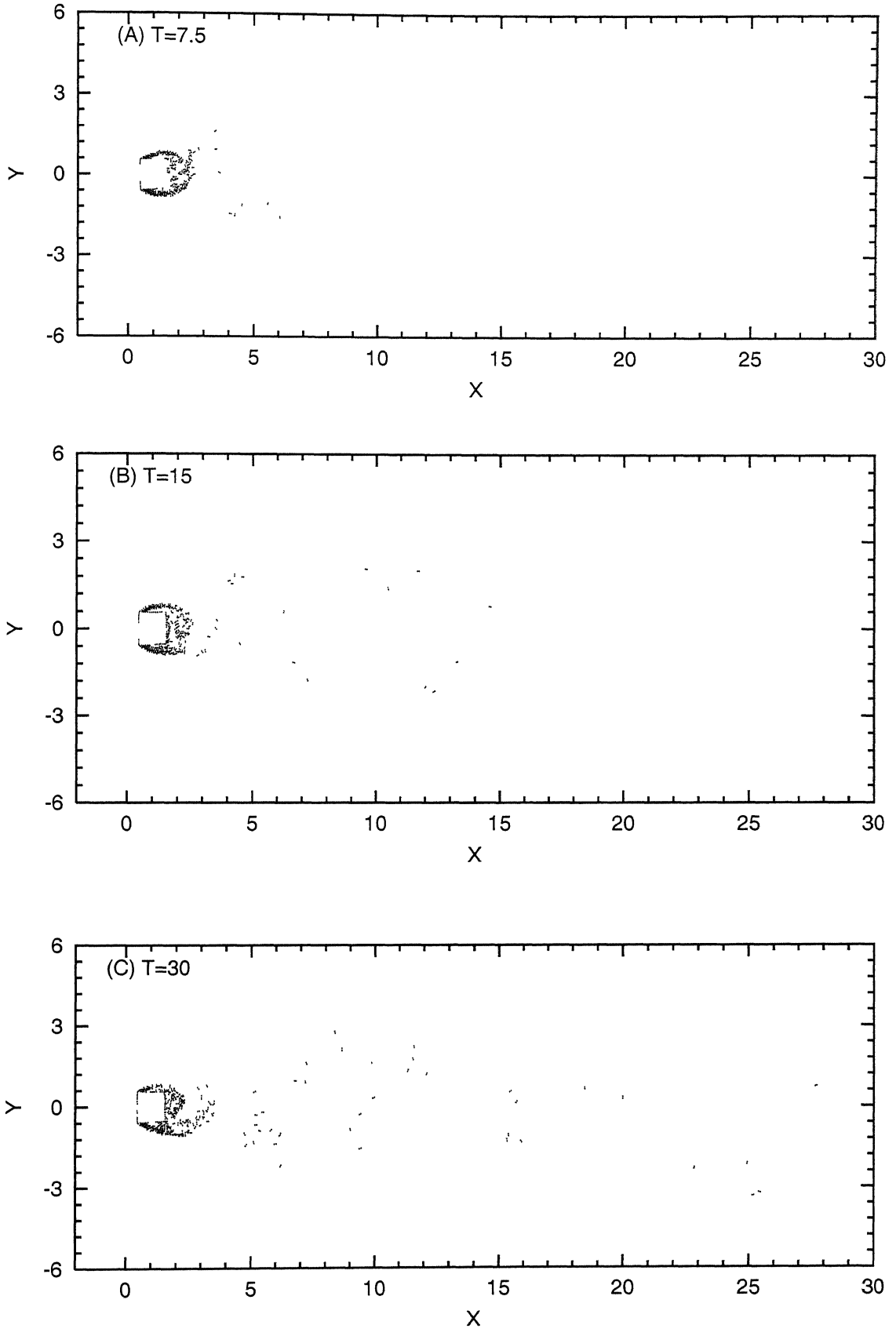

Figure 2.12: Flow diagram for square cylinder at $Re = 1.2 \times 10^6$

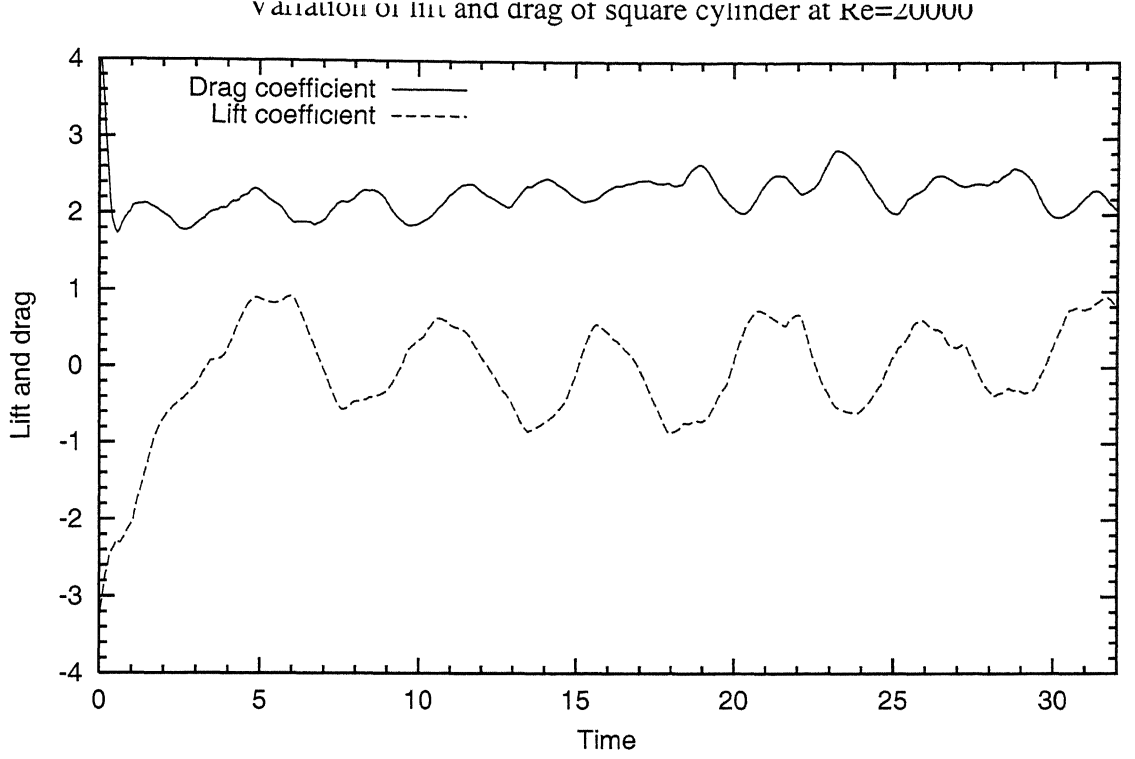

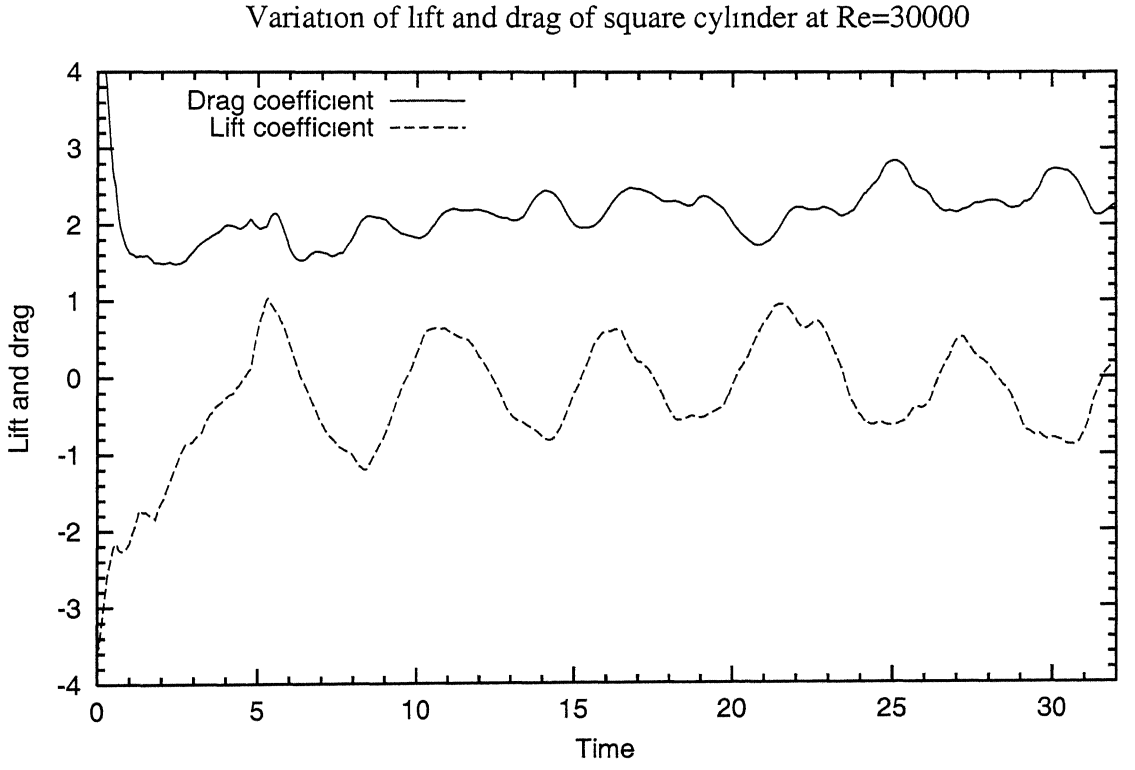

Figure 2.13: Lift and drag variation at $Re = 20000$ & 30000 for square cylinder

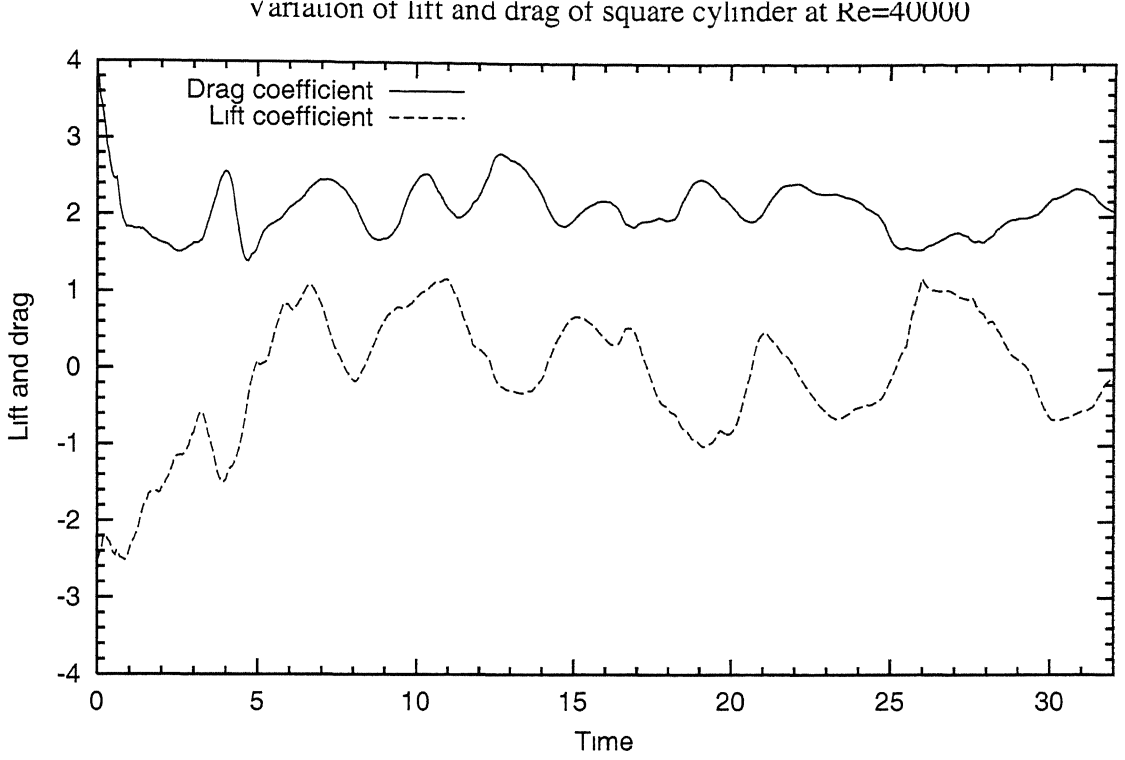

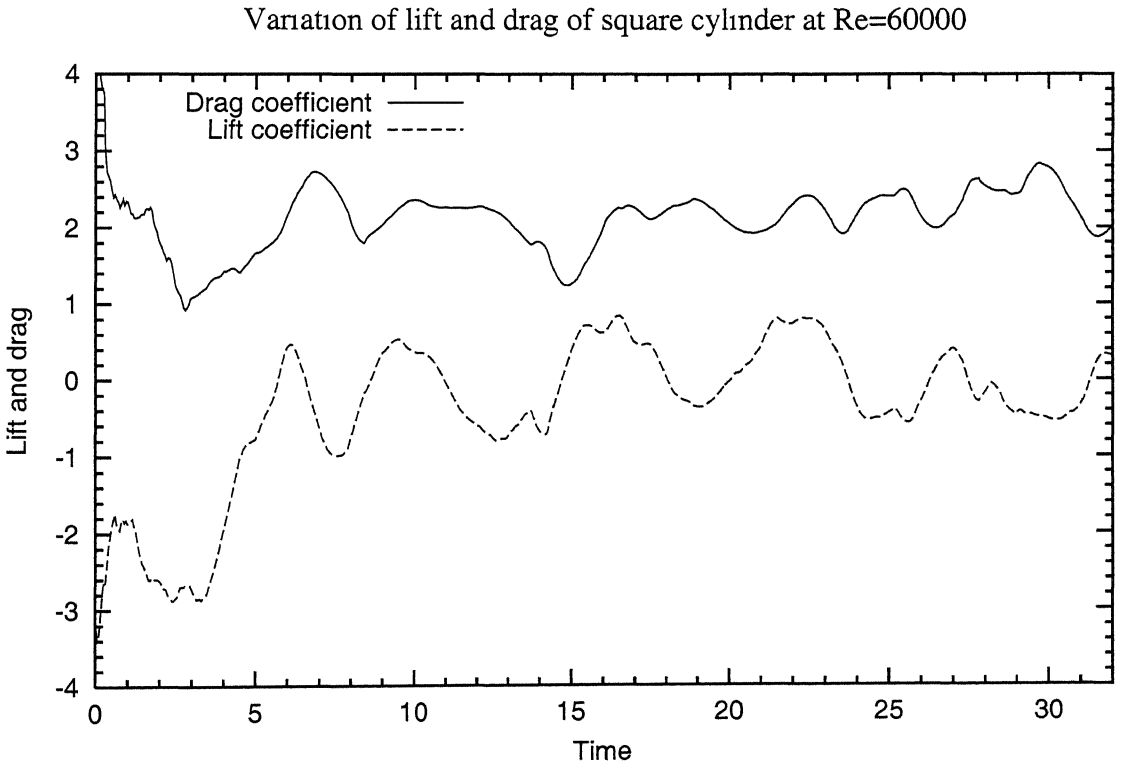

Figure 2.14: Lift and drag variation at $Re = 40000$ & 60000 for square cylinder

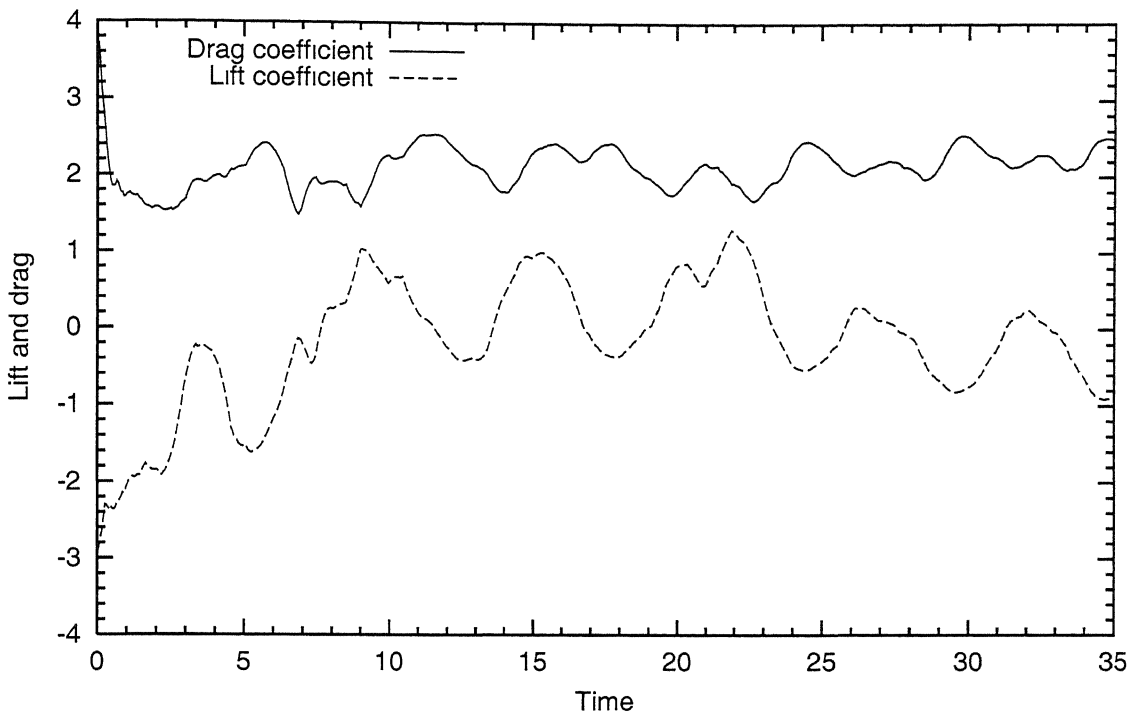

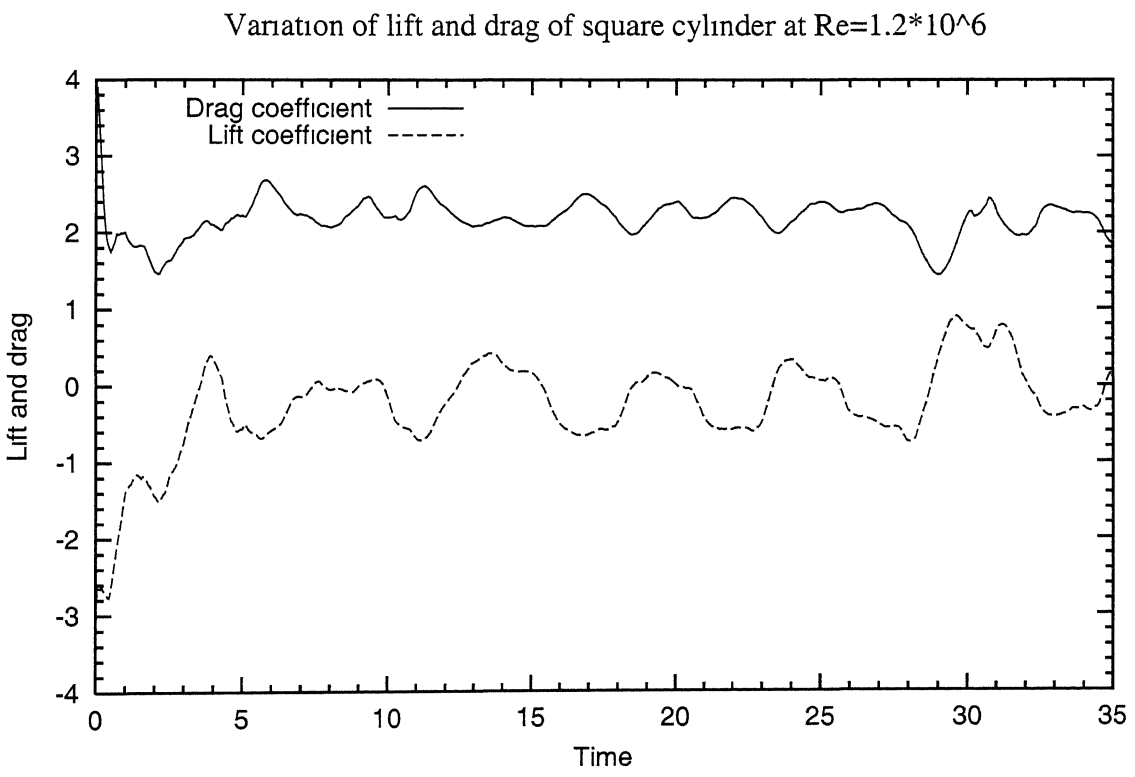

Figure 2.15: Lift and drag variation at $Re = 1\times10^5$ & 1.2×10^6 for square cylinder

Chapter 3

THE FLOW PAST SQUARE CYLINDER WITH ATTACHMENTS

3.1 Introduction

Flow separation on a body prevents complete recovery of pressure and hence responsible for drag. Drag forces are large in case of bodies having sharp edges. So the idea here is to delay the onset of separation by using attachments with the square cylinder. Ritter[16] and Som[21] have proposed techniques, using simple attachments to reduce drag on open railway wagons and on truck bodies. Experimental investigations have shown significant reduction in drag.

We propose here to study some geometries to see if the full-vortex cloud method can predict reduction in drag.

3.2 Mathematical Formulation

To solve the flow past this type of arrangements, we develop the flow past multiple bodies first. The difference in the flow past single bodies and the multiple bodies lies in the determination of coupling coefficient matrix. In latter case, the effect of a body over the other is also taken into account while calculating the coupling coefficient matrix. Rest of the treatment remains the same. Suppose there are P

bodies in $x-y$ plane immersed in uniform flow V_∞ at an angle of attack α_∞ with respect to $x-$ axis. The body q is discretized into M_q number of elements with number of bodies from 1 to P.

Thus the Boundary-Integral equation taking into account the effects of one body over the other can be written as,

$$\sum_{q=1}^{P}\sum_{n=1}^{M_q} K_{mn}^{pq}\gamma(s_{qn}) = -U_\infty cos\beta_{pm} - V_\infty sin\beta_{pm} \qquad (3\,1)$$

where also also $p = 1, 2, \ldots, P$ and $m = 1, 2, ..., M_p$

The above equation 3 1 is the statement of the Dirichlet boundary condition at the element m of body p. The coupling coefficient *i.e.* the velocity induced on one body element due to the element of the other body is given by,

$$K_{mn}^{pq} = \frac{\Delta s_{qn}}{2\pi}\left\{\frac{(y_{pm}-y_{qn})cos\beta_{pm} - (x_{pm}-x_{qn})sin\beta_{pm}}{(x_{pm}-x_{qn})^2 + (y_{pm}-y_{qn})^2}\right\} \qquad (3.2)$$

For special cases when ($p = q$ *and* $m = n$) is the self induced coupling coefficient as given earlier for single body.

The equation 3.1 can be written in the following matrix form,

$$\begin{bmatrix} A_{11} & A_{12} \\ A_{21} & A_{22} \end{bmatrix} [\,\gamma(s)\,] = [\,rhs\,] \qquad (3\,3)$$

Here sub-matrices A_{11} and A_{22} are the coupling coefficient matrices as calculated earlier for single body. And sub-matrices A_{12} and A_{21} contain the effect of one body over the another. Typically, sub-matrix A_{12} contains all of the coefficient accounting for interference experienced by the first body due to the second body.

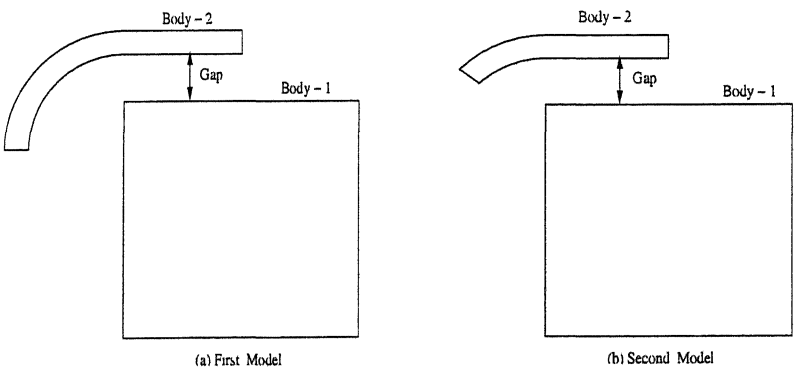

Figure 3.1: Two models used in present investigation

3.3 Results and discussions

We have considered two geometries. In both of the geometries, the side of square cylinder is taken as 1 0, free stream velocity W_∞ is 1.0, angle of attack, $\alpha_\infty = 0$, length of the flat portion of the attachment is 0.5, thickness and inner radius of the curved part of the attachment is 0.1 and 0.4 respectively. Both of the geometries are studied at different positions of attachment and for various Reynolds number.

For first geometry

The geometry is shown in Fig. 3.2. The body of square cylinder and the attachment are discretized into 56 surface elements and 52 surface elements respectively. The Table 3.1 shows the average values of lift and drag coefficients of the main body(square cylinder) and the attachment for various gaps between the square and the attachment at Reynolds number of 20000. Total lift and drag acting on the geometry is also shown in the Table 3.1. It is evident from the Table 3.1 as the gap is reduced the total drag acting on the geometry reduces and reaches to a minimum, and on further reduction of the gap, drag increases. Maximum reduction in drag is around 38% at Reynolds number of 20,000.

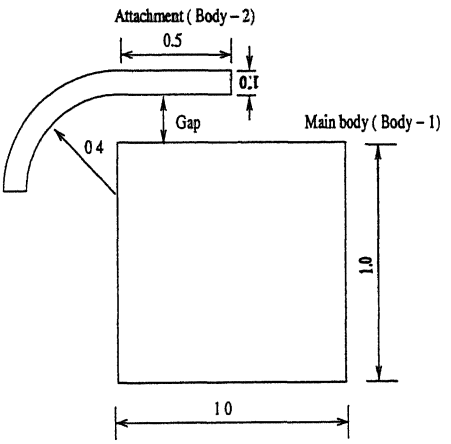

Figure 3.2: First geometry

The case is again run for various Reynolds numbers(at $50,000, 1\times10^5$ *and* 1.2×10^6) when the gap between the two bodies is optimum(*i.e.* when the drag is minimum). The results are shown in the Table 3.2. The flow diagram for various

Gap	*Average lift coefficients*, C_l			*Average drag coefficients*, C_d			*Reduction*
	Body − 1	*Body* − 2	*Total*	*Body* − 1	*Body* − 2	*Total*	*in* C_d(%)
0.20	-1.078648	0.135818	-0.942830	1.548154	0.111806	1.659960	27.80
0.17	-1.194436	0.173199	-1.021237	1.494855	0.117757	1.612612	29.86
0.16	-0.644665	0.192763	**-0.451902**	1.239422	0.186909	**1.426331**	**37.96**
0.15	-1.427683	0.186493	-1 241190	1.732633	0.047211	1.779844	22.58
0.14	-1.116135	0.160531	-0.955604	1.671501	0.134620	1.806121	21.44

Table 3.1: Lift and drag of geometry-1 at various positions of the attachment

gaps are shown in Fig. 3.6 to Fig. 3.9. Fig. 3.10 shows the flow diagram for $Re = 1.2 \times 10^6$ at optimum gap. The variation in lift and drag coefficient with time is shown Fig. 3.11 to Fig. 3.12. The Fig. 3.13 to 3.14 shows the variation in lift and drag at optimum gap and Re=1×10^5 *and* 1.2×10^6 respectively. The present study shows a reduction in drag using drag suppressor from 2.18 to 1.426(*reduction of* 38%) at Reynolds number of 20000.

Re	*Average lift coefficients*, C_l			*Average drag coefficients*, C_d			*Reduction*
	Body − 1	*Body* − 2	*Total*	*Body* − 1	*Body* − 2	*Total*	*in* C_d(%)
20000	-0.644665	0.192763	-0.451902	1.239422	0.186909	1.426331	37.96
50000	-1.716633	0.197500	-1.519133	1.471544	0.070148	1.541693	33.79
1×10^5	-1.072953	0.159764	-0.913189	1.435434	0.140764	1.576198	27.62
1.2×10^6	-1.103621	0.207633	-0.895989	1.376179	0.142850	1.519029	30.65

Table 3.2: Lift and drag of geometry-1 at optimum gap

For second geometry

The geometry under consideration is shown in Fig. 3.3. The body of square cylinder and attachment are discretized into 56 and 38 surface elements respectively. The Table 3.3 shows the lift and drag coefficients of individual bodies and the total lift and drag on the geometry at Reynolds number of 20,000 when the gap between the bodies vary from 0.14 to 0.20. It can also be seen from the Table 3.3 that the drag acting on the geometry is minimum when the gap is 0.16 and

increases when the gap is either reduced or increased.

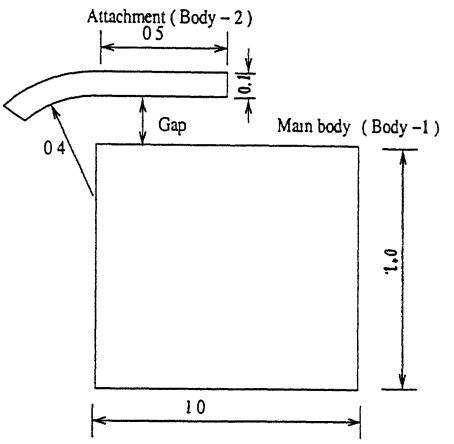

Figure 3.3: Second geometry

The case is again run for the configuration of minimum drag for various Reynolds numbers(at $50,000, 1 \times 10^5$ *and* 1.2×10^6). The results are shown in the Table 3.4. Flow diagrams for various gaps are shown in Fig. 3.15 to Fig. 3.18. Fig. 3.19 shows the flow diagram for $Re = 1.2 \times 10^6$ and optimum gap. The variation in lift and drag with time is shown in Fig. 3.20 to Fi.g 3.23. Fig. 3.24 to Fig. 3.25 shows the variation in lift and drag of the geometry with time when the gap is kept at optimum and $Re = 1 \times 10^5$ and $Re = 1.2 \times 10^6$ respectively.

Gap	*Average lift coefficients,* C_l			*Average drag coefficients,* C_d			*Reduction*
	$Body-1$	$Body-2$	*Total*	$Body-1$	$Body-2$	*Total*	*in* $C_d(\%)$
0.20	-0.966711	0.187977	-0.778734	1.723650	0.071530	1.795180	21.90
0.17	-1.272374	0.263100	-1.009274	1.490483	0.024947	1.515430	34.08
0.16	1.610553	0.268493	**-1.342060**	1.344694	0.014013	**1.358707**	**40.90**
0.15	-1.949026	0.324388	-1.624638	1.432042	0.016343	1.448385	37.00
0.14	-1.660850	0.257079	-1.403771	1.582787	0.038369	1.621156	29.48

Table 3.3: Lift and drag of geometry-2 at various positions of the attachment

Fig. 3.4 shows the variation in drag of geometries when gap between the bodies is varied and average drag of square cylinder is also plotted. The plot shows that

Re	*Average lift coefficients, C_l*			*Average drag coefficients, C_d*			*Reduction in C_d(%)*
	Body − 1	*Body − 2*	*Total*	*Body − 1*	*Body − 2*	*Total*	
20000	-1.610553	0 268493	-1.342060	1.344694	0.014013	1.358707	40.90
50000	-1 365549	0 239934	-1.125615	1.421387	0.016249	1.437636	38.26
1×10^5	-1 383413	0.230505	-1 152908	1.441183	0.046595	1.487778	31.68
1.2×10^6	-1.565719	0.276271	-1.289448	1.498898	0.004638	1.503535	31.36

Table 3.4: Lift and drag of geometry-2 at optimum gap

the drag of cylinder with attachments is less than that of square cylinder alone The drag of both the geometries is minimum when the gap is 0.16.

In Fig. 3 5A drag for square cylinder and attachments for both of the geometries are plotted for increasing Reynolds number. In the same plot, drag of square cylinder is also plotted. In Fig. 3 5B, total drag acting on the geometries are compared with the drag of square cylinder. It is clear form the plot that drag reduces to a good extent when using drag suppressor.

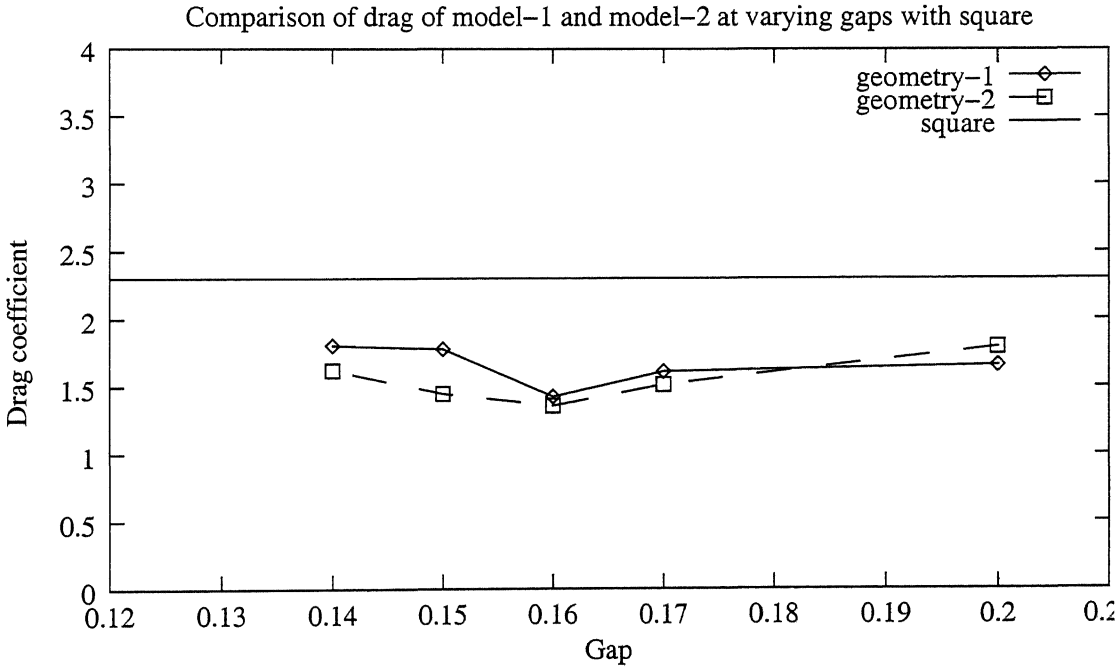

Figure 3.4: Comparison of drag of geometries at various gaps between the two bodies

(A)

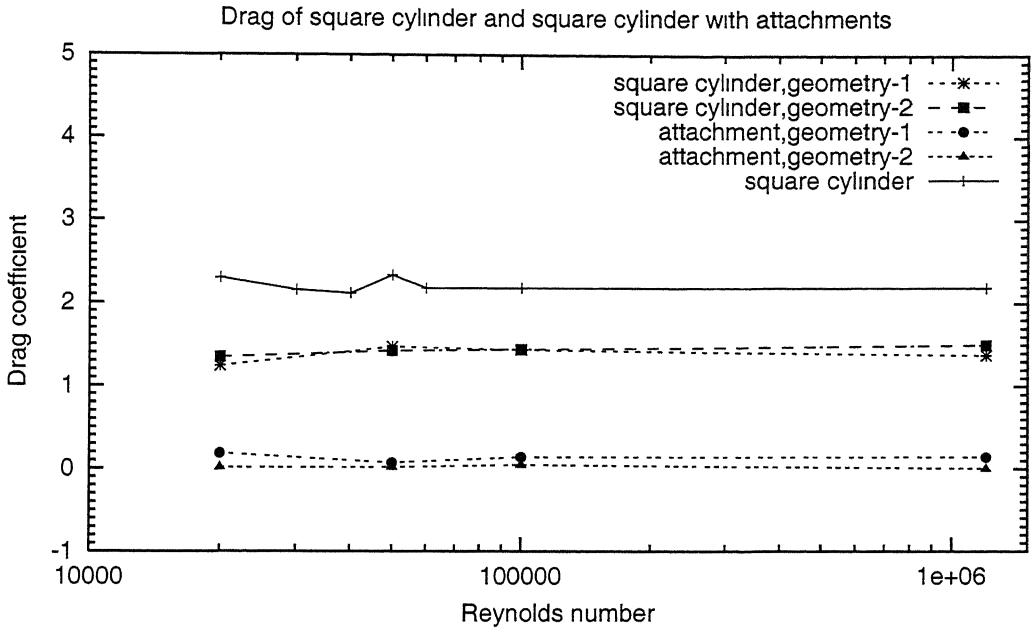

(B)

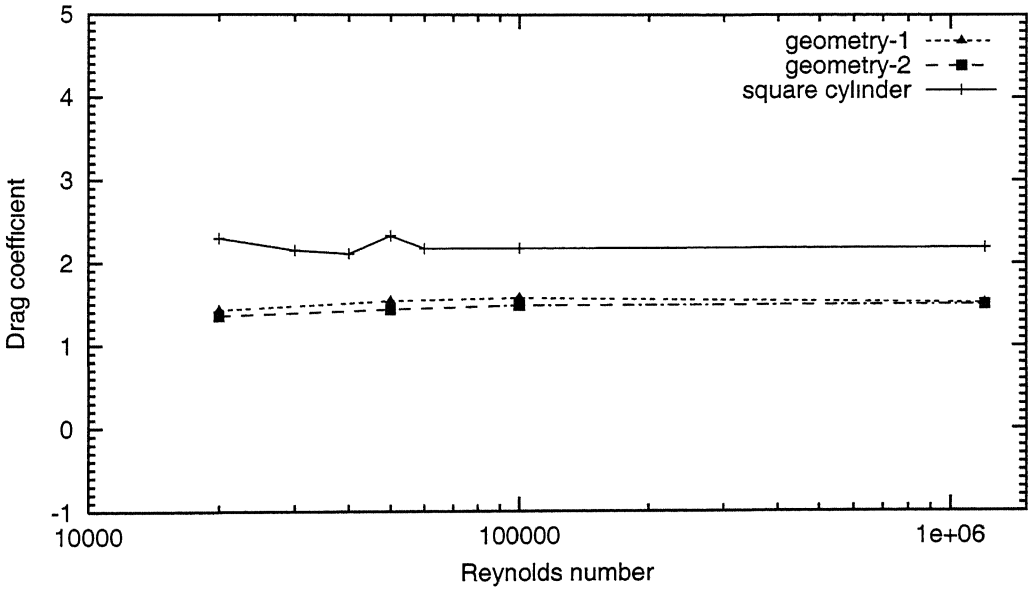

Figure 3.5: Comparison of drag of square cylinder with both of the geometries

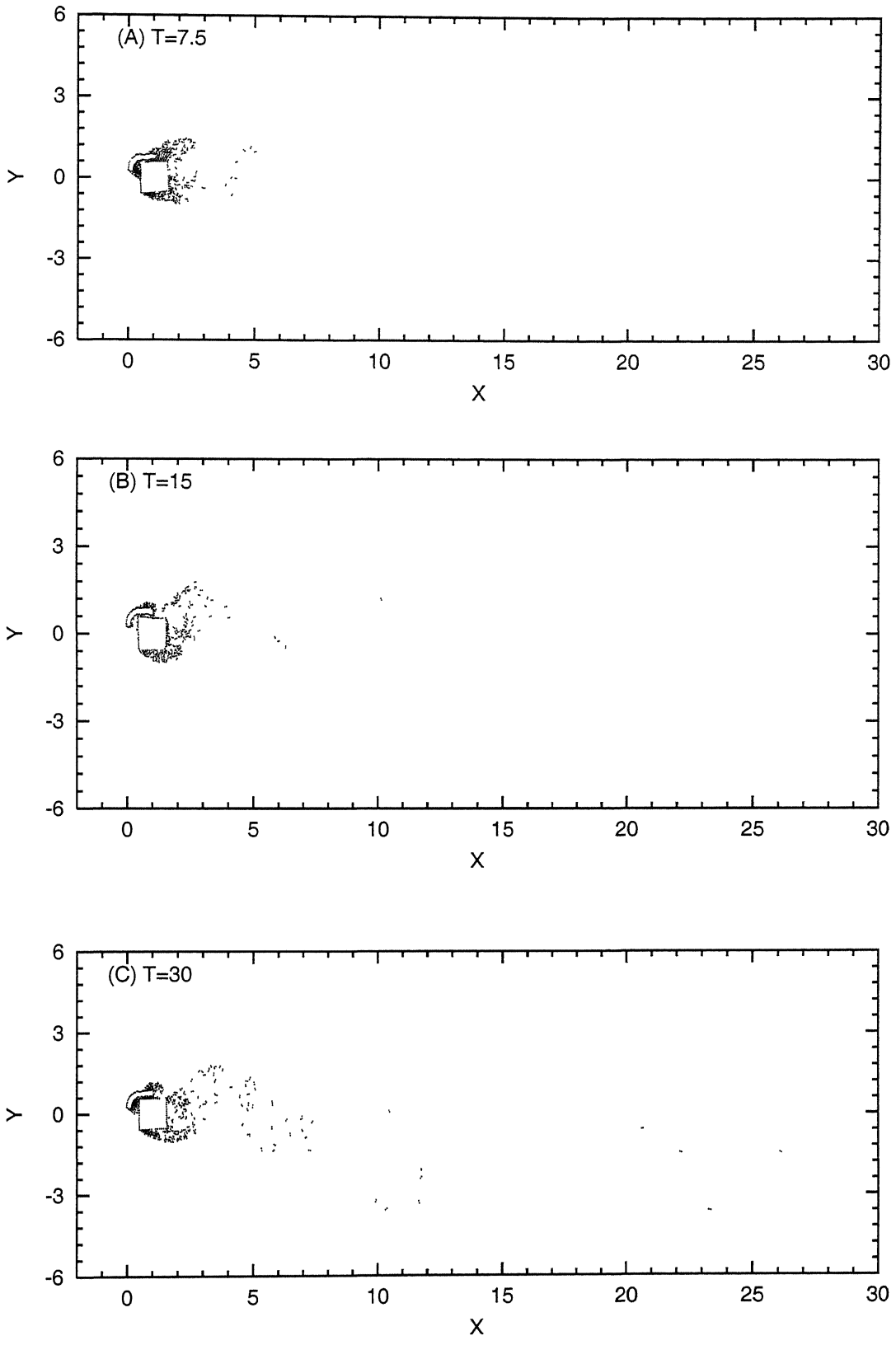

Figure 3.6: Flow diagram for geometry-1 at $\sqrt{Re} = 20000$ and $gap = 0.20$ between the two bodies

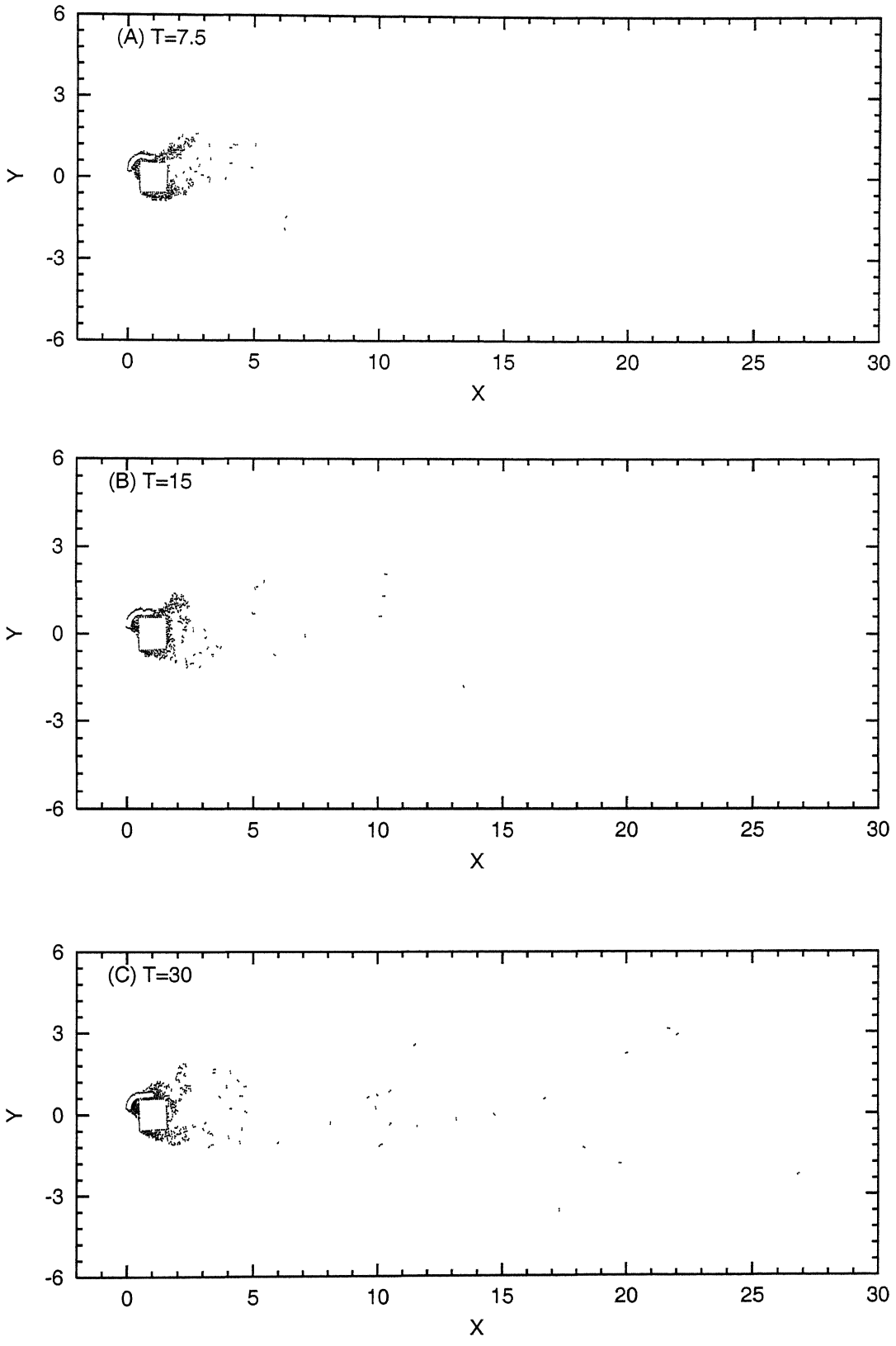

Figure 3.7: Flow diagram for geometry-1 at $Re = 20000$ and $gap = 0.17$ between the two bodies

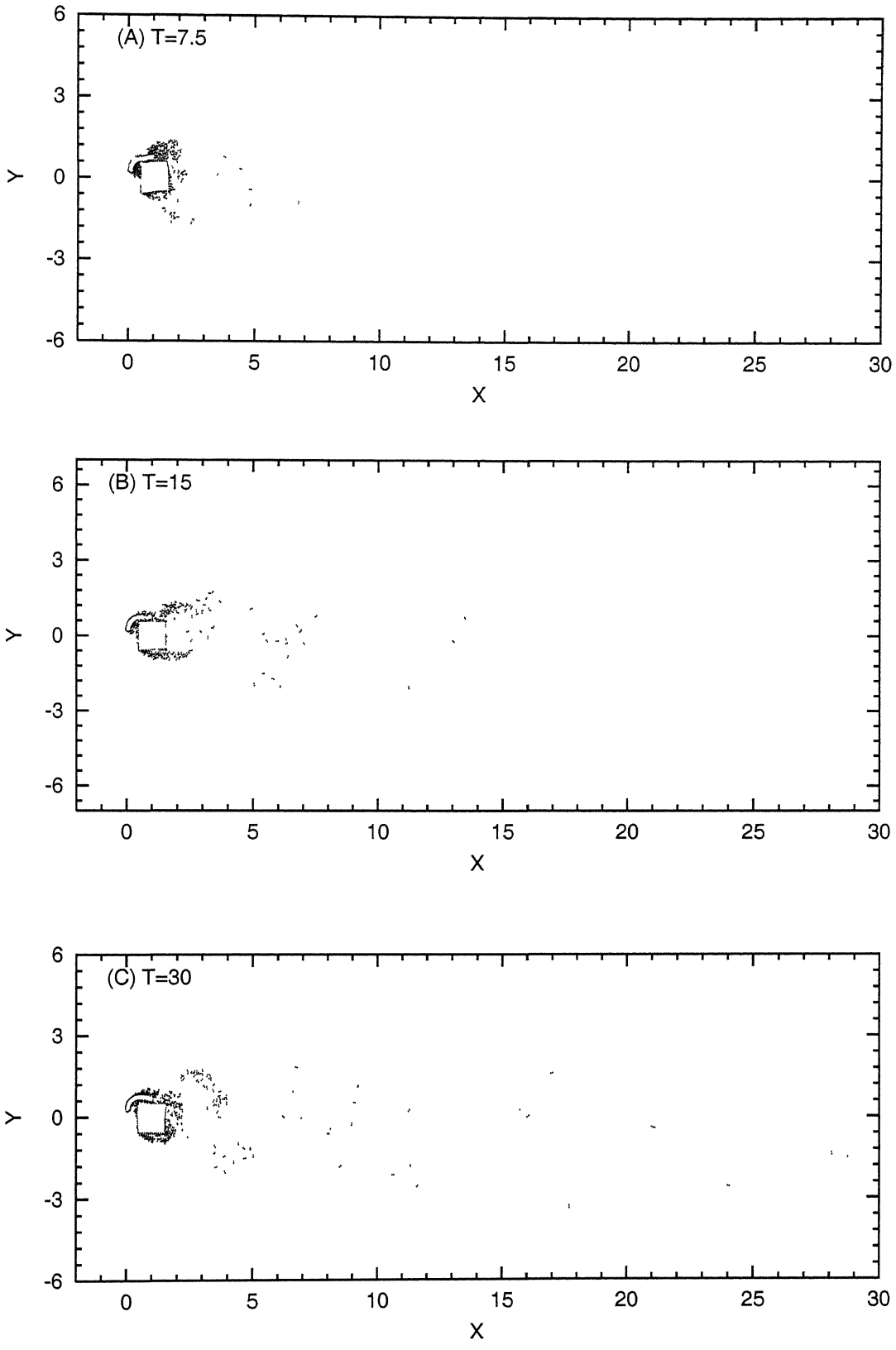

Figure 3.8: Flow diagram for geometry-1 at $Re = 20000$ and $gap = 0.16$ between the two bodies

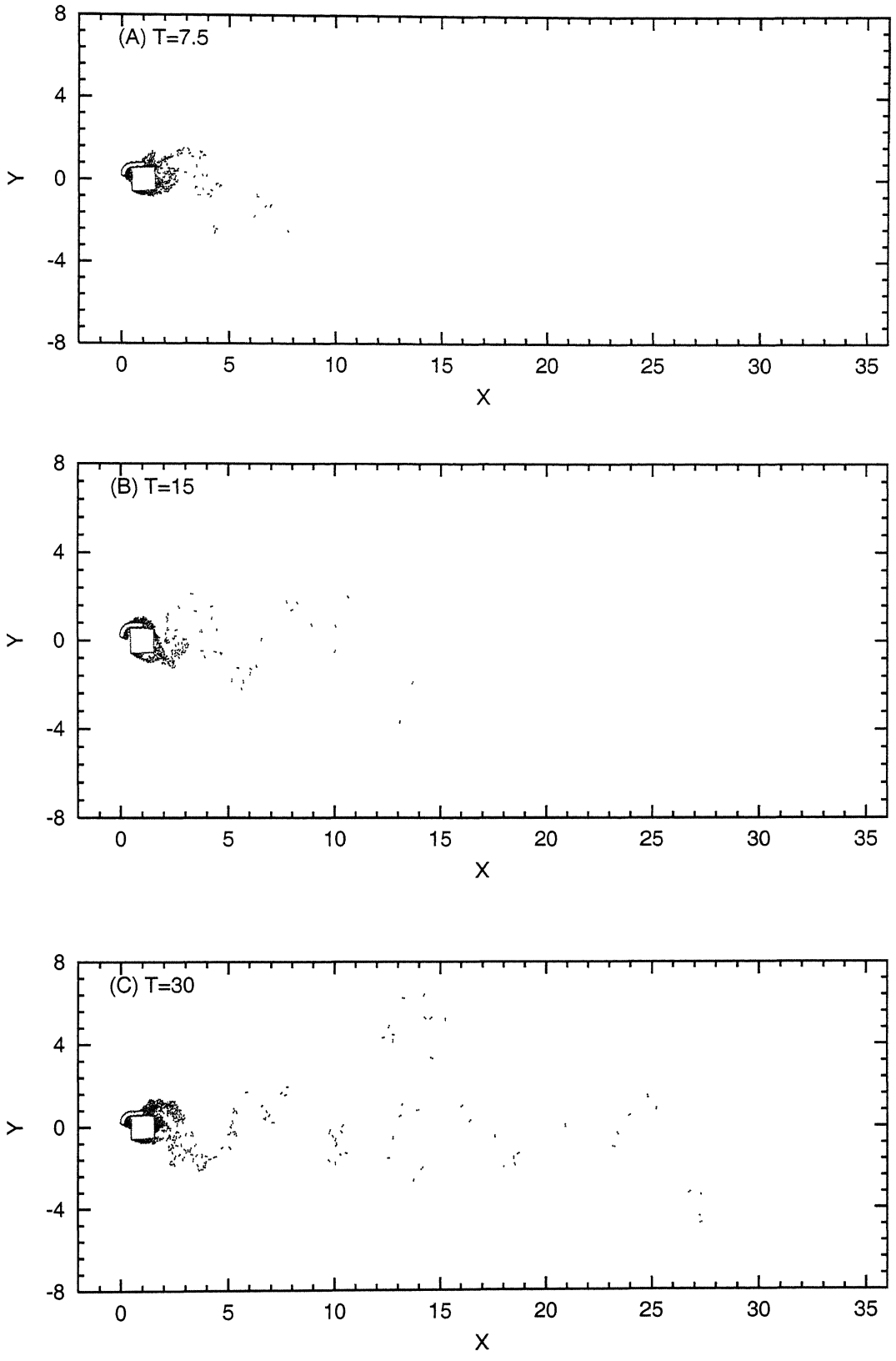

Figure 3.9: Flow diagram for geometry-1 at $Re = 20000$ and $gap = 0.14$ between the two bodies

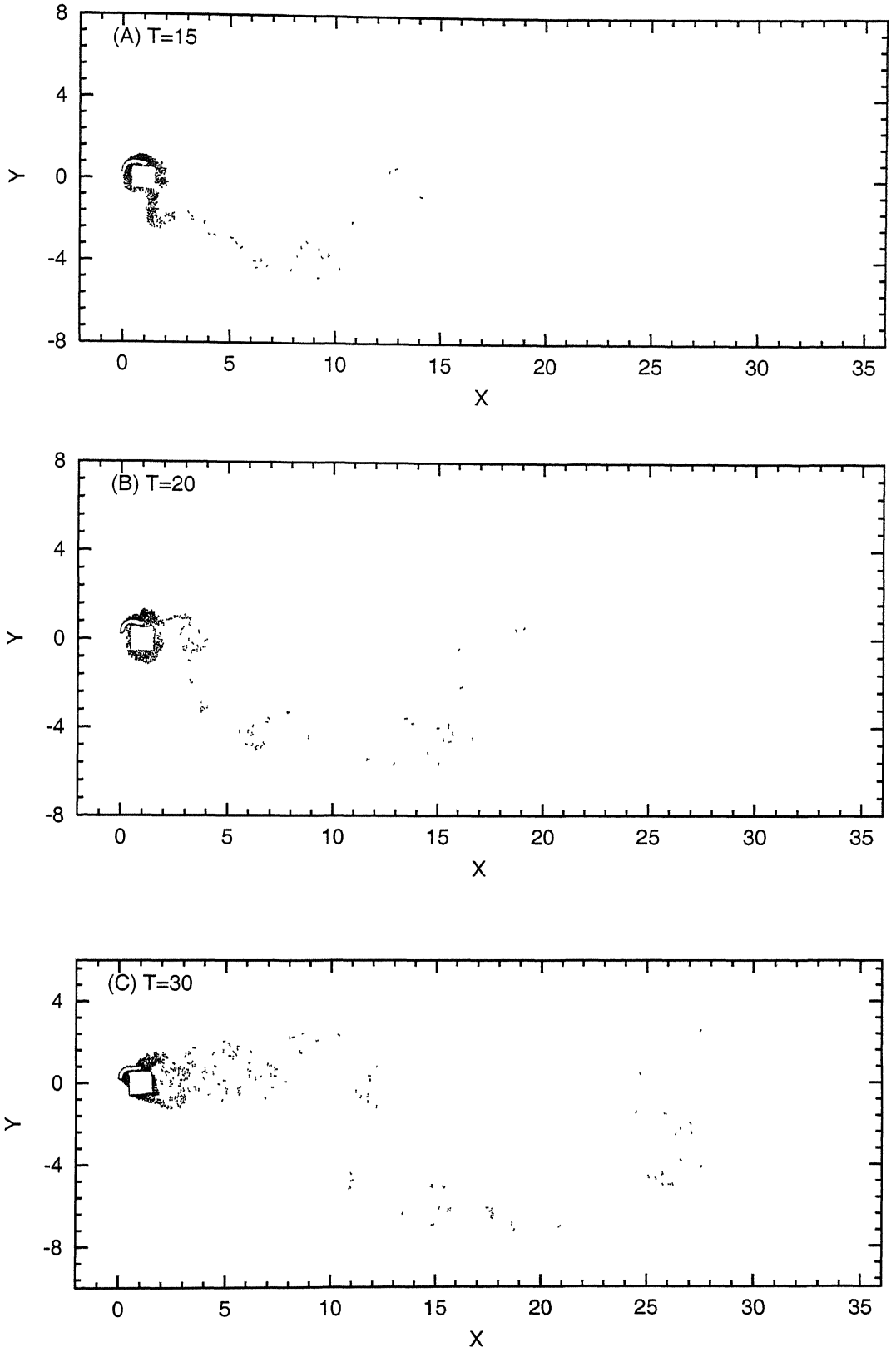

Figure 3.10: Flow diagram for geometry-1 at $Re = 1.2 \times 10^6$ and optimum gap between the two bodies

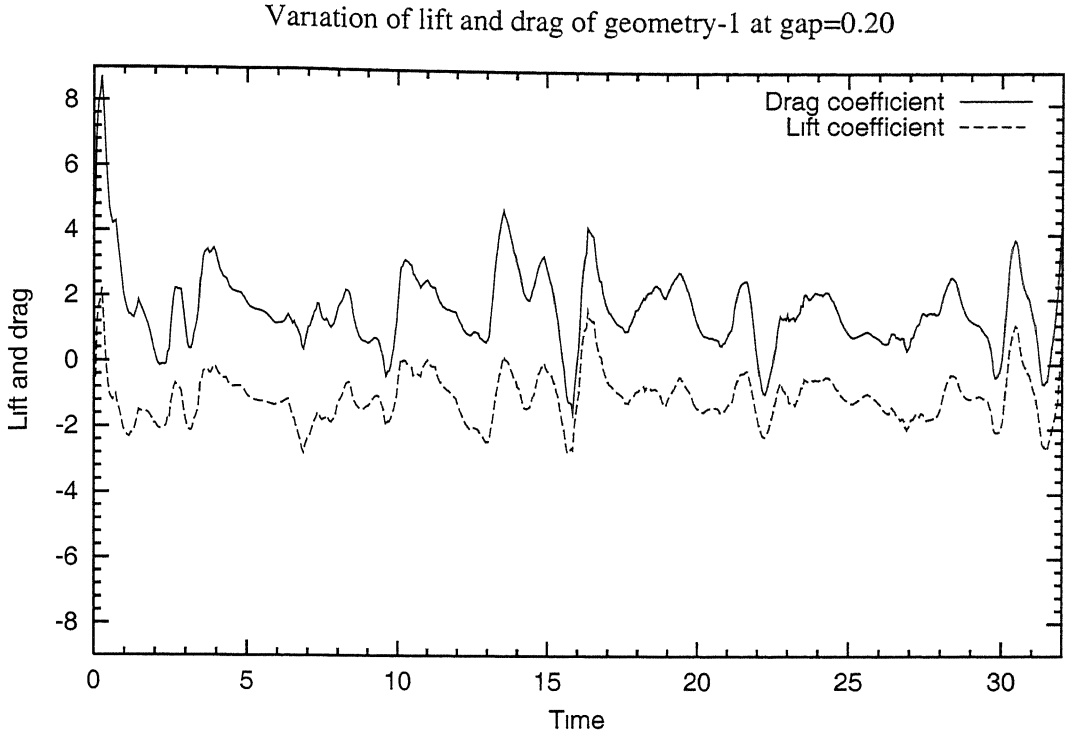

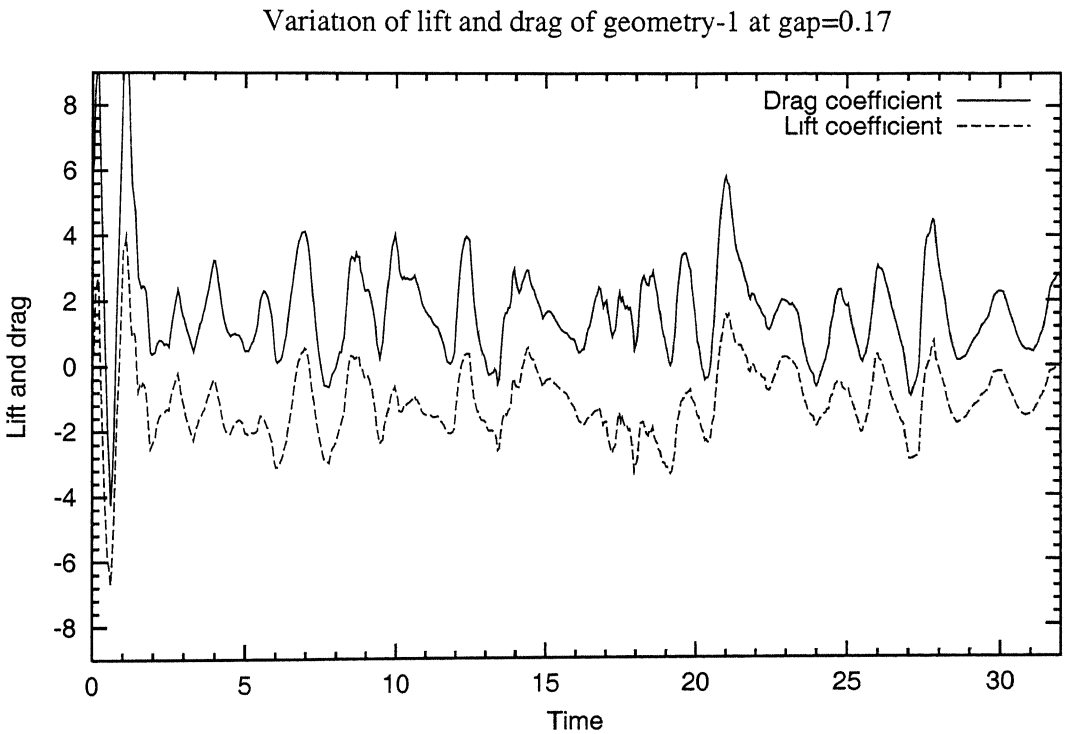

Figure 3.11: Variation of lift and drag of geometry-1 at varying gaps between the bodies at Reynolds number 20000

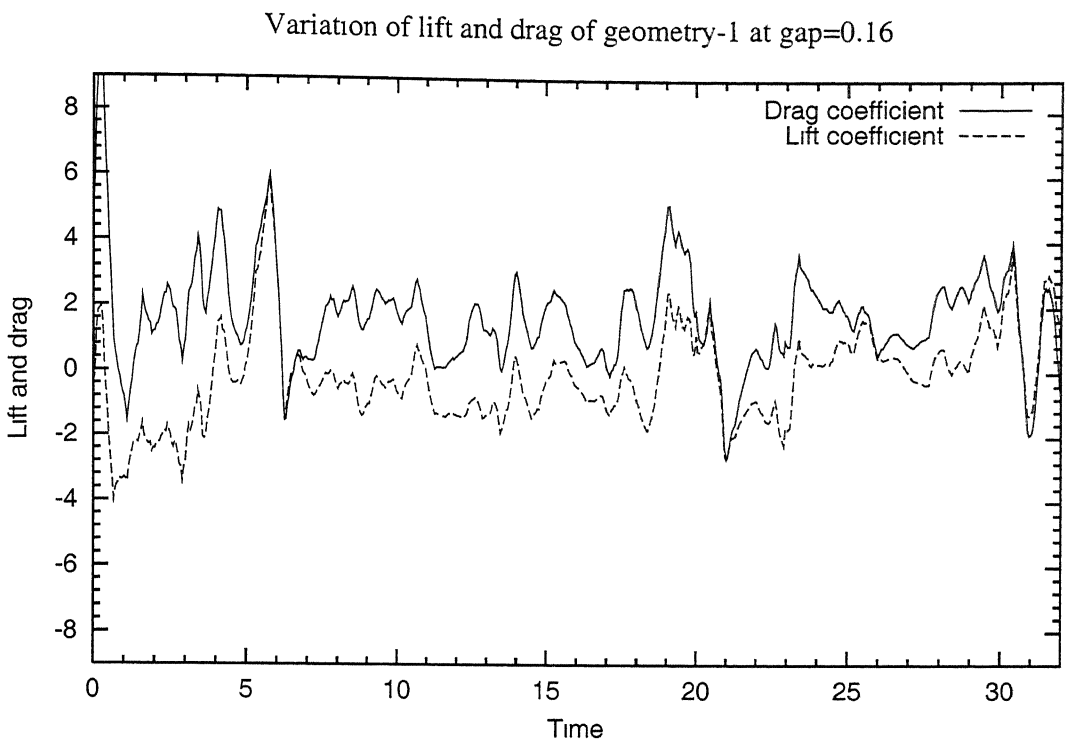

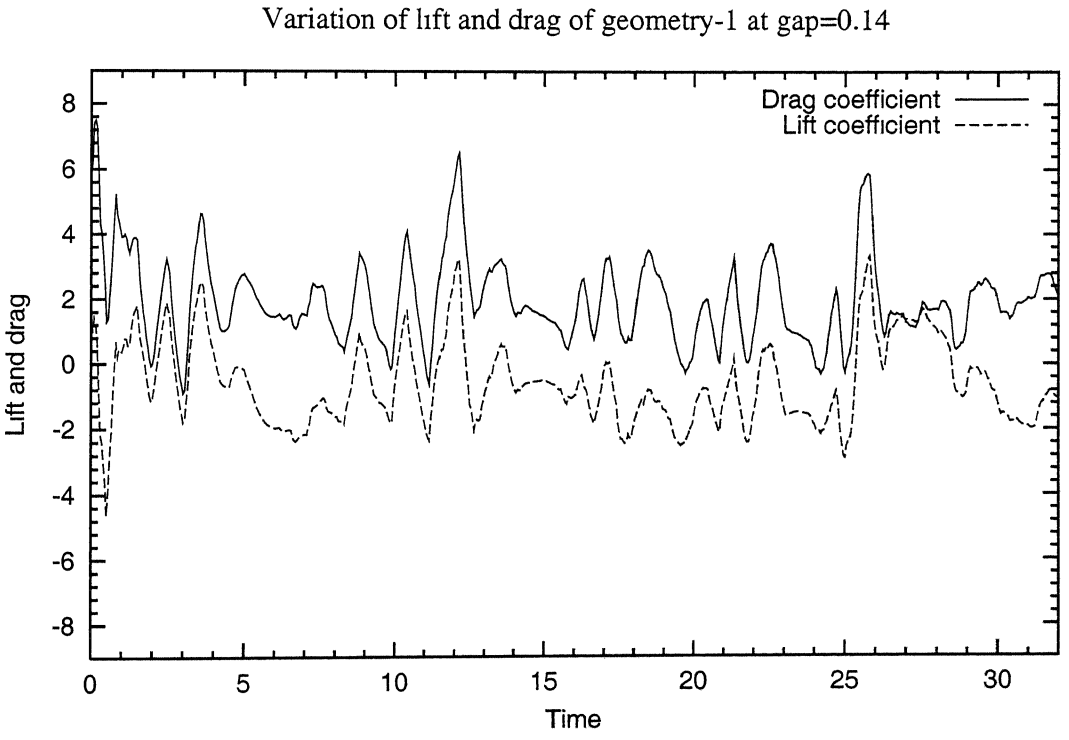

Figure 3.12: Variation of lift and drag of geometry-1 at varying gaps between the two bodies at Reynolds number 20000

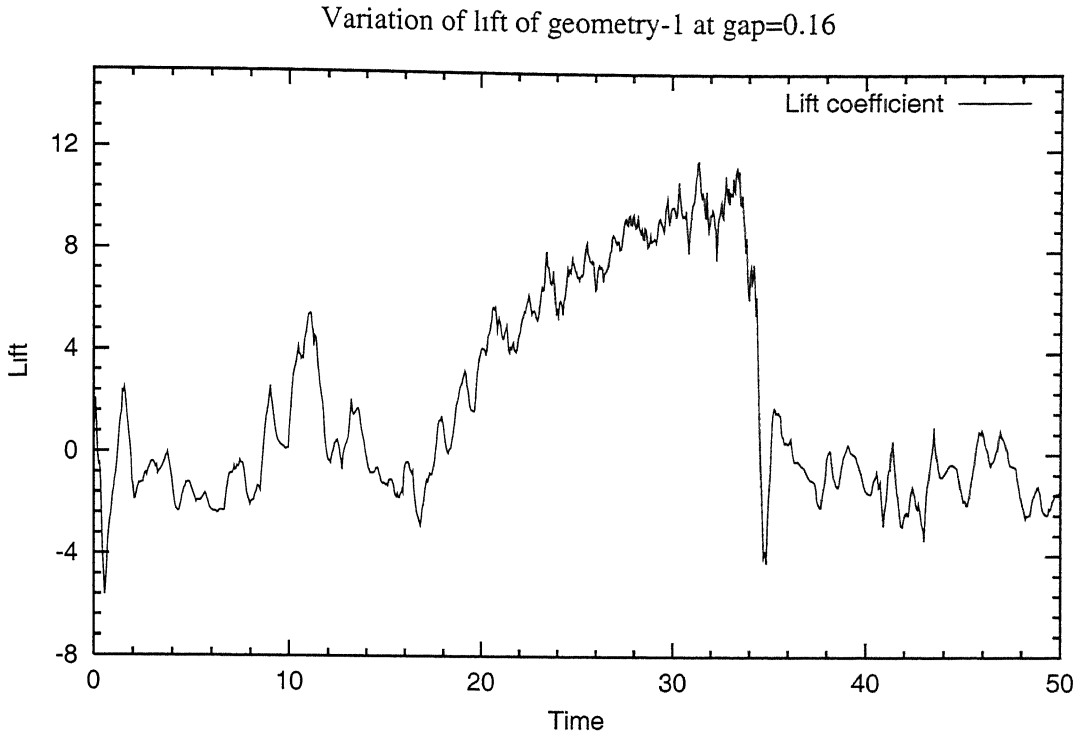

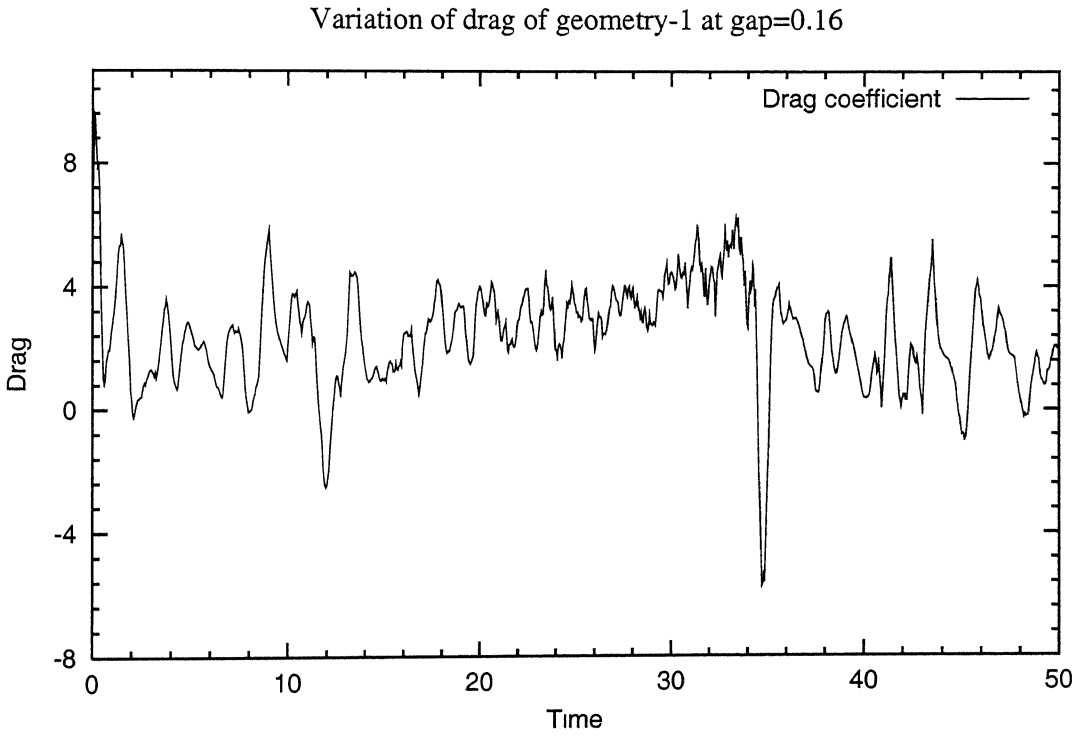

Figure 3.13: Variation of lift and drag of geometry-1 at optimum gap between the two bodies at $Re = 1 \times 10^5$

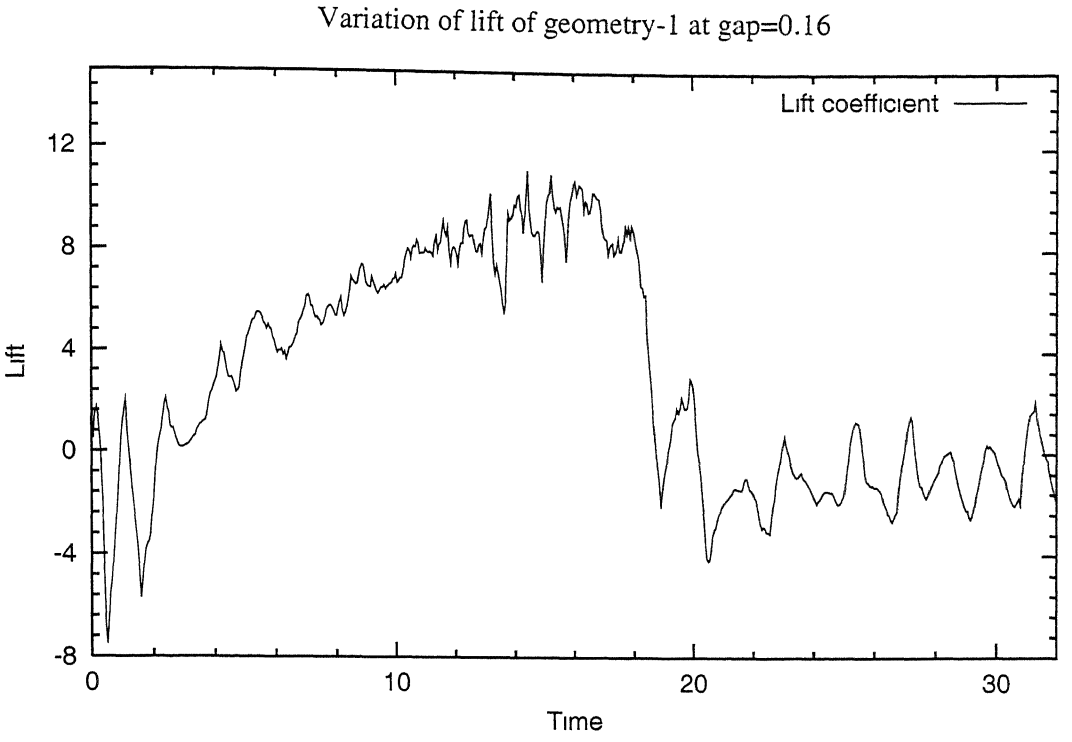

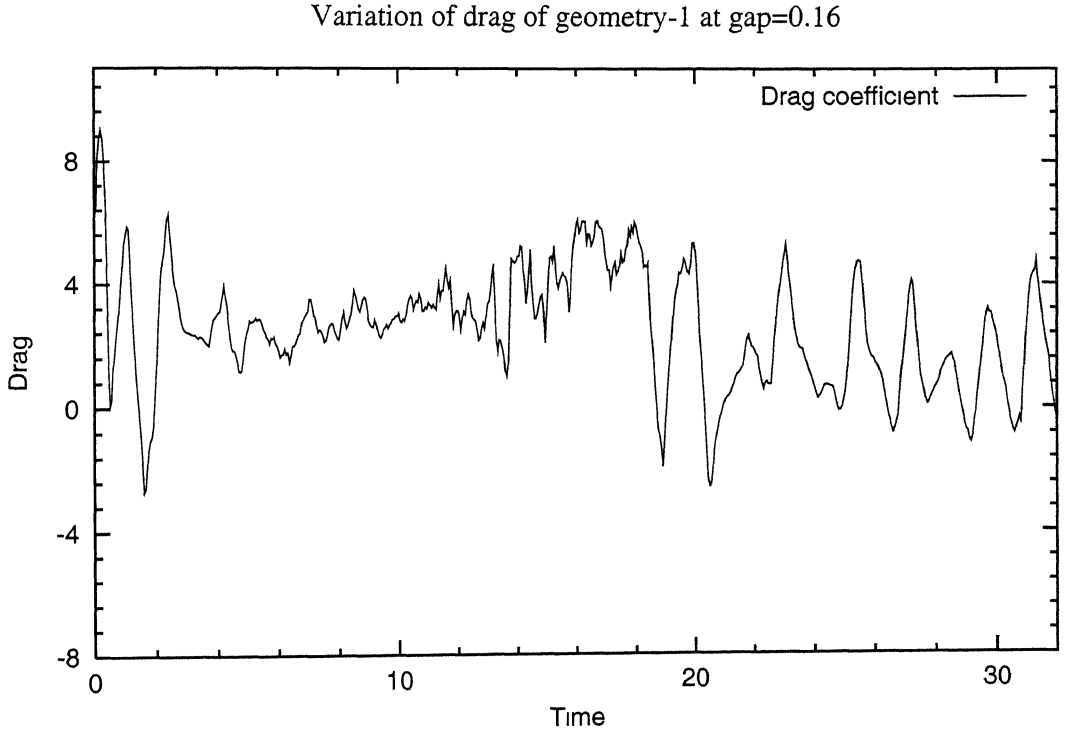

Figure 3.14: Variation of lift and drag of geometry-1 at optimum gap between the two bodies at $Re = 1.2 \times 10^6$

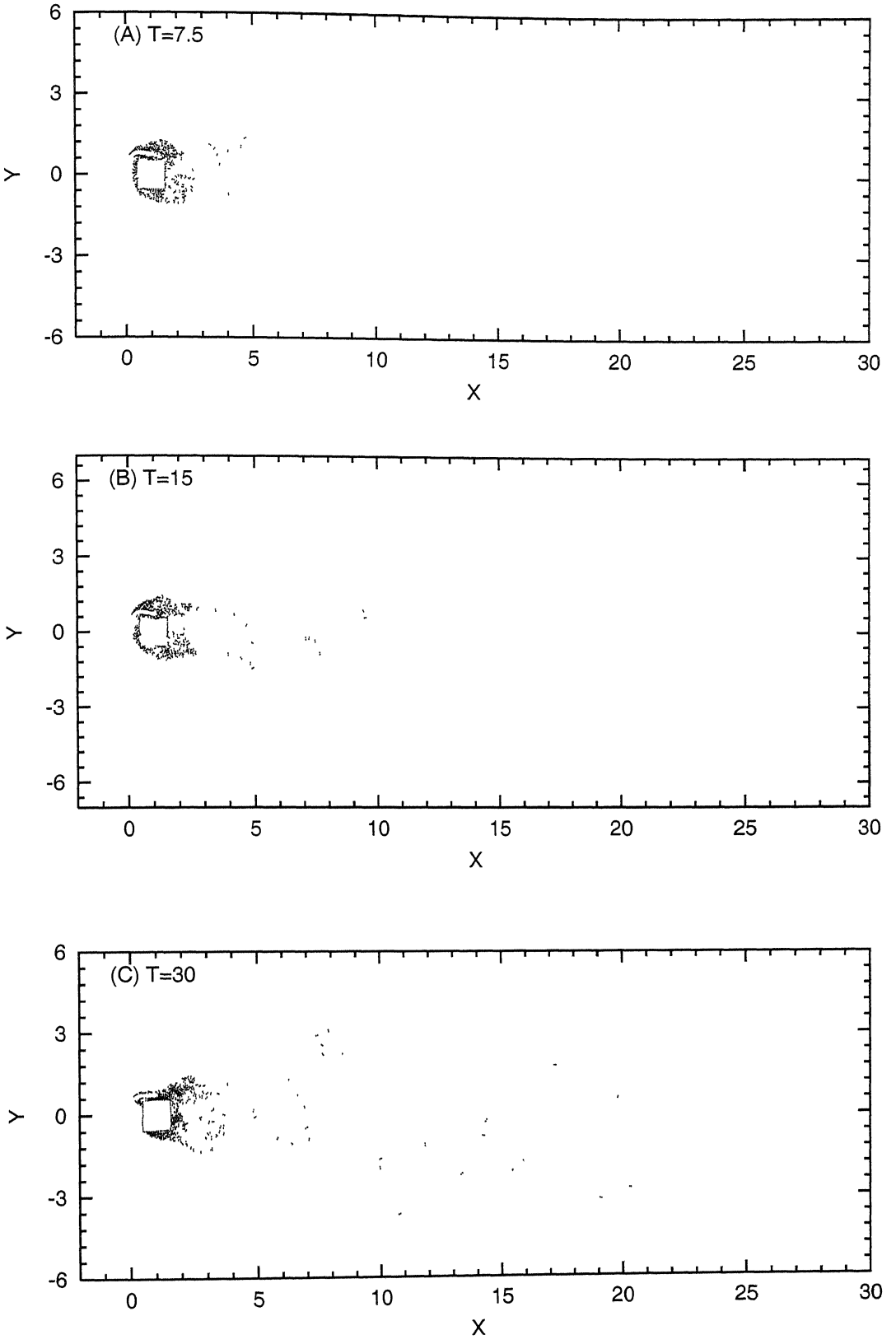

Figure 3.15. Flow diagram for geometry-2 at $Re = 20000$ and $gap = 0.20$ between the two bodies

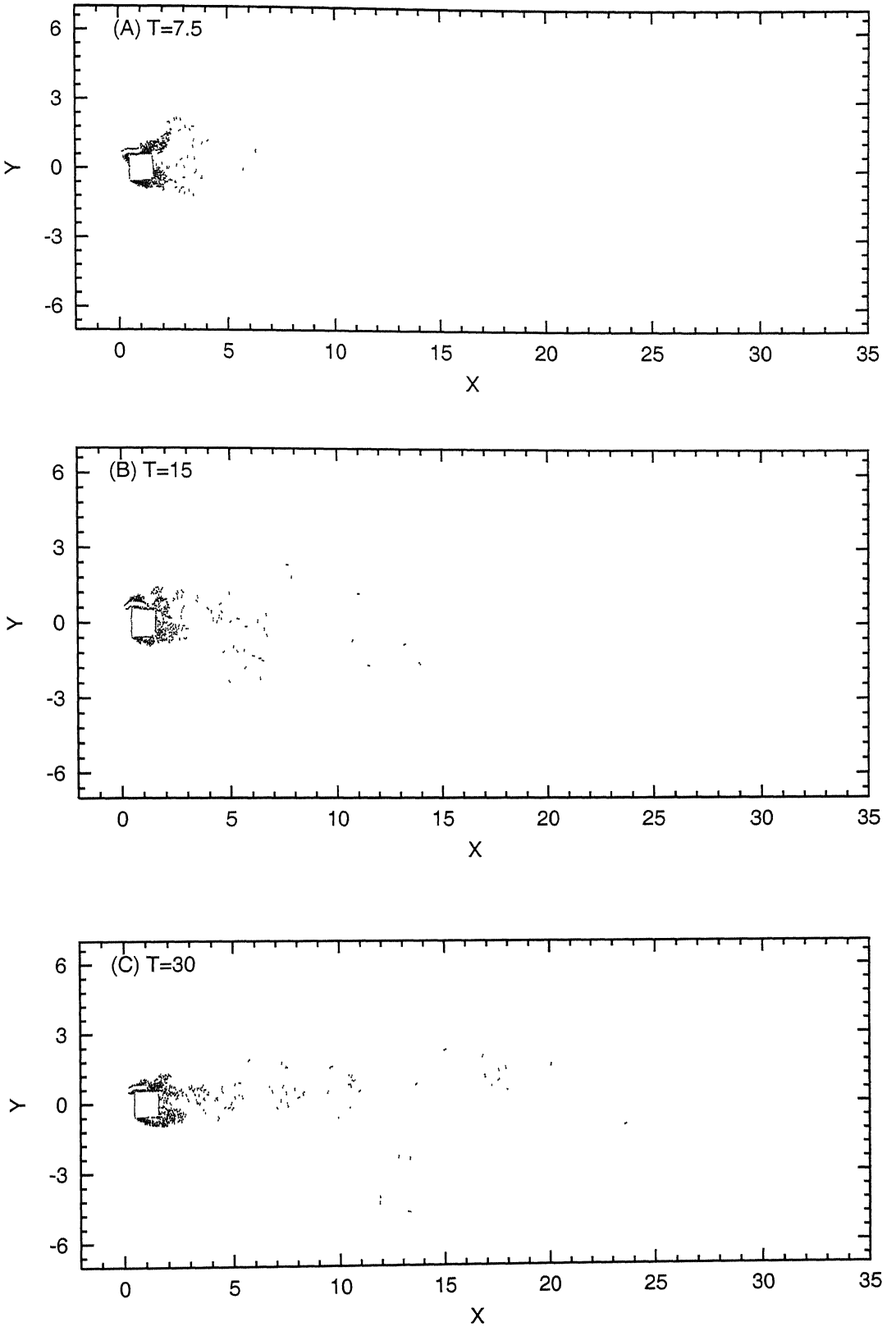

Figure 3.16: Flow diagram for geometry-2 at $Re = 20000$ and $gap = 0.17$ between the two bodies

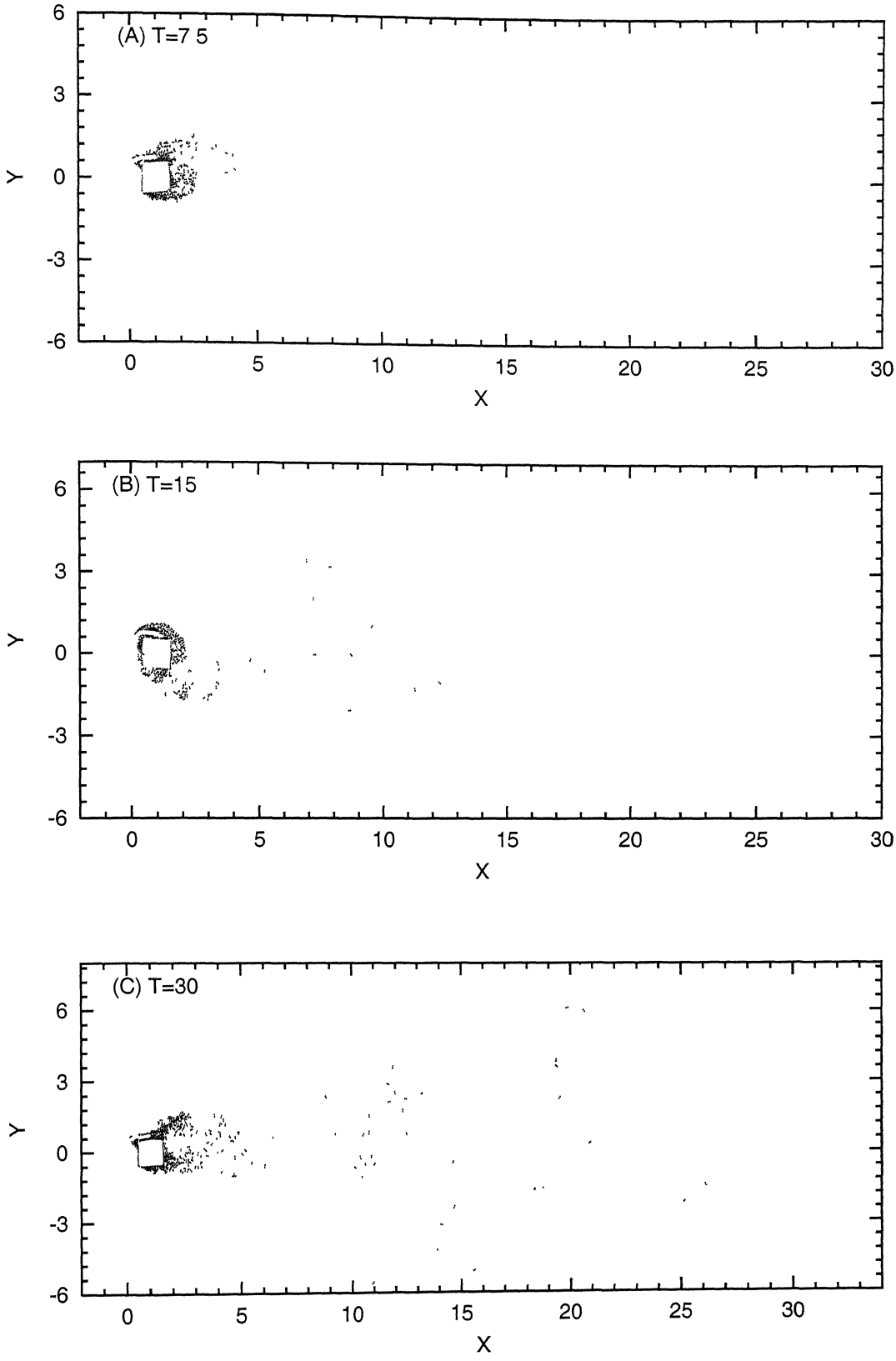

Figure 3.17: Flow diagram for geometry-2 at $Re = 20000$ and $gap = 0.16$ between the two bodies

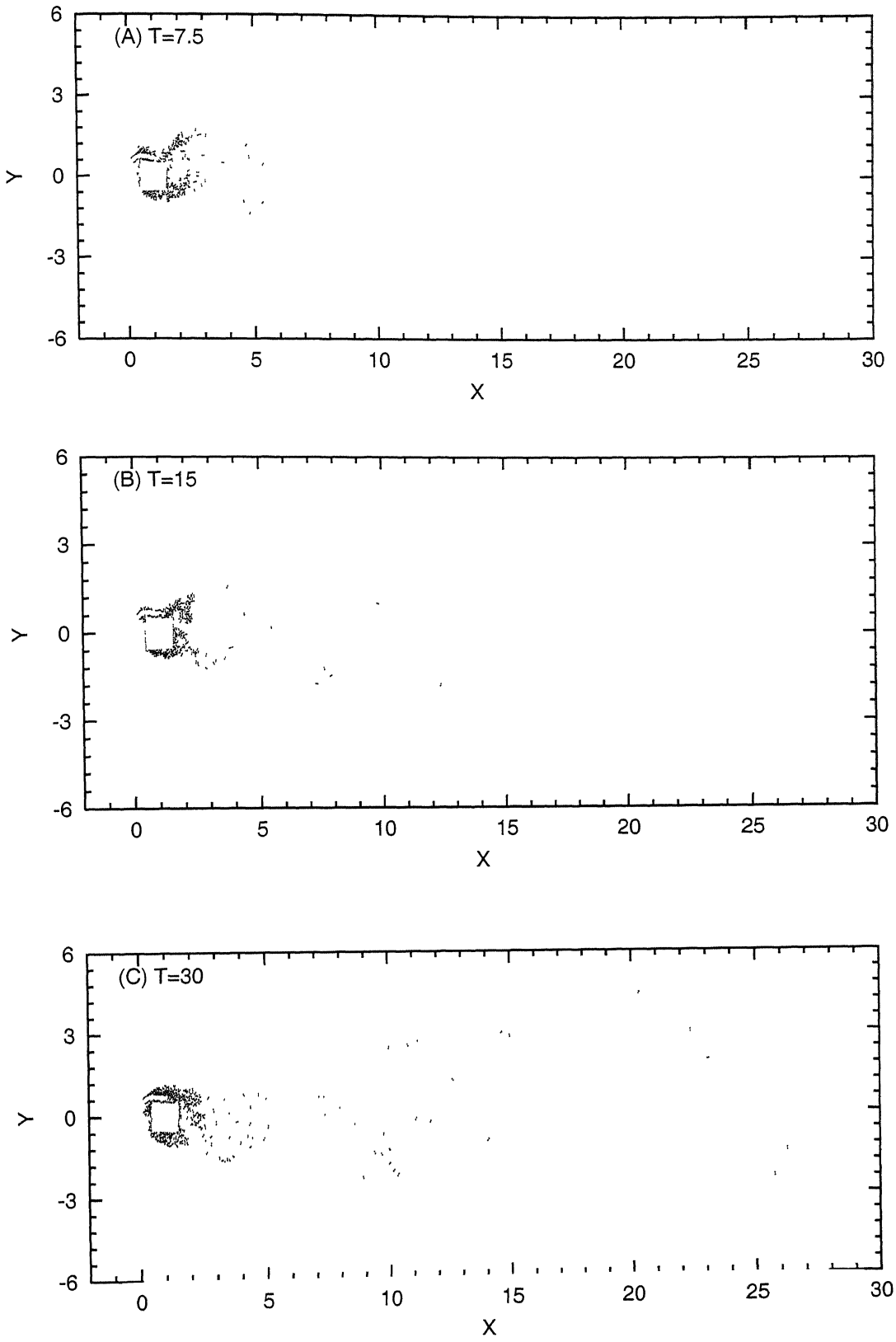

Figure 3.18: Flow diagram for geometry-2 at $Re = 20000$ and $gap = 0.14$ between the two bodies

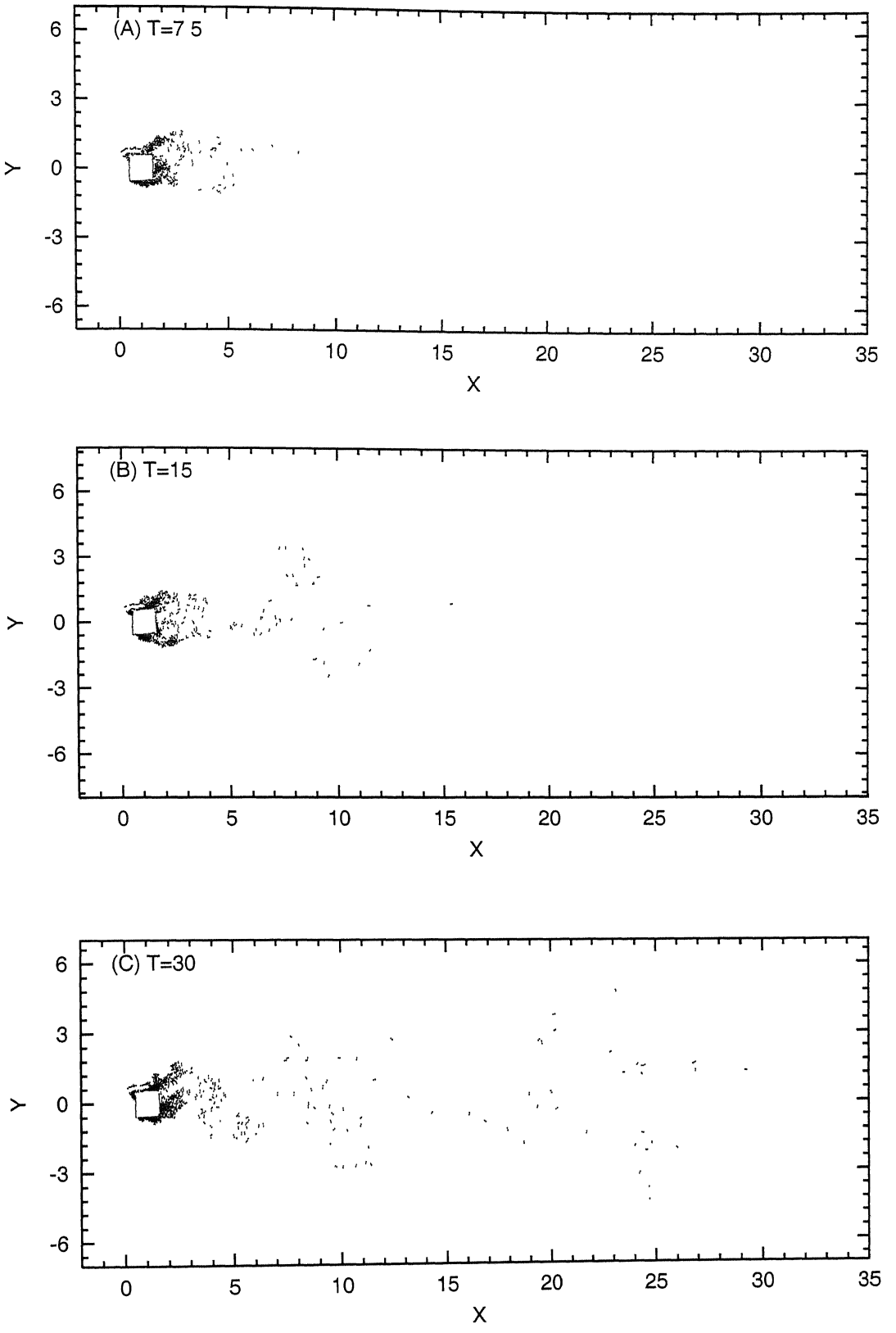

Figure 3.19: Flow diagram for geometry-2 at $Re = 1.2 \times 10^6$ at optimum gap between the two bodies

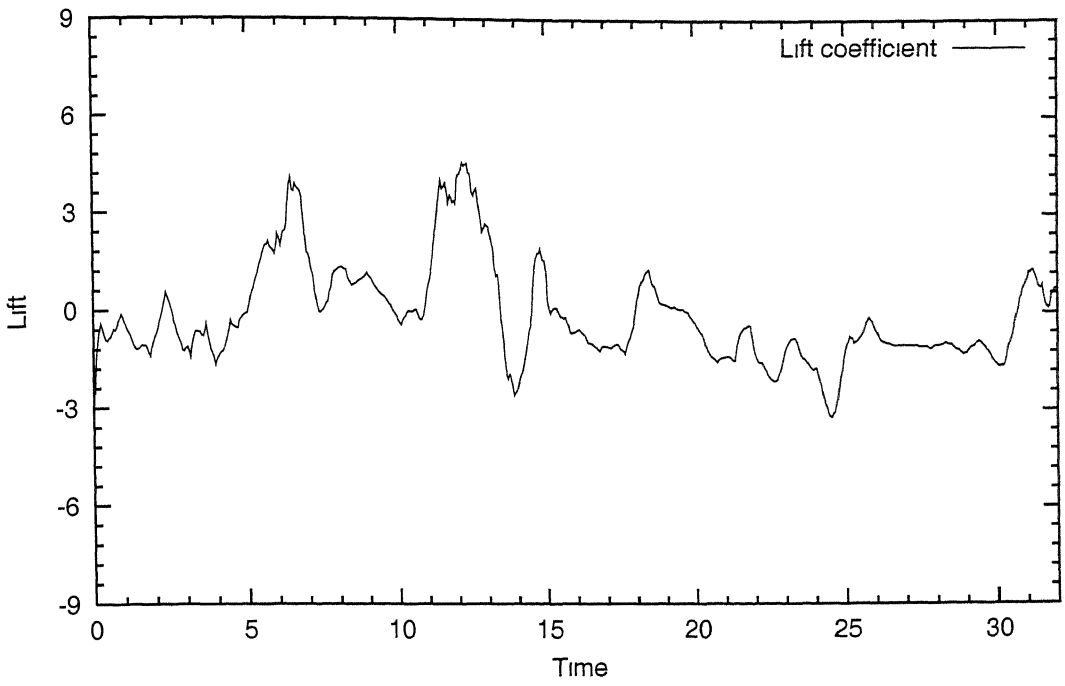

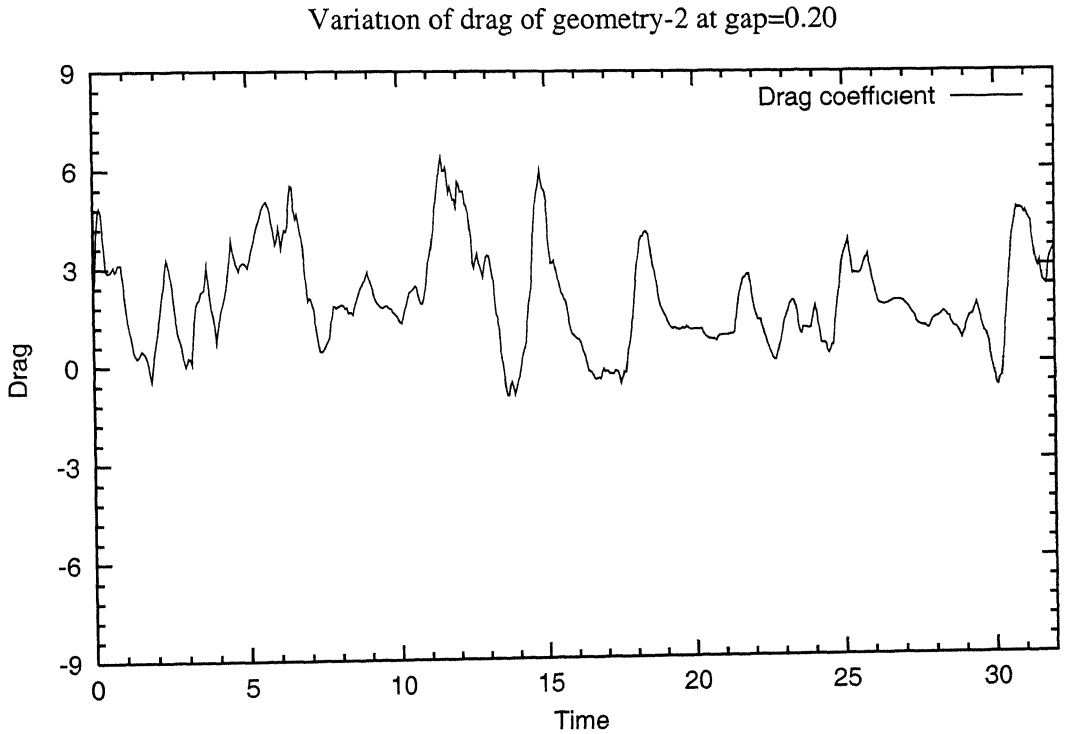

Figure 3.20: Variation of lift and drag of geometry-2 at Reynolds number 20000 and gap=0.20 between the two bodies

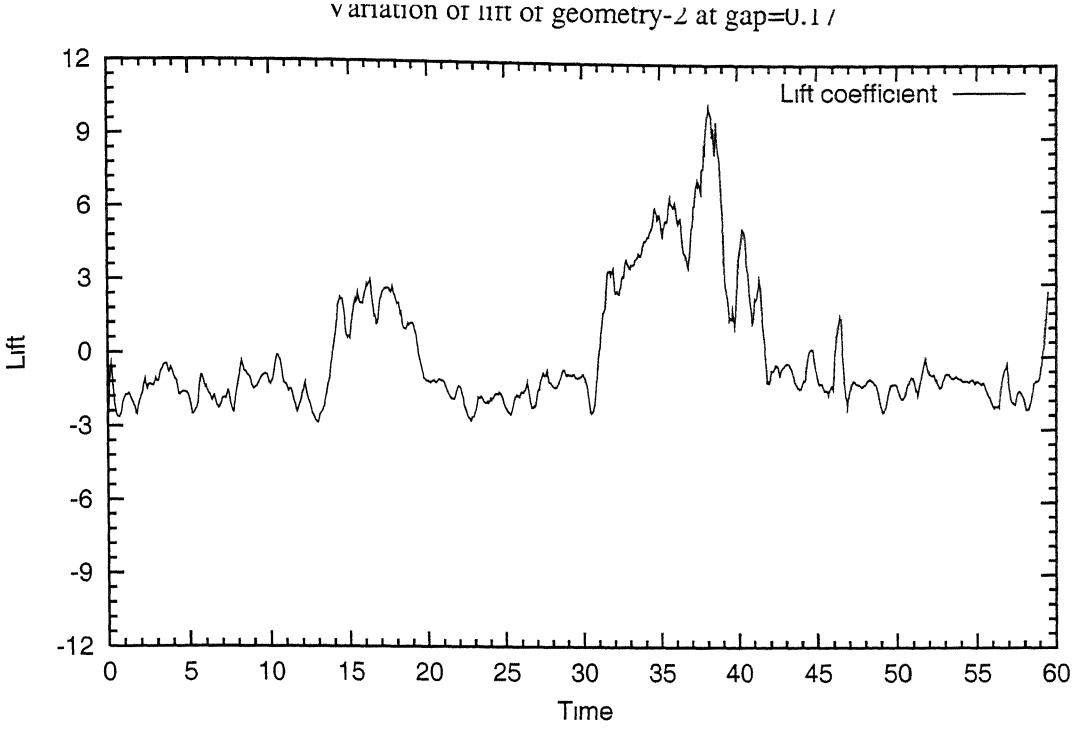

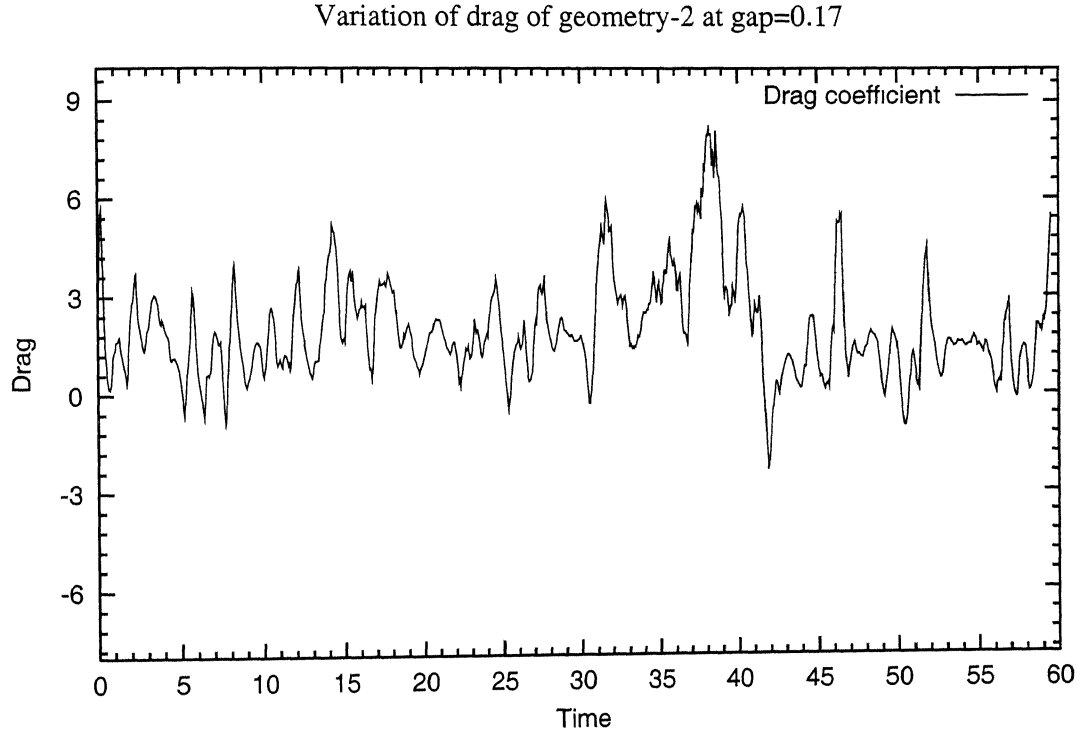

Figure 3.21: Variation of lift and drag of geometry-2 at Reynolds number 20000 and gap =0.17 between the two bodies

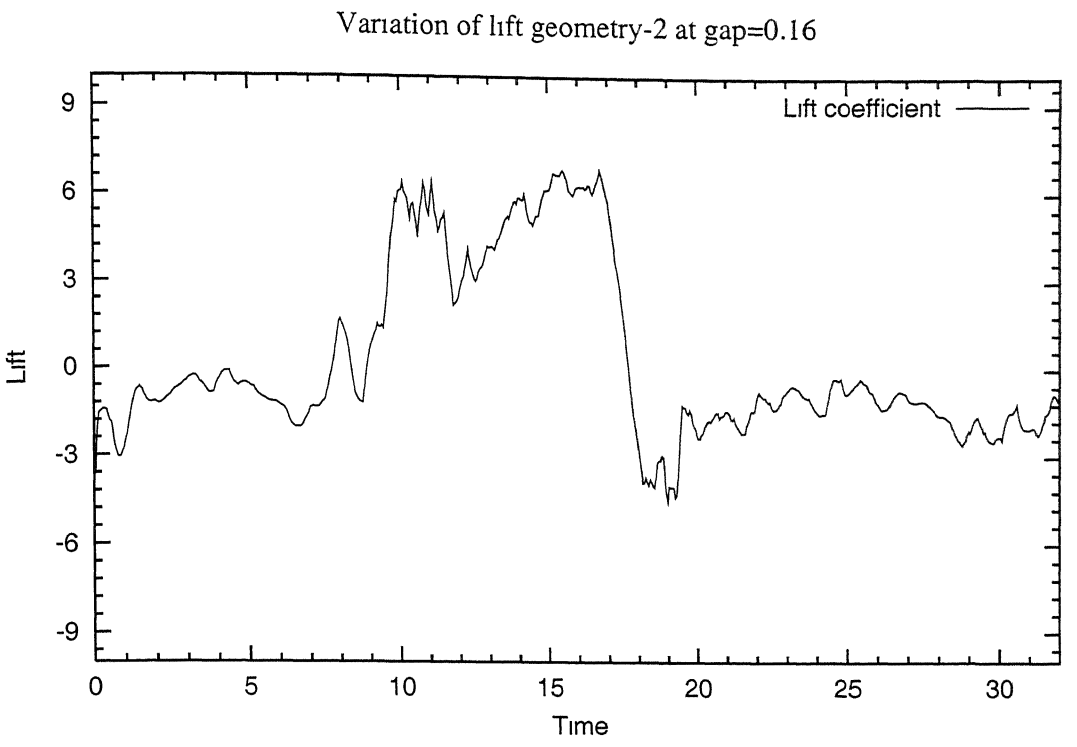

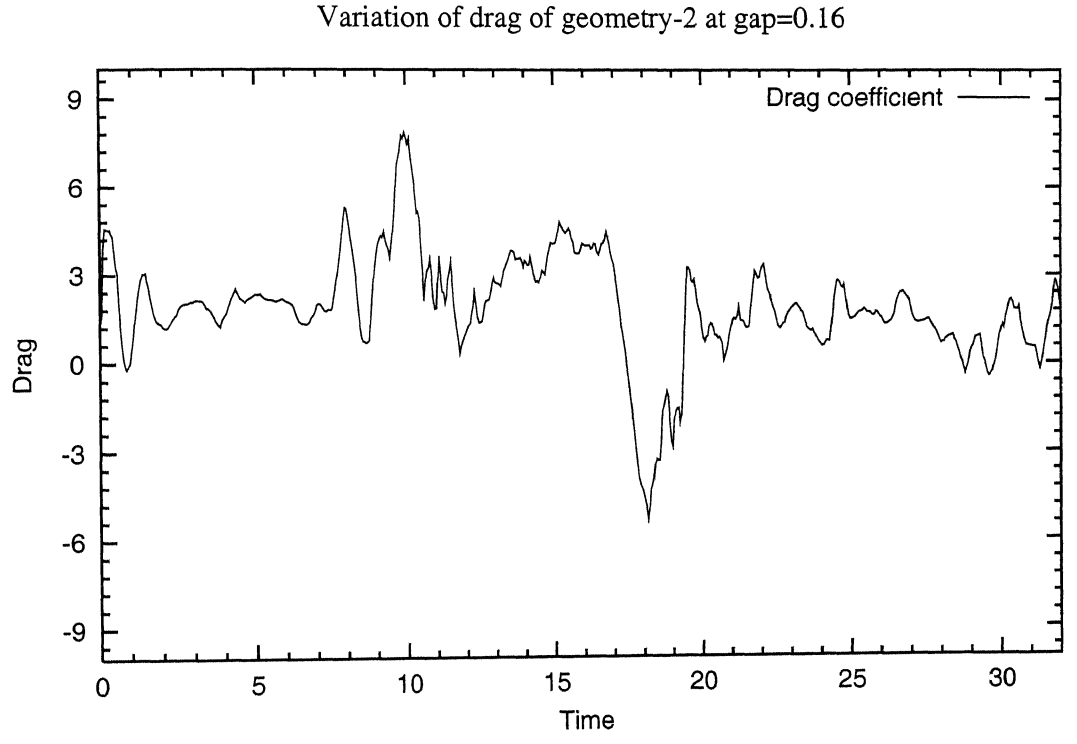

Figure 3.22: Variation of lift and drag of geometry-2 at Reynolds number 20000 and gap= 0.16 between the two bodies

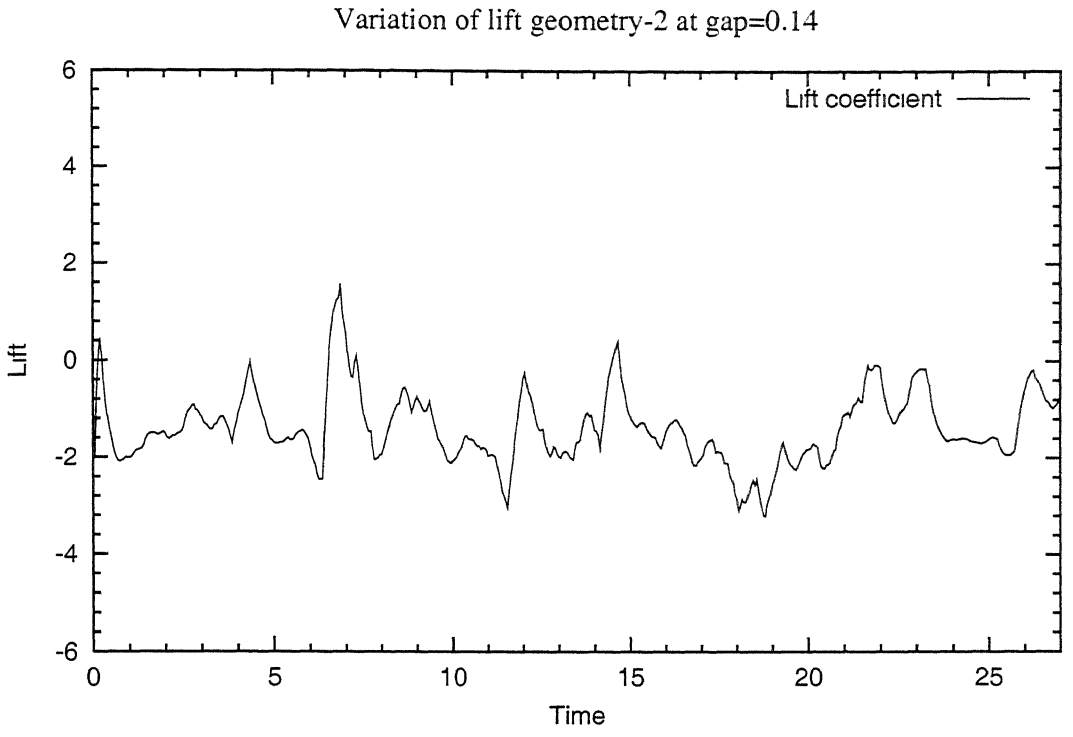

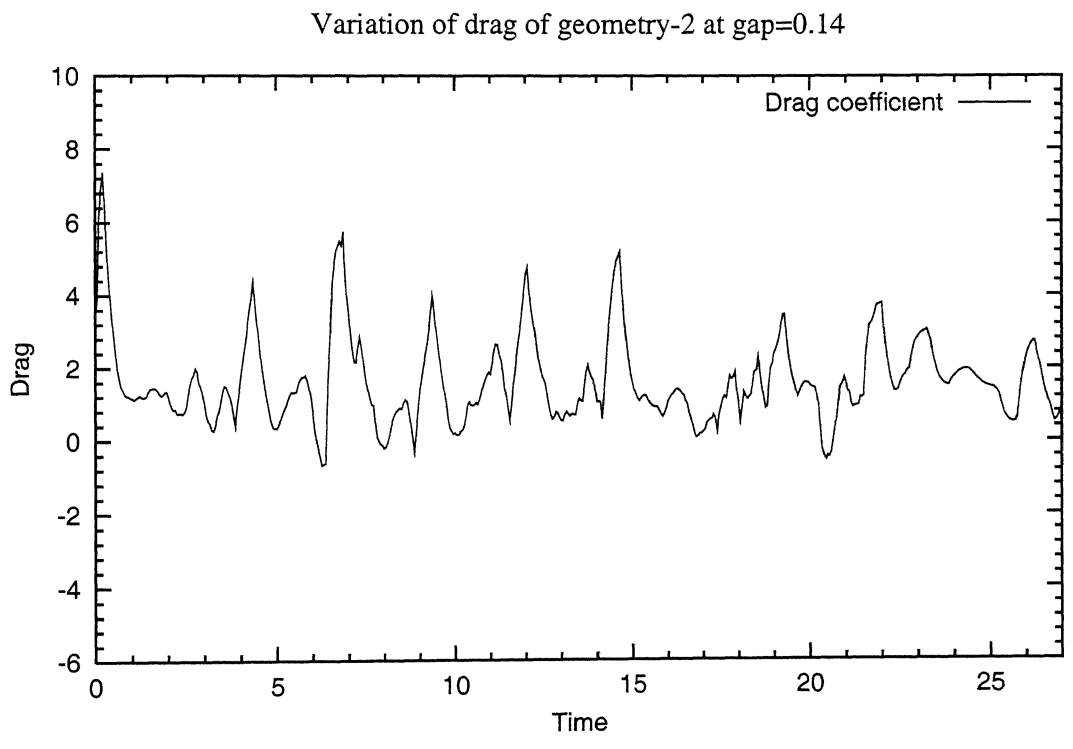

Figure 3.23: Variation of lift and drag of geometry-2 at Reynolds number 20000 and gap= 0.14 between the two bodies

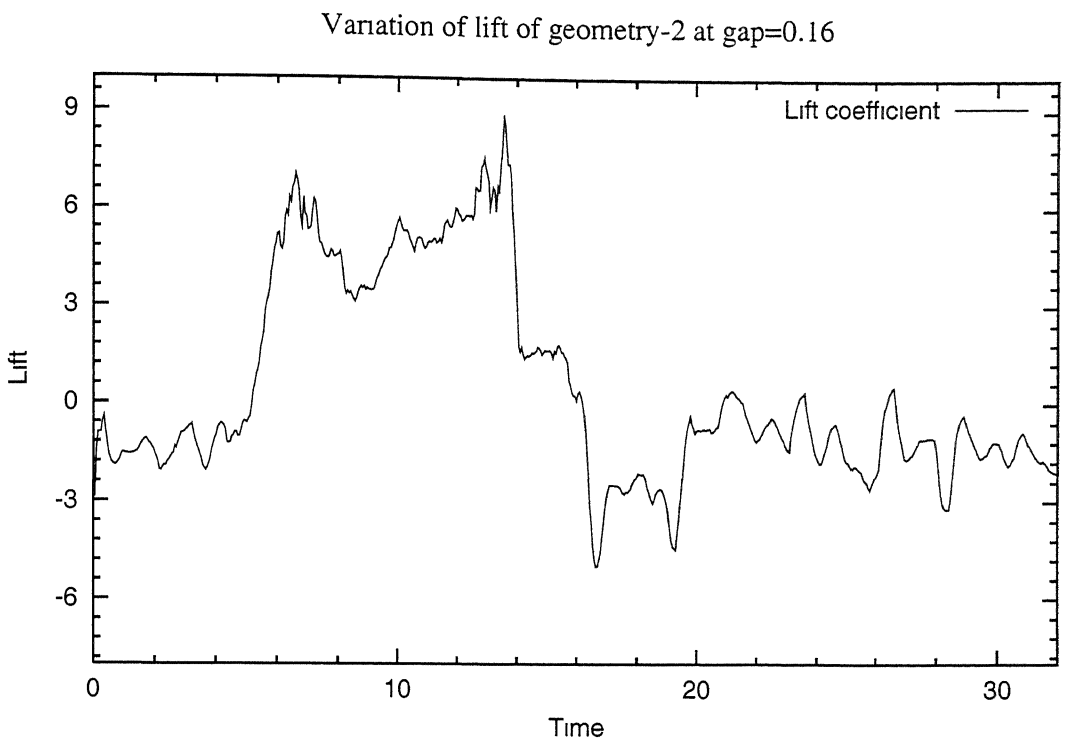

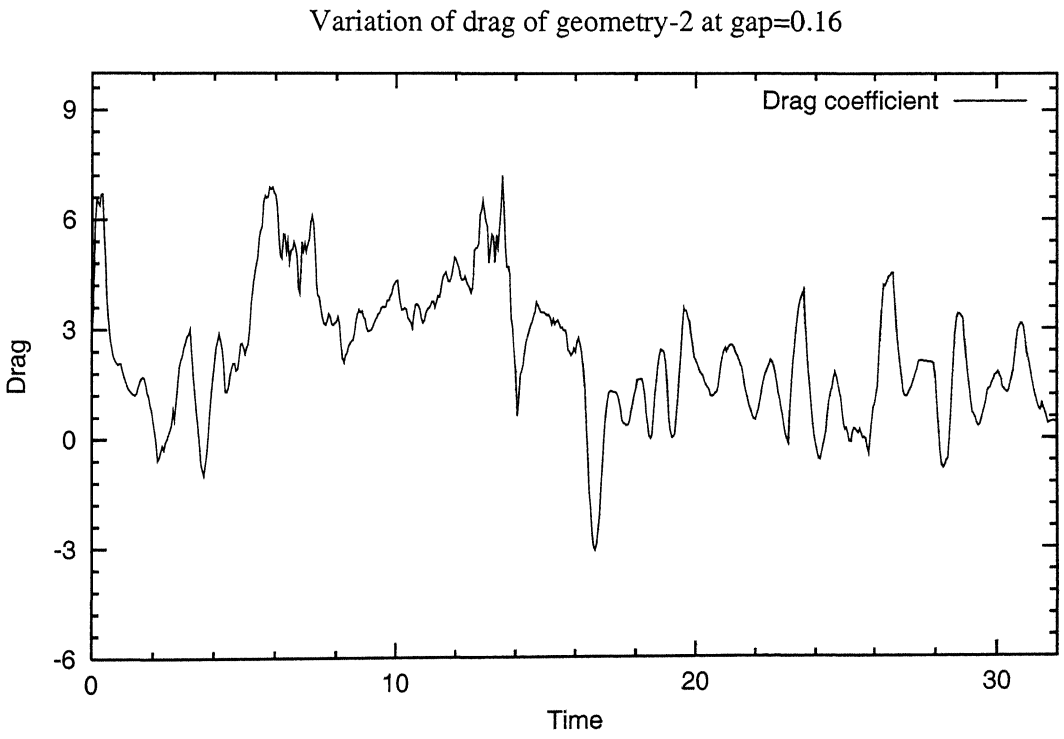

Figure 3.24: Variation of lift and drag of geometry-2 at optimum gap between the two bodies at $Re = 1 \times 10^5$

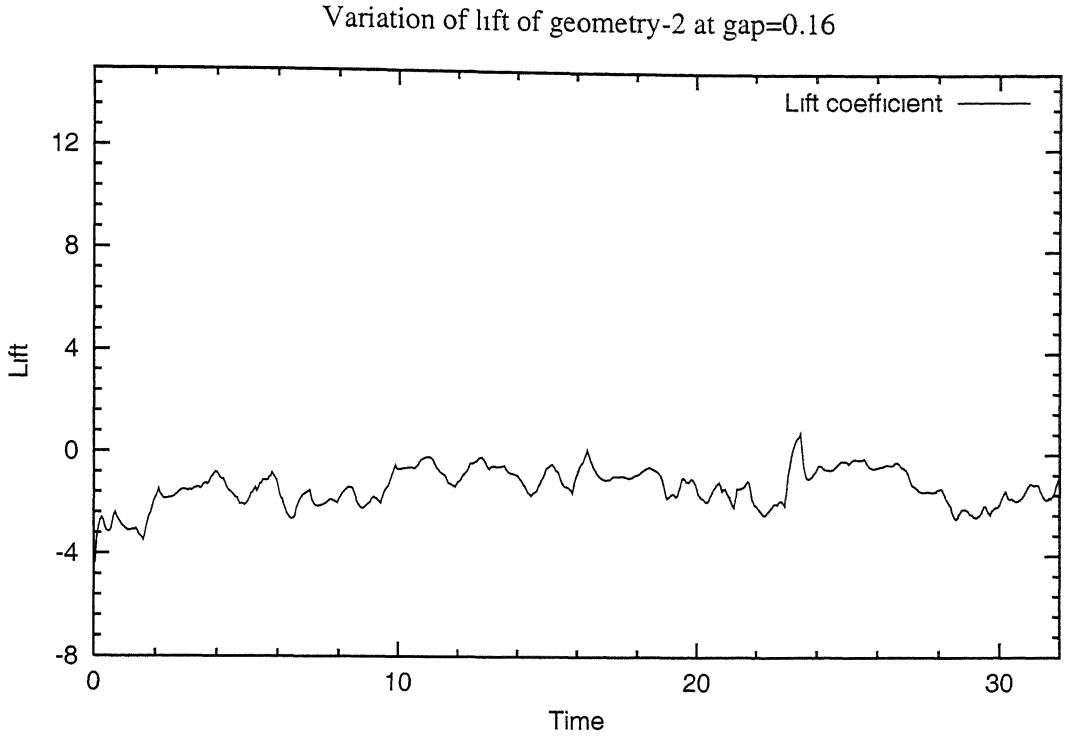

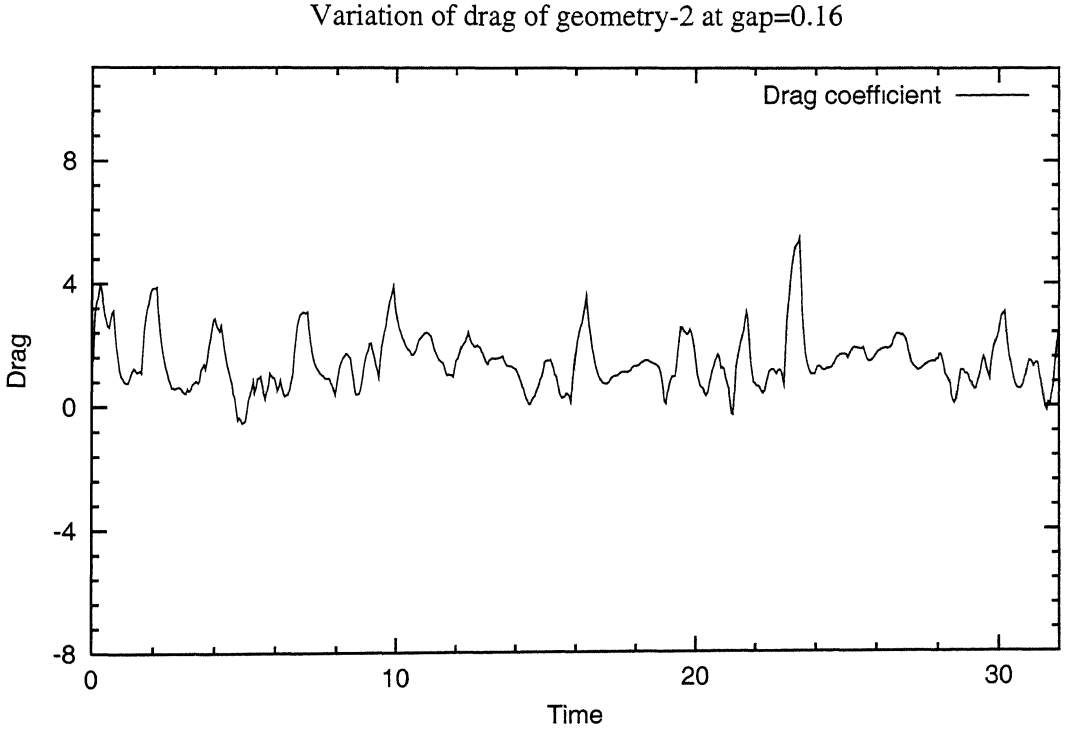

Figure 3.25: Variation of lift and drag of geometry-2 at optimum gap between the two bodies at $Re = 1.2 \times 10^6$

Chapter 4

THE FLOW PAST ROTATING CIRCULAR CYLINDER

4.1 Problem Formulation

Flow past rotating circular cylinder can be modeled by introducing a bound vortex Γ at the centre of cylinder. The bound vortex Γ can be related to the bound vorticity by,

$$\Gamma = \oint \gamma(s)ds \tag{4.1}$$

or in numerical form,

$$\Gamma = \sum_{n=1}^{M} \gamma(s_n)\Delta s_n \tag{4.2}$$

and Martensen's boundary integral equation for plane two dimensional flow is,

$$\sum_{n=1}^{M} K(s_m, s_n)\gamma(s_n) = -(U_\infty cos\beta_m + V_\infty sin\beta_m) \tag{4.3}$$

Adding equations (4.2) and (4.3), the modified form of Martensen equations is,

$$\sum_{n=1}^{M} (K(s_m, s_n) + \Delta s_n)\gamma(s_n) = -(U_\infty cos\beta_m + V_\infty sin\beta_m) + \Gamma \tag{4.4}$$

In presence of cloud of vortices the equation 4.4 is modified as

$$\sum_{n=1}^{M}(K(s_m, s_n) + \Delta s_n)\gamma(s_n) = -(U_\infty cos\beta_m + V_\infty sin\beta_m) + \Gamma$$

$$+\Gamma_{circ} - \sum_{j=1}^{Z} \Delta\Gamma_j(U_{mj}cos\beta_m + V_{mj}sin\beta_m + 1) \qquad (4.5)$$

where U_{mj} *and* V_{mj} are the same as given earlier for square cylinder.

The bound vortex Γ can be related to the rotation Ω by $\Gamma = 2\pi r_0^2 \Omega$. Thus the only change for solving the flow past rotating circular cylinder is change in Martensen equation and the rest of the analysis(*i.e.* shedding, diffusion, convection *etc.*) remains unchanged.

4.2 Results and discussions

The diameter of cylinder is taken as 1.0, mainstream flow W_∞ is 1.0, and rotation(Ω) of cylinder is varied. The cylinder is discretized into 32 surface elements The flow is calculated for 720 time steps, each time step is 0.05. We also solved the flow for infinite Reynolds number(Potential flow). The result for infinite Reynolds number and for vortex cloud solution are given in Table 4.1 The results obtained for lift and drag are not correct. Flow diagrams for different rotation speeds are given in Fig. 4.2 to Fig 4.6. Variation in lift and drag with time is shown in Fig. 4.7 to Fig. 4.11. The Fig. 4.1 shows the variation in lift and drag of the rotating cylinder with increasing velocity ratio($r\Omega/U_\infty$).

Rotation Ω	*At Infinite Reynolds number (Potential flow)*		*Vortex cloud analysis, at* $Re = 1 \times 10^5$	
	C_l	C_d	C_l	C_d
0.1	0.313943	0.000000	-0.218555	0.643247
0.2	0.627886	0 000000	-0.612226	0.421329
0.4	1.255773	0 000000	-0.654632	0.715022
0.6	1 883659	0 000000	-0.759954	0.575640
0.8	2.511545	0.000000	-0.901063	0.395768
1.0	3.139432	0 000000	-0.103302	0.799423
1 2	3.767318	0.000000	-0.688595	0.548724
1.4	4.395204	0.000000	-0.589837	0.647782
1 6	5.023091	0.000000	-0.506253	0.398093
1.8	5 650977	0.000000	-0.446093	0.612781
2.0	6 278863	0.000000	-0.105586	0 748433

Table 4.1: Lift and drag of rotating circular cylinder at varying rotation speeds

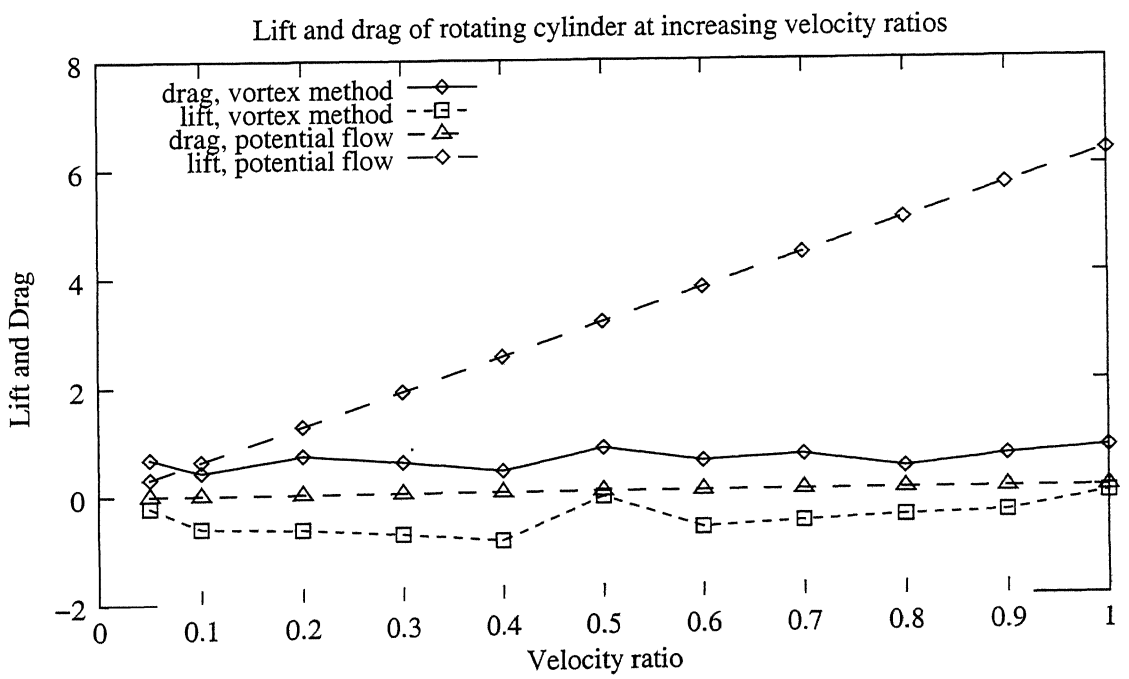

Figure 4.1: Lift and drag of rotating cylinder at increasing velocity ratio, $\frac{D\Omega}{2U_\infty}$

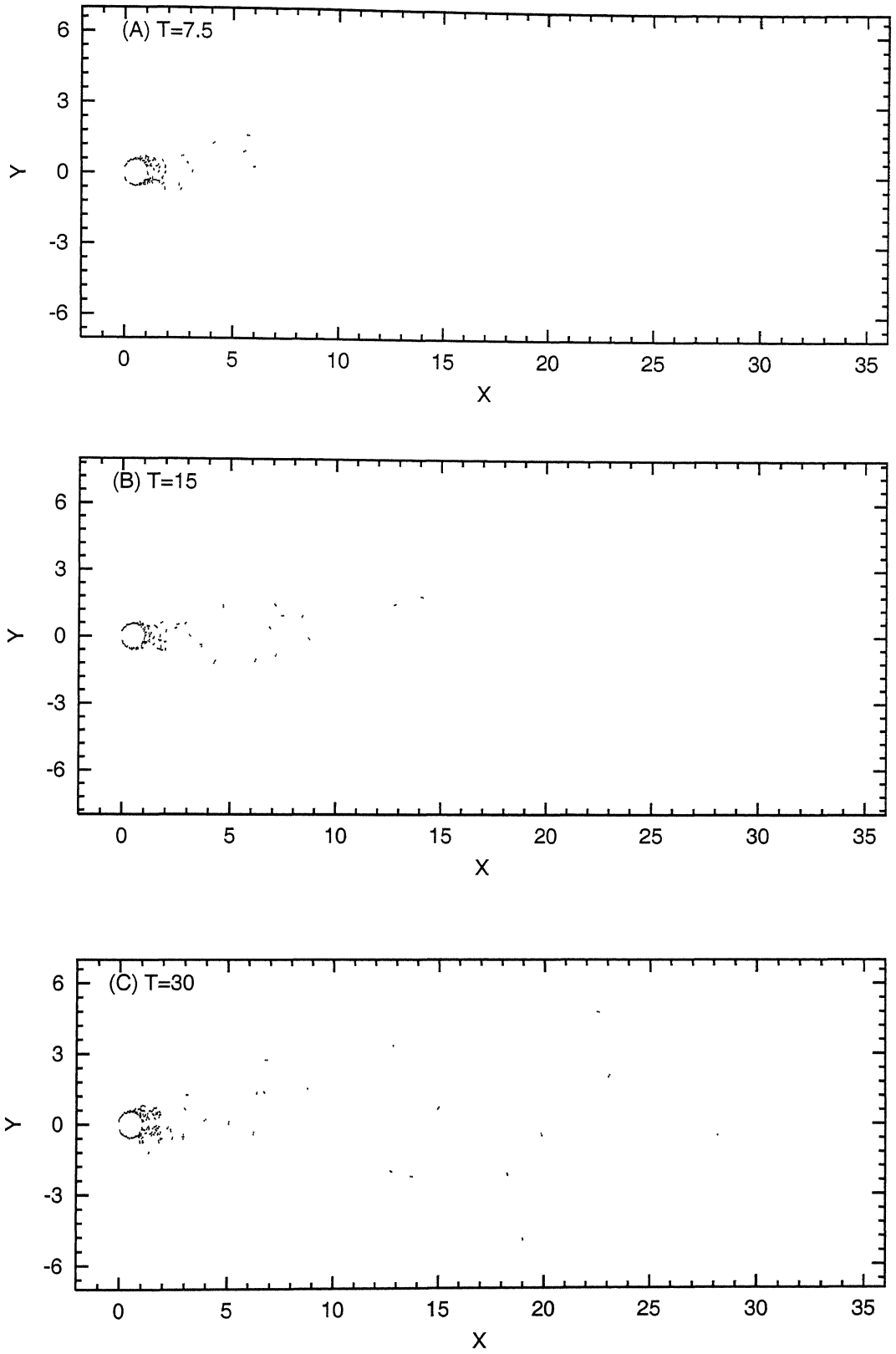

Figure 4.2: Flow diagram of rotating circular cylinder at Reynolds number, $Re = 1 \times 10^5$ and $\Omega = 0.4$

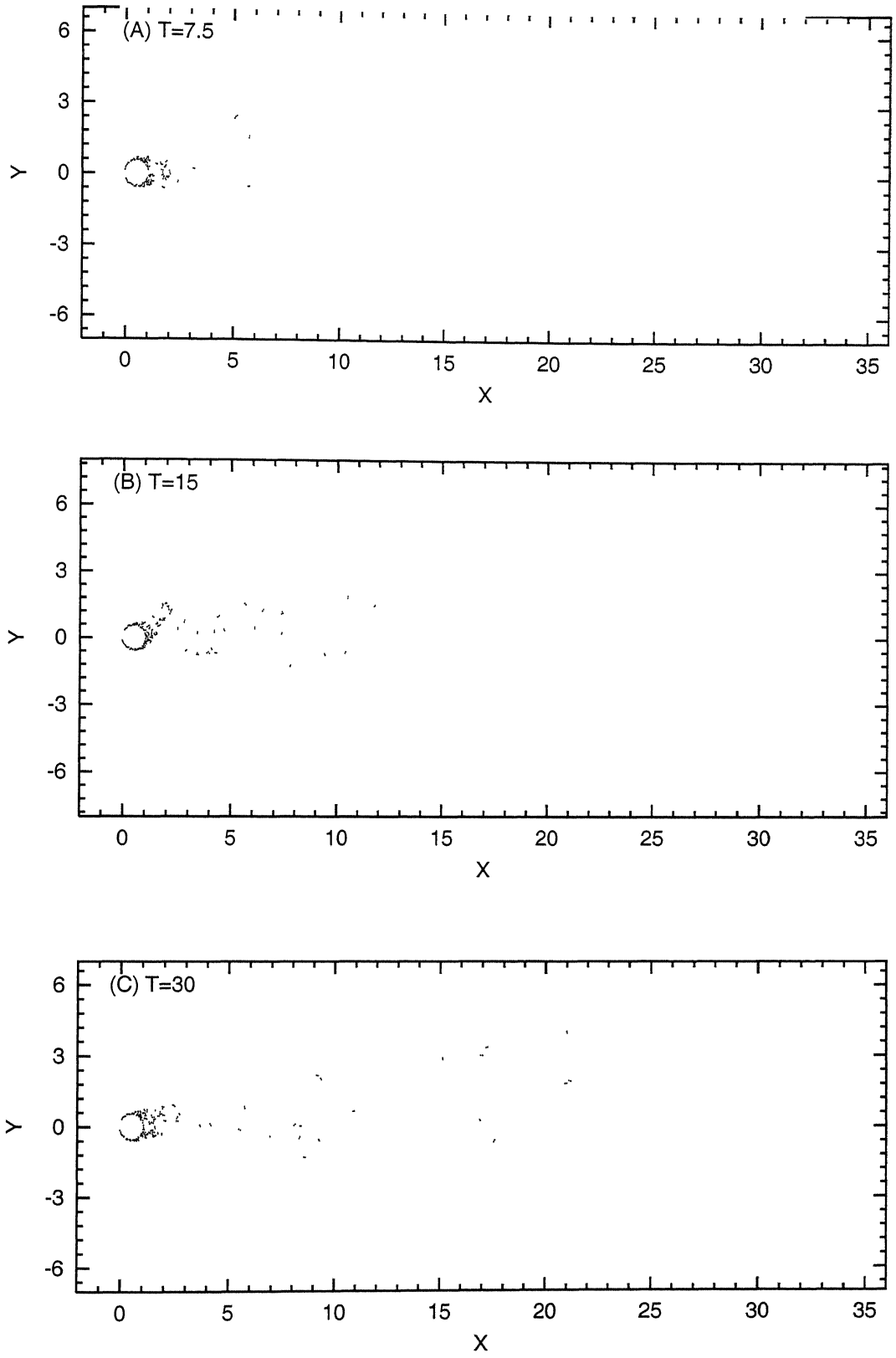

Figure 4.3: Flow diagram of rotating circular cylinder at Reynolds number, $Re = 1 \times 10^5$ and $\Omega = 0.8$

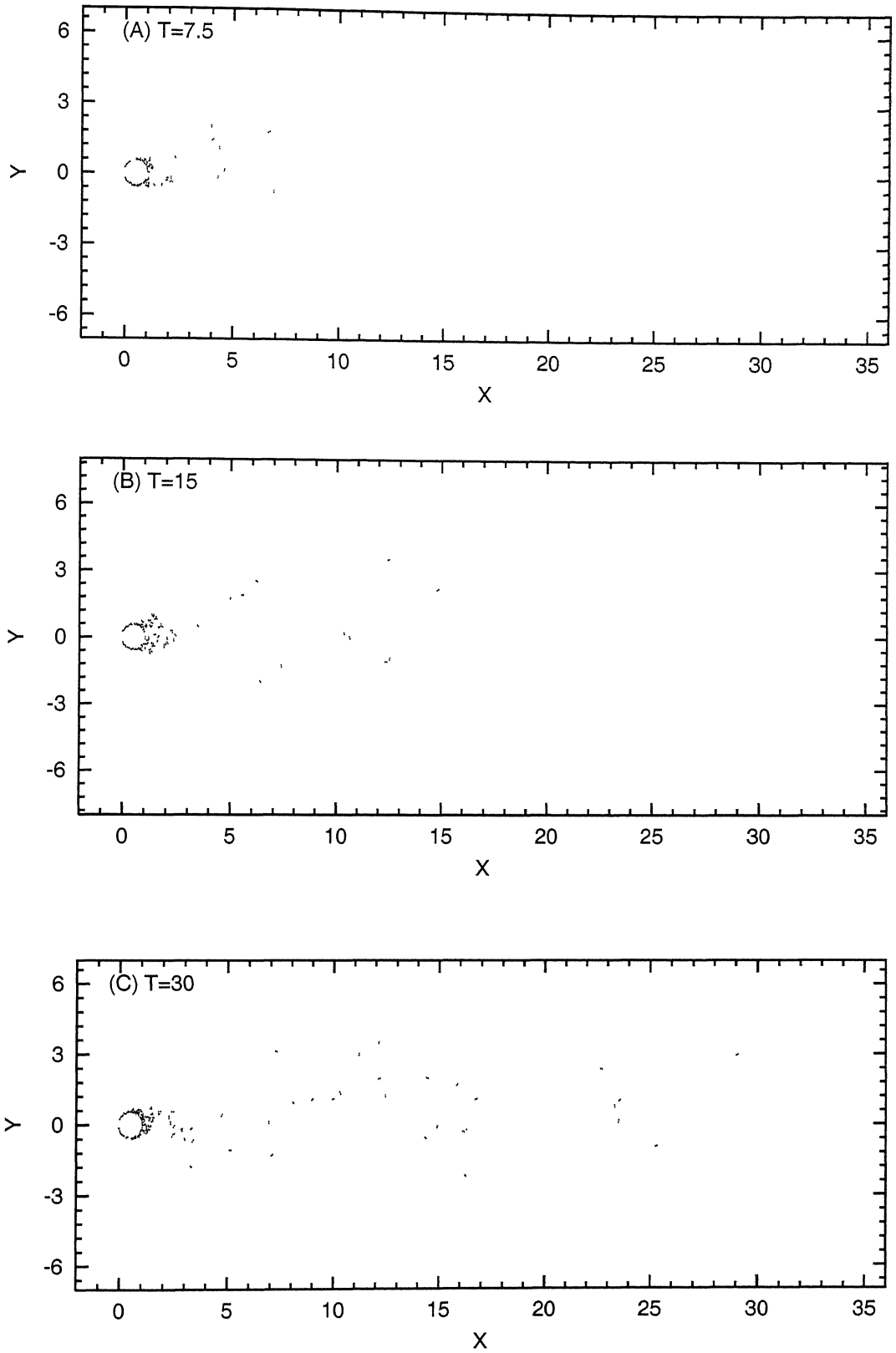

Figure 4.4: Flow diagram of rotating circular cylinder at Reynolds number, $Re = 1 \times 10^5$ and $\Omega = 1.2$

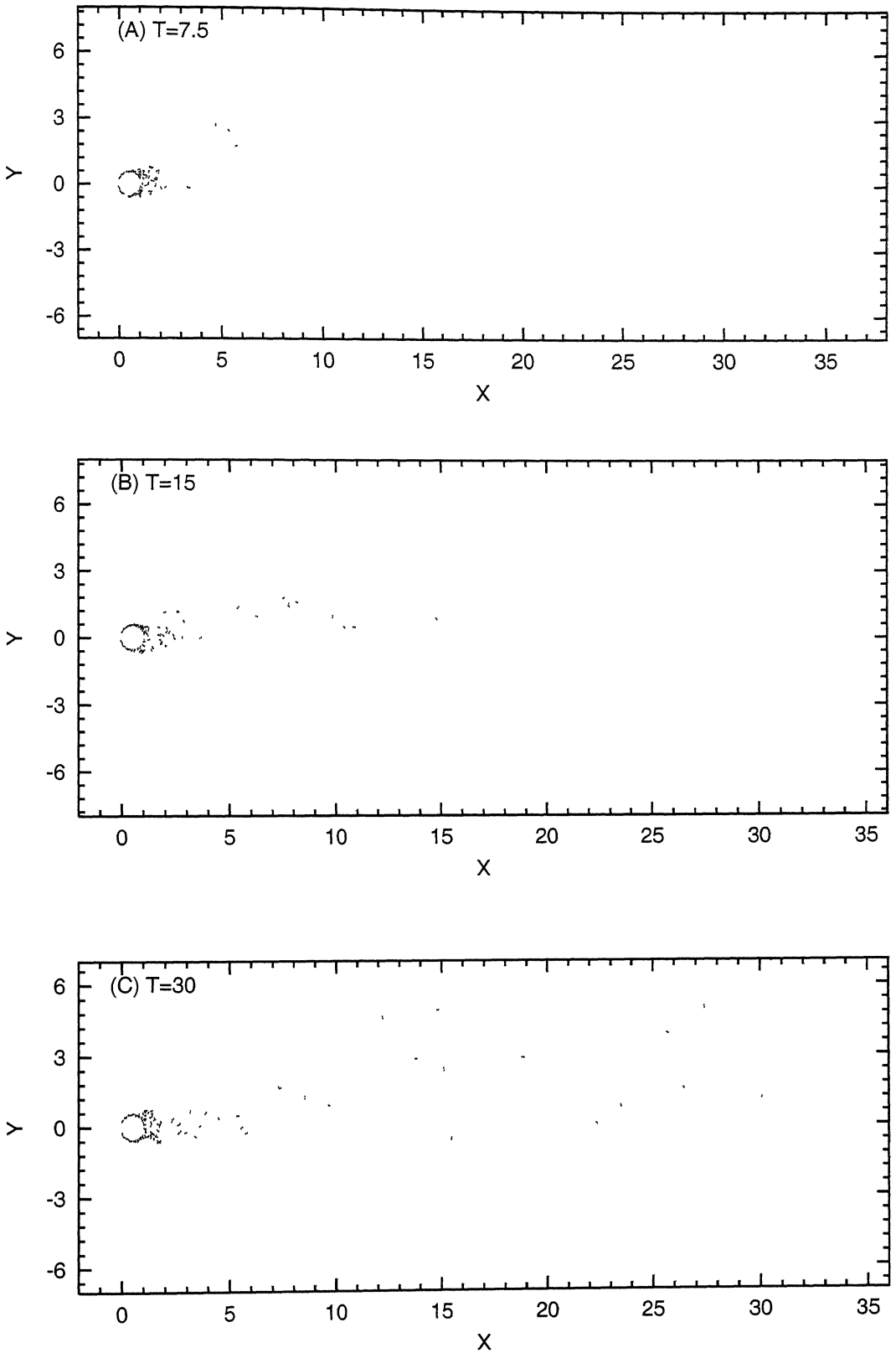

Figure 4.5: Flow diagram of rotating circular cylinder at Reynolds number, $Re = 1 \times 10^5$ and $\Omega = 1.6$

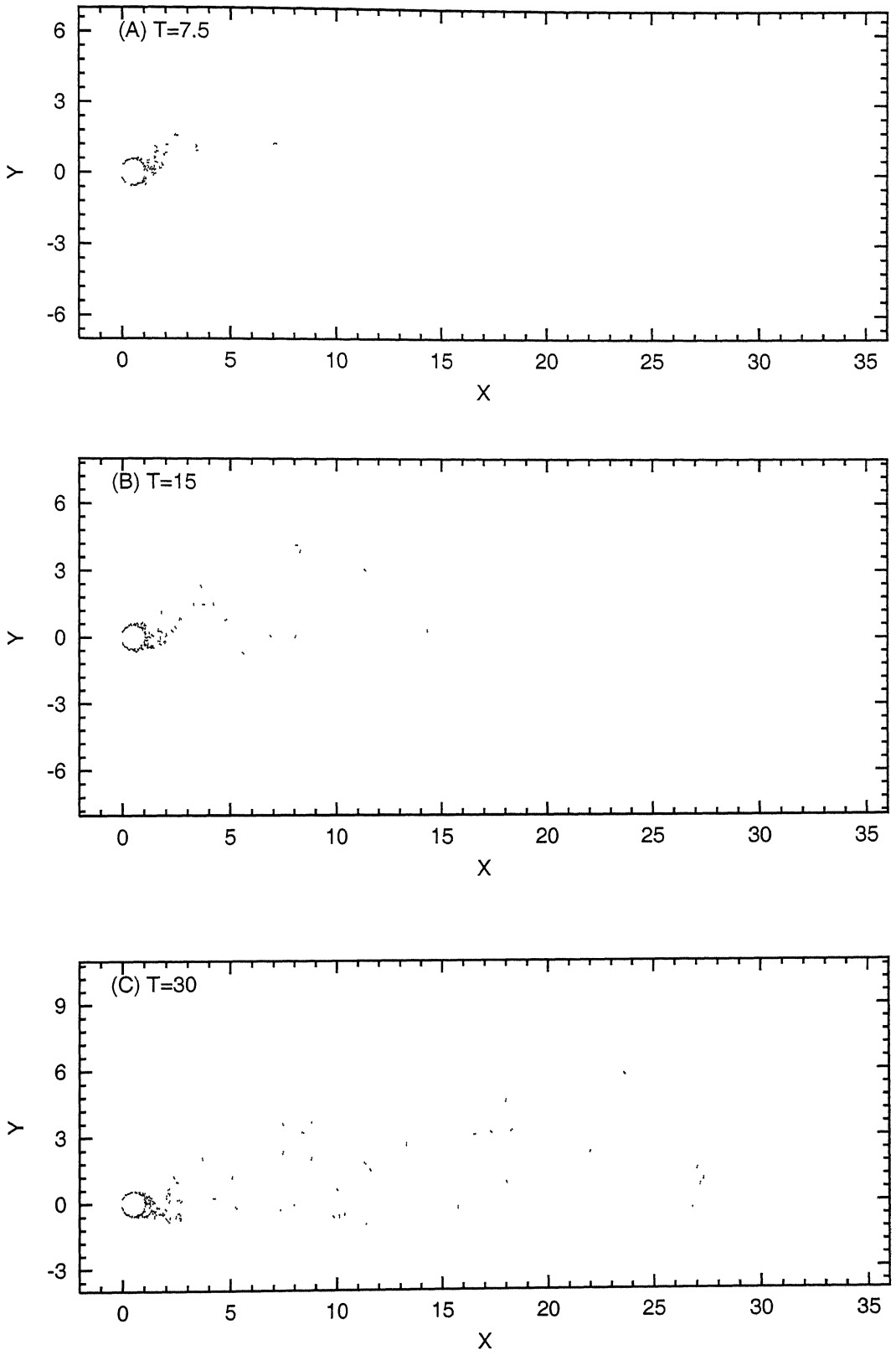

Figure 4.6: Flow diagram of rotating circular cylinder at Reynolds number, $Re = 1 \times 10^5$ and $\Omega = 2.0$

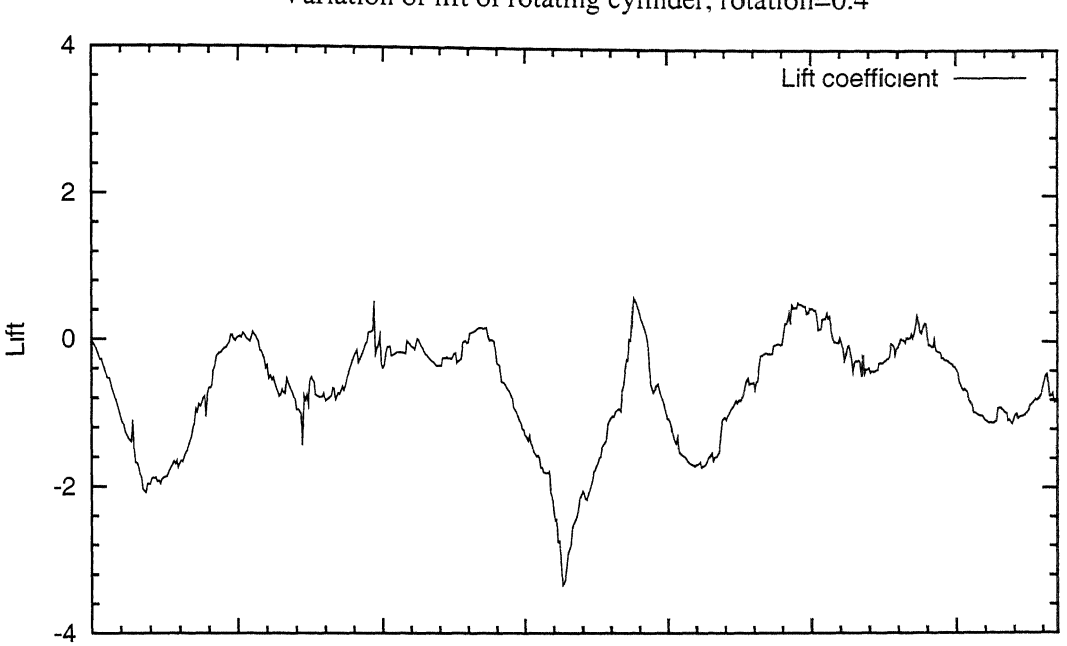

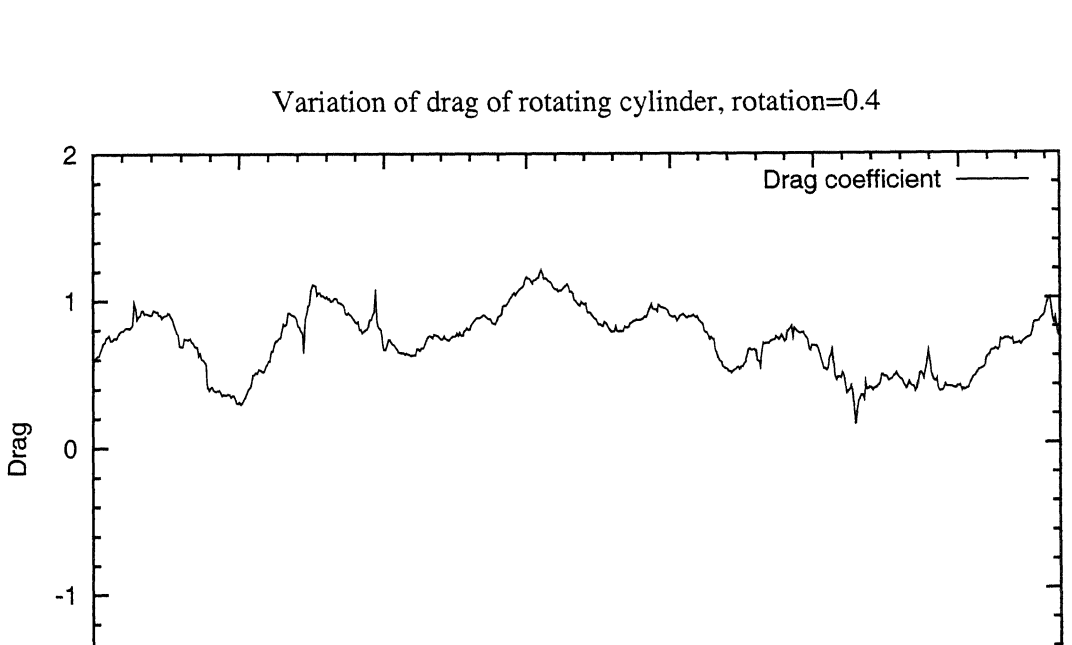

Figure 4.7: Variation of lift and drag of rotating circular cylinder at Reynolds number, $Re = 1 \times 10^5$ and $\Omega = 0.4$

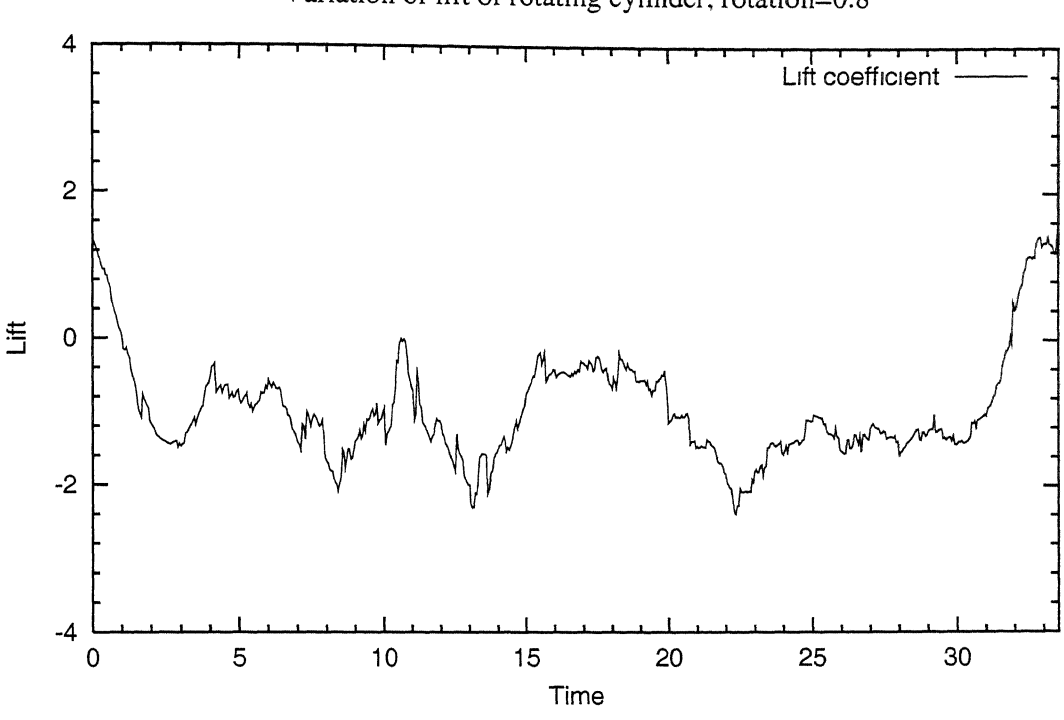

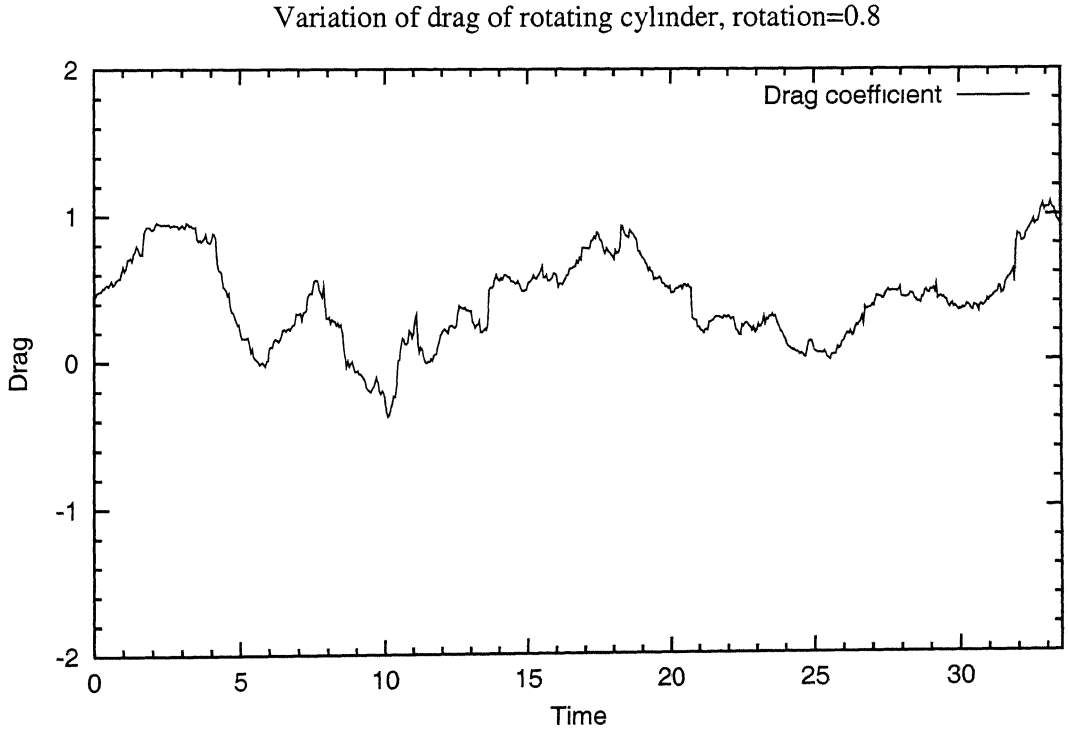

Figure 4.8: Variation of lift and drag of rotating circular cylinder at Reynolds number, $Re = 1 \times 10^5$ and $\Omega = 0.8$

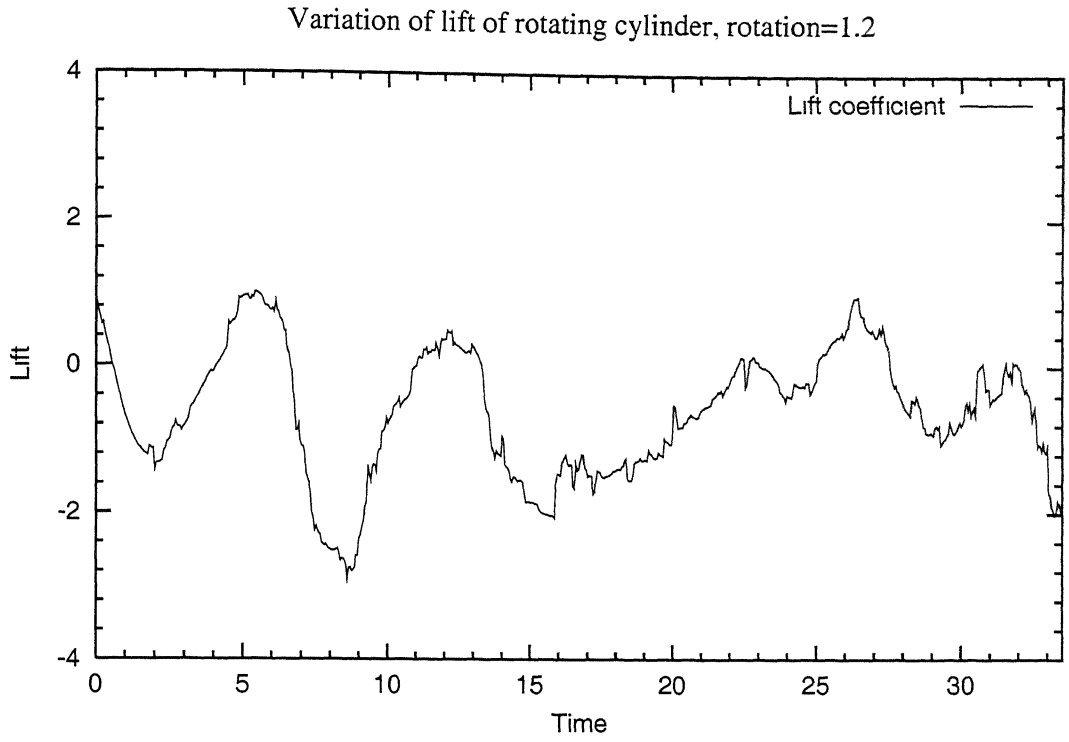

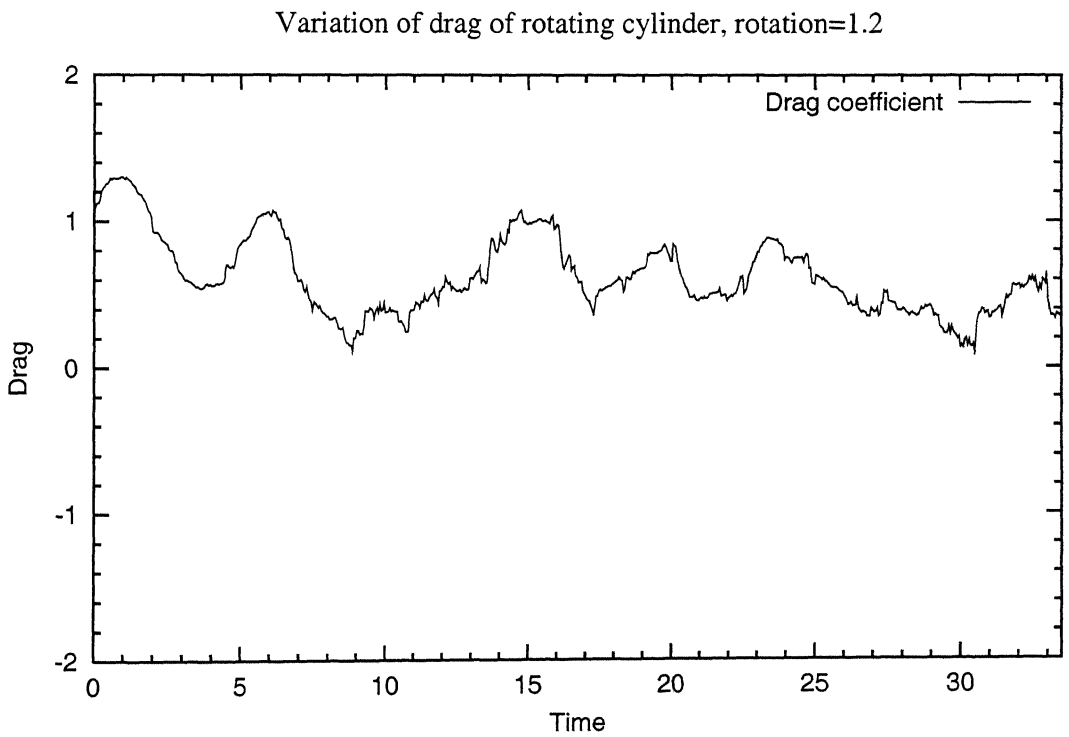

Figure 4.9: Variation of lift and drag of rotating circular cylinder at Reynolds number, $Re = 1 \times 10^5$ and $\Omega = 1.2$

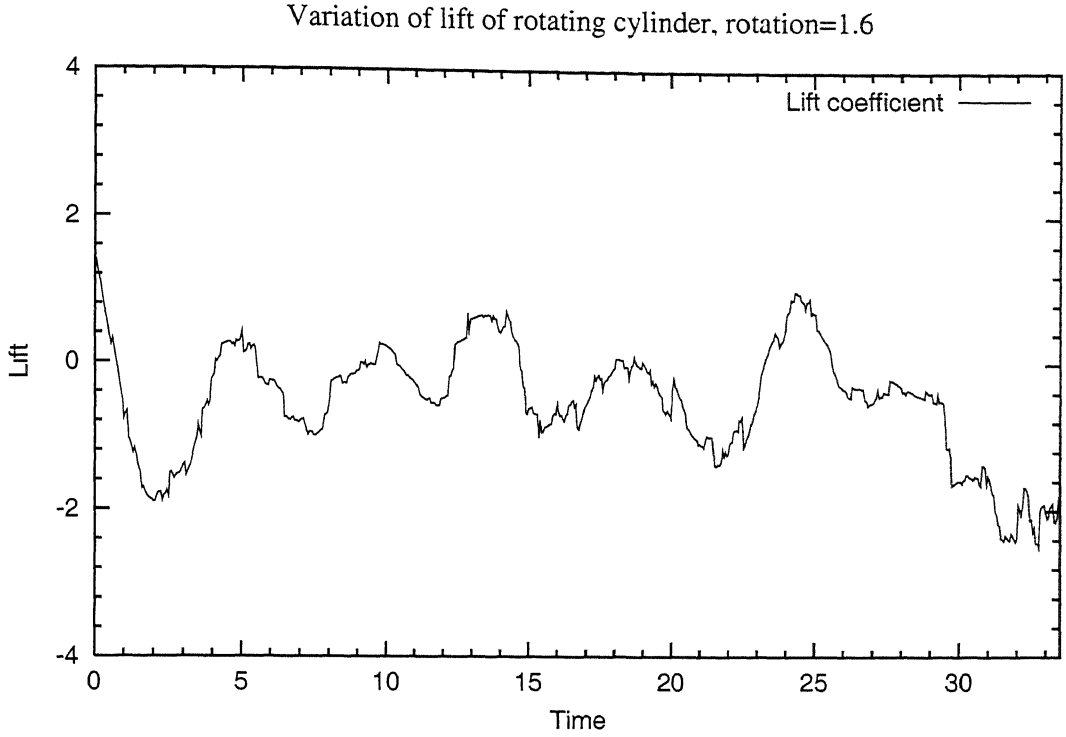

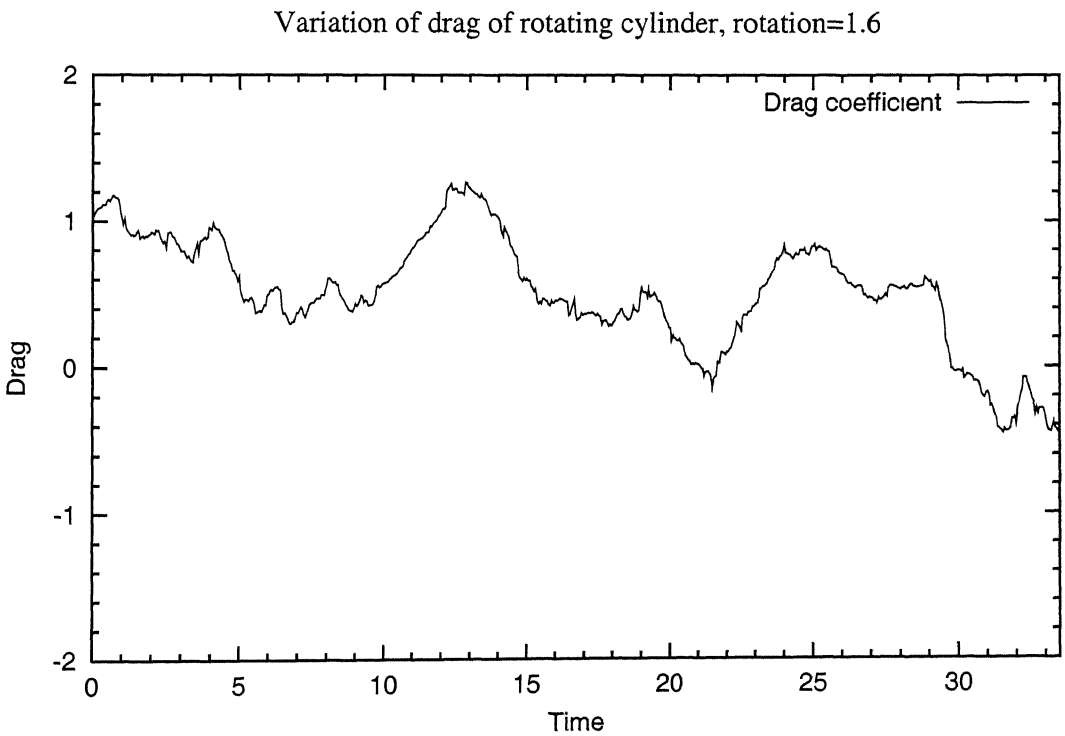

Figure 4.10: Variation of lift and drag of rotating circular cylinder at Reynolds number, $Re = 1 \times 10^5$ and $\Omega = 1.6$

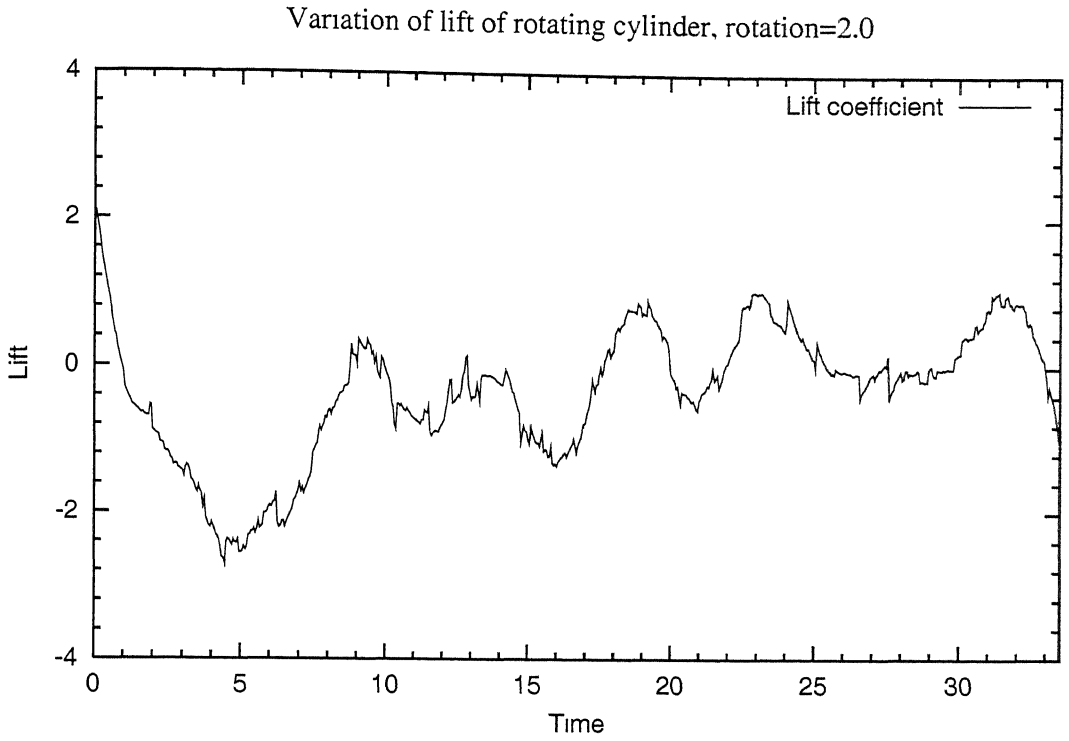

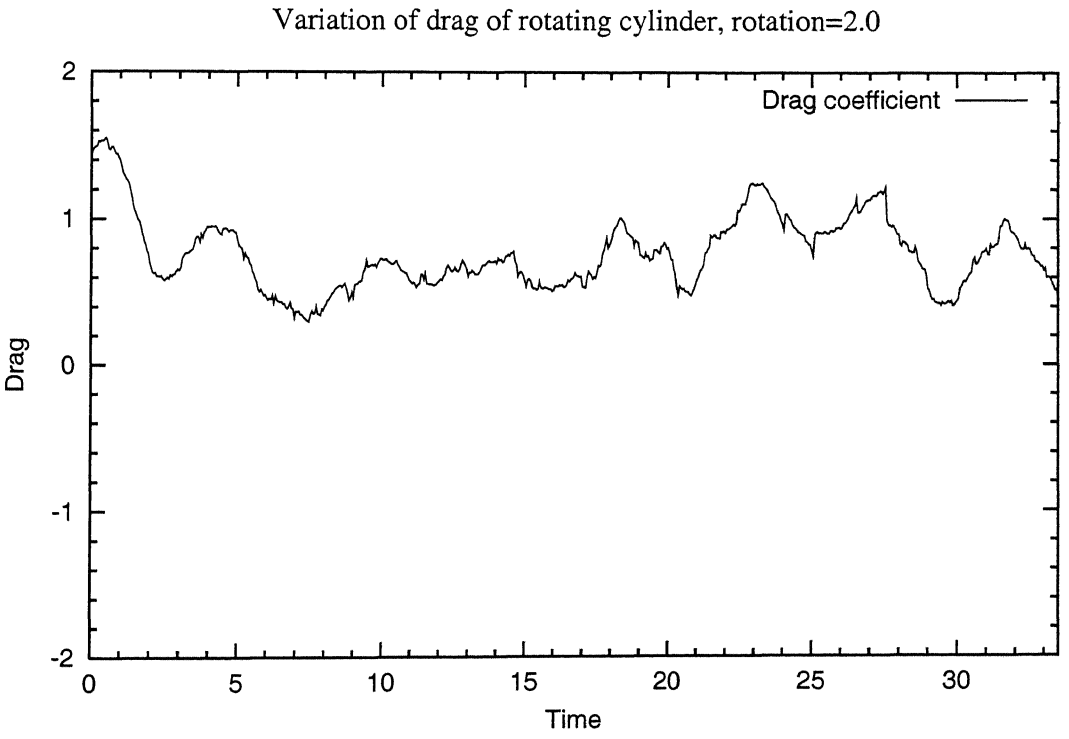

Figure 4.11· Variation of lift and drag of rotating circular cylinder at Reynolds number, $Re = 1 \times 10^5$ and $\Omega = 2.0$

Chapter 5

CONCLUSIONS

In first part of the present work we developed a procedure for the flow past square cylinder in flow field. The lift and drag coefficients are calculated by obtained pressure distribution on the surface of the cylinder, and are compared with the available experimental results. The drag and lift coefficients obtained are in fairly good agreement with the available experimental results.

The second part of the thesis deals with the extension of flow past square cylinder to flow past square cylinder with drag suppressors. We first developed a general procedure to solve the flow past two-dimensional multiple bodies. Two geometries of drag suppressors are dealt in with and it is found that drag of square cylinder can be reduced to a large extent, as has been reported in the literature.

In the last part of thesis, we tried to solve the flow past rotating circular cylinder. In the available time, this part could not be taken to a satisfactory conclusion and the results obtained are not correct.

References

1. Baker, G.R(1979) The cloud-in-cell technique applied to the roll-up of vortex sheets *J. Compt. Phys. Vol* 31, pp. 76-95.

2. Clements, R.R. and Maull, D.J (1973) The rolling up of a trailing vortex sheet.*Aero. J Vol.*77 pp. 46.

3. Chorin, A J.(1973) Numerical study of slightly viscous flow.*J. Compt. Phys. Vol.*57, pp. 785-796.

4. Chorin, A.J.(1978) Vortex sheet approximation of boundary layers.*J. Compt. Phys. Vol.*27, pp 428-442.

5. Chorin, A.J. and Bernard, P.S.(1973) Discretization of a vortex sheet, with an example of roll-up.*J. Compt. Phy Vol.*13, pp. 423.

6. Hoerner, S.J.(1965) Fluid-dynamic drag.*Published by The Author*

7. Jain, Manish Kumar(1996) Flow about the bluff bodies by the full-vortex cloud approach.*M.Tech.Thesis IIT Kanpur*

8. Krasny, R.(1987) Computation of vortex sheet roll-up in the Trefftz plane.*J. Fluid. Mech. Vol.*184, pp. 123-155.

9. Kuwahara, K. and Takami, H.(1973) Numerical studies of two-dimensional vortex motion by a system of point vortices.*J. Phys. Soc. Japan. Vol*34, pp. 247.

10. Leonard, A.(1980) Vortex methods for flow simulation.*J. Compt. Phys. Vol.*37, pp. 289-335.

11. Lewis, R.I.(1991) Vortex element methods for fluid dynamic analysis of engineering systems.*Cambridge University Press* 1991.

12. Lewis, R.I. and Porthouse, D.T.C.(1983b) Recent advances in theoretical simulation of real fluid flows.*Trans. N.E.C.I.* 99, *No.* 3

13. Milizanno, F. and Saffman, P.G.(1977) The calculation of large Reynolds number two dimensional flow using discrete vortices with random walk. *J. Compt. Phys. Vol.*23, pp. 380-392.

14. Moore D.W.(1974) A numerical study of the roll-up of a finite vortex sheet.*J. Fluid Mech. Vol.*63, pp. 225-335.

15. Parag Kumar(1993) Discrete vortex modelling of the wake of a flat plate. *M.Tech. Thesis, IIT Kanpur.*

16. Ritter, J.A Aluminium/steel "AERO-LITE" Rapid discharge.$ASME\,84 - WA/RT - 8$.

17. Rosenhead, L.(1932) The point vortex approximation of the vortex sheet.*Proc. Roy. Soc. London Ser.A* 134, pp.170-192.

18. Saffman, P.G.(1981) Dynamics of vorticity.*J. Fluid Mechanics Vol.*106, pp. 49-58.

19. Sarpkaya, T.(1989) Vortex induced oscillation.*A.S.M.E. J. Appl. Mechanics Vol.*68, pp. 109-128.

20. Smith, P.A. and Stansby, P.K.(1988) Impulsively started flow around a circular cylinder by the vortex method *J. Fluid Mechanics Vol.*198, pp. 45-77.

21. Som, Anup(1987) Aerodynamic treatment of open trucks with a view to minimising drag.*B.Tech. Project, IIT, Kanpur*

22. Takami, H.(1964) A numerical experiment with discrete vortex approximation with reference to the rolling-up of a vortex sheet.*Dept. Aero. & Astron., Stanford Univ. SUDAER* 202.

23. Verma, Chaman Singh(1994) Flow about bluff bodies by surface vorticity method.*M.Tech.Thesis IIT Kanpur*

24. Westwater, F.L.(1935) Rolling-up of the surface of discontinuity behind an aerofoil of finite span.*Aero. Res. Counc. R&M. No.*1962.

25. White, Frank M.(1979) Fluid Mechanics.*McGraw – Hill, Inc.* 1979.

A 134263

Date Slip

The book is to be returned on the date last stamped.

.....	.....
.....	.....
.....	.....
.....	.....
.....	.....
.....	.....
.....	.....
.....	.....
.....	.....
.....	.....
.....	.....
.....	.....